



Technische Universität München

Fakultät für Medizin

Development of innovative chelators for the synthesis of ^{89}Zr and ^{18}F AIF protein-based PET tracers

Lisa Russelli

Vollständiger Abdruck der von der Fakultät für Medizin der Technischen Universität München zur Erlangung des akademischen Grades einer **Doktorin der Naturwissenschaften (Dr.rer.nat.)** genehmigten Dissertation.

Vorsitz: Prof. Dimitrios Karampinos

Prüfer*innen der Dissertation: 1. Prof. Dr. Wolfgang A. Weber

2. Prof. Dr. Gabriele Multhoff

Die Dissertation wurde am 09.08.2022 bei der Technischen Universität München eingereicht und durch die Fakultät für Medizin am 13.12.2022 angenommen.

To all the beautiful things that science can accomplish

Abstract

Molecular imaging is a technique that exploits molecular biology to perform *in vivo* diagnosis using highly sensitive imaging methodologies such as Positron Emission Tomography (PET). ImmunoPET (iPET) is based on the use of radiopharmaceuticals made of antibodies and their derivatives, including engineered constructs with fast blood clearance and tissue uptake. Research in this field is quite active in many aspects, starting from the selection/design of new biological ligands up to the development of innovative radiolabelling approaches to label them and develop new PET probes. In this regard, the aim of this work was to develop new chelators for the complexation of relevant PET radioisotopes such as zirconium-89 (^{89}Zr) and fluorine-18 (^{18}F) to expand the number of proteins that can be labelled with these isotopes without affecting their biological properties. Zirconium-89 has a high interest in the field since is easily available, gives good resolution PET images and is already available in GMP (good manufacturing practice) quality, hence, has good possibilities to be extensively translated into clinic. Even though the labelling of protein-based biomolecules with ^{89}Zr is already feasible using the chelator DFO, there remains unmet need to increase labeling efficiency and in-vivo stability. To achieve these goals a new class of chelators were then conceptually designed, synthesised and characterized in depth in collaboration with the University of Piemonte Orientale in Italy. Among them, after preliminary tests *in vivo* in healthy nude mice, the chelator AAZTHAG was selected, being the best candidate for the goal mentioned above. The functionalized version, named AAZTHAG- $\text{C}_5\text{-OH}$, was then prepared in order to permit the conjugation with selective proteins of interest, followed by their labelling with ^{89}Zr . As a proof-of-concept, the chelator was conjugated with the mAb Trastuzumab and the resulting tracer characterized in depth. A similar approach was used for the development of new chelators for the complexation of [^{18}F]AIF to enable the labelling of heat-sensitive proteins with the widely available ^{18}F . Since common radiofluorination methods require harsh conditions, they cannot be implied in the direct labelling of sensitive protein-based vectors. A solution to this limitation is given by the [^{18}F]AIF methodology, where the ^{18}F radioisotope is strongly bound to an

aluminium atom, which is complexed, in soft conditions, by a bifunctional chelator previously conjugated to the protein construct. So far there are not many options available in the literature, with the NOTA chelator being the gold standard for this labelling approach but still requiring high temperatures (>100°C) to give high quality performances. The goal here was then to synthesise new chelators for the complexation of ^{18}F at room temperature in order to include in this method also the labelling of heat-sensitive molecules (e.g. svFab or nanobodies). Among the various ligands synthesised and fully characterized, the 2-AMPDA-HB molecule gave the best results in terms of radiochemical yield and stability *in vitro*. The resulting [^{18}F]AlF-2-AMPDA-HB was tested in healthy nude mice to validate its stability *in vivo* showing low accumulation in bones and no remarkable accumulation in other organs.

Zusammenfassung

Die molekulare Bildgebung ist eine Technik, die sich die Molekularbiologie zunutze macht, um eine hochselektive In-vivo-Diagnosen mit Hilfe hochempfindlicher Bildgebungsverfahren wie z.B. der Positronen-Emissions-Tomographie (PET) durchzuführen. Die ImmunoPET (iPET) basiert auf der Verwendung von Radiopharmaka, die aus Antikörpern und deren Derivaten inklusiver von Konstrukten mit niedrigem Molekulargewicht, die eine schnelle Blutclearance aufweisen und rasch von Geweben aufgenommen werden. Die Forschung auf diesem Gebiet ist in vielerlei Hinsicht sehr aktiv, angefangen bei der Auswahl/Design neuer biologischer Liganden bis hin zur Entwicklung innovativer Radiomarkierungsverfahren, um sie zu markieren und neue PET-Sonden zu entwickeln. Ziel dieser Arbeit war es, neue Chelatoren für die Komplexierung relevanter PET-Radioisotope wie Zirkonium-89 (^{89}Zr) und Fluor-18 (^{18}F) zu validieren, um die Anzahl der Proteine zu erhöhen, die mit diesen Isotopen ohne eine Veränderung ihrer biologischen Eigenschaften markiert werden können. Zirkonium-89 ist in diesem Bereich von großem Interesse, da es in GMP (good manufacturing practice) Qualität für klinische Studien verfügbar ist und PET- Bilder mit guter Auflösung liefert so dass es gute Chancen bestehen, es in naher Zukunft in der Klinik einzusetzen. Obwohl die Markierung von Biomolekülen auf Proteinbasis mit ^{89}Zr unter Verwendung des Chelators DFO bereits möglich ist, werden in der Literatur ständig neue Chelatoren vorgestellt, um die Markierungsleistung zu erhöhen und stabilere Radiotracer *in vivo* bereitzustellen. In Zusammenarbeit mit der Universität von Piemonte Orientale in Italien wurde eine neue Klasse von Chelatoren konzipiert, synthetisiert und eingehend charakterisiert. Nach vorläufigen Tests *in vivo* an gesunden Nacktmäusen wurde der Chelator AAZTHAG ausgewählt, da er für das oben genannte Ziel am besten geeignet ist. Die funktionalisierte Version mit der Bezeichnung AAZTHAG-C₅-OH wurde dann hergestellt, um die Konjugation mit Proteinen von Interesse zu ermöglichen, gefolgt von deren Markierung mit ^{89}Zr . Als Nachweis wurde der Chelator mit dem mAb Trastuzumab konjugiert und der resultierende Tracer eingehend charakterisiert. Parallel dazu wurde ein ähnlicher Ansatz für die Entwicklung neuer Chelatoren für die Komplexierung

von [^{18}F]AlF verwendet, um die Markierung hitzeempfindlicher Moleküle mit dem weit verbreiteten ^{18}F zu ermöglichen. Da die üblichen Radiofluorierungsmethoden harsche Bedingungen erfordern, können sie nicht für die direkte Markierung empfindlicher proteinbasierter Vektoren eingesetzt werden. Eine Lösung für diese Einschränkung bietet die [^{18}F]AlF-Methode, bei der das ^{18}F -Radioisotop an ein Aluminiumatom gebunden wird, das unter schonenden Bedingungen durch einen bifunktionellen Chelator komplexiert wird, der zuvor an das Proteinkonstrukt konjugiert wurde. Bislang gibt es dafür in der Literatur nicht viele Optionen, wobei der NOTA-Chelator der Goldstandard für diesen Markierungsansatz ist, aber immer noch hohe Temperaturen ($>100^\circ\text{C}$) erfordert, um eine hohe Markierungsausbeute zu erzielen. Ziel war es daher, neue Chelatoren für die Komplexierung von ^{18}F bei Raumtemperatur zu synthetisieren, um diese Methode auch für die Markierung hitzeempfindlicher Moleküle (z. B. svFab oder Nanobodies) zu nutzen. Unter den verschiedenen synthetisierten und vollständig charakterisierten Liganden lieferte das 2-AMPDA-HB Moleküle die besten Ergebnisse in Bezug auf die radiochemische Ausbeute und die Stabilität *in vitro*. Der resultierende [^{18}F]AlF-2-AMPDA-HB wurde in gesunden Nacktmäusen getestet, um seine Stabilität *in vivo* zu validieren. Dabei zeigte sich eine geringe Anreicherung in den Knochen und keine bemerkenswerte Anreicherung in anderen Organen.

Work on the presented PhD thesis resulted in the following publications:

Russelli L*, De Rose F, Leone L, Reder S, Schwaiger M, D'Alessandria C, Tei L. A Semi Rigid Novel Hydroxamate AMPED-Based Ligand for ⁸⁹Zr PET Imaging. *Molecules*. 2021 Sep 25;26(19):5819. doi: 10.3390/molecules26195819. PMID: 34641362; PMCID: PMC8512011.

Russelli L*, Martinelli J*, De Rose F, Reder S, Herz M, Schwaiger M, Weber W, Tei L, D'Alessandria C. Room Temperature Al¹⁸F Labeling of 2-Aminomethylpiperidine-Based Chelators for PET Imaging. *ChemMedChem*. 2020 Feb 5;15(3):284-292. doi: 10.1002/cmdc.201900652. Epub 2020 Jan 7. PMID: 31830368.

Studies described in the PhD thesis resulted in the following conference presentations:

Russelli L*, Martinelli J*, De Rose F, Reder S, Herz M, Weber W, Tei L, D'Alessandria C. Al¹⁸F Labeling of new AMPTA-based chelators for application in Positron Emission Tomography imaging. 03-06th April 2019, 57th Symposium of German Society of Nuclear Medicine (DGN), Bremen, Germany.

Russelli L*, Martinelli J*, De Rose F, Reder S, Herz M, Weber W, Tei L, D'Alessandria C. Al¹⁸F Labeling of new AMP-based chelators for application in Positron Emission Tomography imaging. 25-28th September 2019, XIIIth Workshop „Imaging of diagnostic and therapeutic biomarkers in Oncology“ of Cancéropôle grand ouest, Le Bono, France.

Russelli L*, Martinelli J*, De Rose F, Reder S, Herz M, Weber W, Tei L, D'Alessandria C. Al¹⁸F Labeling at room temperature and in vivo study of new AMP-based chelators for application in PET imaging. 18th October 2019, 1st MGC Science Day of the School of Medicine (TUM), Munich, Germany.

Russelli L*, De Rose F, Leone L, Reder S, Schwaiger M, D'Alessandria C, Tei L. A Semi Rigid Novel Hydroxamate AMPED-Based Ligand for ⁸⁹Zr PET Imaging. 5th November 2021, 3rd MGC Science Day of the School of Medicine (TUM), Munich, Germany.

Studies described in this PhD thesis resulted in the following best poster award:

Russelli L*, Martinelli J*, De Rose F, Reder S, Herz M, Schwaiger M, Weber W, Tei L, D'Alessandria C. Room Temperature Al¹⁸F Labeling of 2-Aminomethylpiperidine-Based Chelators for PET Imaging. 24-28th August 2020, Poster Walk „PET/SPECT, Radionuclide, X-Ray, CT I | Probe Chemistry“ of the 15th European Molecular Imaging Meeting (EMIM), Virtual.

Table of Contents

1	INTRODUCTION.....	1
1.1	POSITRON EMISSION TOMOGRAPHY	1
1.2	TUMOR TARGETING PROTEIN-BASED TRACERS	5
1.3	ANTIBODY-DERIVATIVES VECTORS.....	9
1.4	T CELLS TRACKING.....	12
2	METHODOLOGY	14
2.1	⁸⁹ Zr RADIOCHEMISTRY	14
2.1.1	<i>⁸⁹Zr production and properties.....</i>	<i>14</i>
2.1.2	<i>⁸⁹Zr radiolabelling.....</i>	<i>15</i>
2.2	[¹⁸ F]AIF RADIOCHEMISTRY	19
2.2.1	<i>¹⁸F production and properties</i>	<i>19</i>
2.2.2	<i>¹⁸F labelling via prosthetic group.....</i>	<i>20</i>
2.2.3	<i>[¹⁸F]AIF labelling via complexation.....</i>	<i>21</i>
3	OBJECTIVES.....	24
4	RESULTS.....	26
4.1	A SEMI RIGID NOVEL HYDROXAMATE AMPED-BASED LIGAND FOR ⁸⁹ Zr PET IMAGING.....	26
4.2	ROOM TEMPERATURE AL ¹⁸ F LABELING OF 2-AMINOMETHYLPYPERIDINE-BASED CHELATORS FOR PET IMAGING	28
5	SUMMARY AND OUTLOOKS.....	30
5.1	A SEMI RIGID NOVEL HYDROXAMATE AMPED-BASED LIGAND FOR ⁸⁹ Zr PET IMAGING.....	30
5.2	ROOM TEMPERATURE AL ¹⁸ F LABELING OF 2-AMINOMETHYLPYPERIDINE-BASED CHELATORS FOR PET IMAGING	32

6	REPRINT PERMISSIONS	35
6.1	PUBLICATION ON "MOLECULES" JOURNAL.....	35
6.2	PUBLICATION ON "CHEMMEDCHEM" JOURNAL	36
7	ABBREVIATIONS.....	37
8	LIST OF PUBLICATIONS.....	39
9	ACKNOWLEDGEMENTS.....	40
10	REFERENCES.....	41
11	APPENDIX	51
	APPENDIX I	51
	APPENDIX II	51

1 INTRODUCTION

1.1 Positron Emission Tomography

Nuclear medicine can be defined as the branch of medicine which make use of radioactivity for two different applications: diagnosis and therapy. In particular, diagnosis can be performed via two main methodologies called PET and SPECT, which are complementary since they used different radionuclides that consent the *in vivo* visualization of tumor-specific metabolic processes or selected targets on a molecular level to provide functional information of biochemical processes (Vallabhajosula, 2009). Normally, they are coupled with such techniques like MRI or CT in order to provide both anatomic/morphological and functional information at the same time: this results in one single PET/CT, SPECT/CT or PET/MRI scan (Beyer *et al.*, 2000; Even-Sapir *et al.*, 2001; Maurer, 2008; Townsend, 2008; Bockisch *et al.*, 2009; Pichler *et al.*, 2010; Sauter *et al.*, 2010; Delso *et al.*, 2011).

SPECT is the acronyms of single-photon emission computed tomography and, indeed, measures the emissions of single photons of γ -emitters, which are detected by a set of rotating scintillation detectors (γ -cameras, Anger cameras). It is generally performed using radioisotopes such as iodine-123, technetium-99m, xenon-133, thallium-201, and indium-111 (Crişan *et al.*, 2022).

PET imaging (abbreviation of Positron Emission Tomography), as showed in **Figure 1**, is based on the annihilation of a positron with an electron in the matter, which generates a photon pairs in opposite directions between them. More in detail, the positron emission is due to the β^+ -decay of a selected neutron-deficient isotope, and once a positron is emitted will lose its kinetic energy until will encounter its antiparticle (an electron) from the surrounding matters to form a positronium. These will mutually annihilate and their masses converted into two ~ 511 keV γ -rays emitted in approximate opposite direction ($\sim 180^\circ$) (Turkington, 2001). Based on this particular characteristic, the two γ -rays can be detected by two detectors (or a circular array of multiple detector pairs of scintillation crystals) placed around the patient. The output

1. INTRODUCTION

is only generated when the incident photon pairs from positron annihilation are detected in coincidence by opposite detector pairs and when detection occurs simultaneously, typically within a time window of 6-12 ns (Vallabhajosula, 2009). This coincidence event represents a line in space and allows the localization of the annihilation occurrence. Subsequently, due to the acquisition of a large number of coincidence events along all lines and different angles, a three dimensional image is reconstructed from the two-dimensional projections via mathematical algorithms (Turkington, 2011; Cherry, Sorenson and Phelps, 2012).

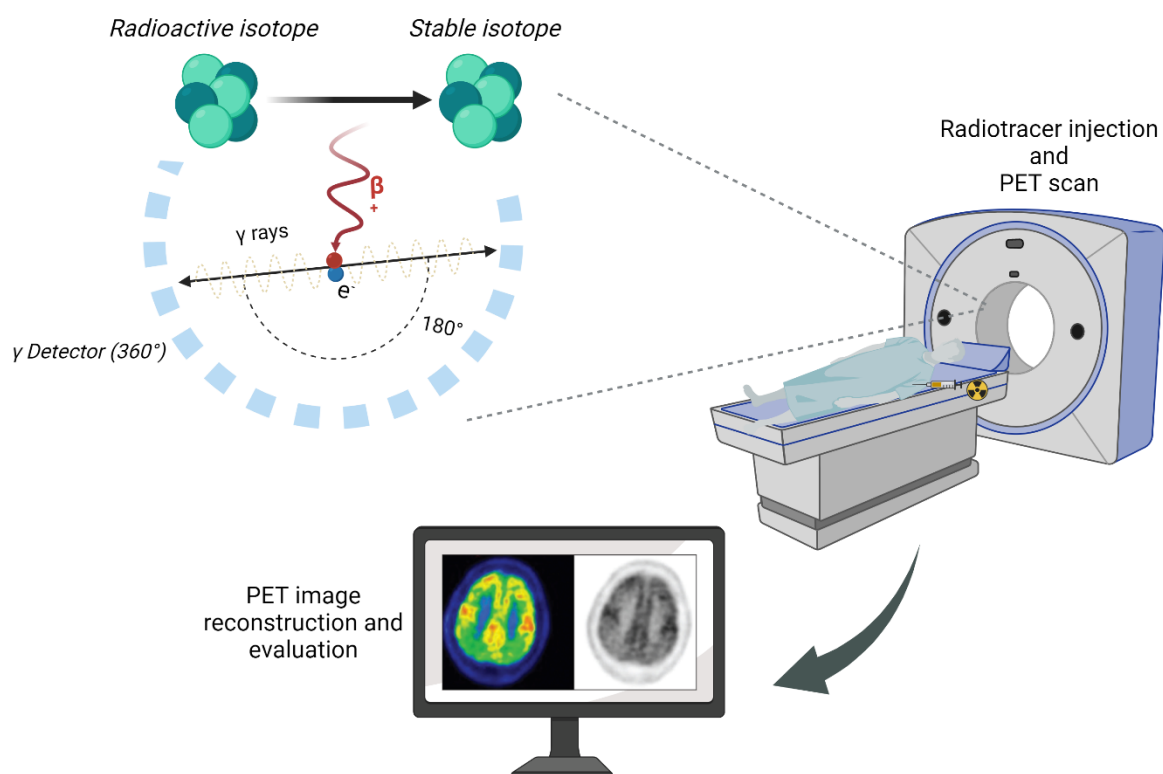


Figure 1: Basics of a PET scan. After a patient is injected with a radiotracer, the radioactive isotope start decaying emitting β^+ radiation. A β^+ particle then collide with an electron in the space: this collision emit two γ rays in the opposite directions (at $\sim 180^\circ$ between them). The two γ rays are afterwards detected by the crystals of the detector and the signal is then multiplied. After a software reconstruction the PET image is ready to be evaluate from the physician in order to assess the patient condition - brain PET image from (Sarikaya *et al.*, 2021). Figure created with BioRender.com.

During the evaluation of the scans is important to measure the amount of radioactivity accumulated in tumors and this quantification can be done since PET scanners are designed

1. INTRODUCTION

to measure the *in vivo* radioactivity concentration, generally expressed in kBq/ml (Kinahan and Fletcher, 2010). The tissue uptake can be influenced mostly by the amount of activity injected and by the patient size, and in order to compensate for these two variables and standardize the quantification, the standardized uptake value (SUV) is commonly used as a relative measure of the radioactivity uptake (Thie, 2004). The SUV is expressed with the equation:

$$SUV = \frac{\text{activity concentration} \left[\frac{kBq}{ml} \right] \times \text{patient body weight} [kg]}{\text{injected activity} [kBq]}$$

In preclinical studies a derivative of this equation equally used is named %ID/g and expressed as reported below:

$$\% \frac{ID}{g} \text{ tumor} = \frac{\text{tumor activity} [MBq]}{\text{injected activity} [MBq] \times \text{tumor weight} [g]} \times 100$$

where the tumor activity is given after a specific ROI is drawn around the tumor, the injected activity is decay corrected and the weight of the tumor is measured post-mortem.

PET acquisition can then be performed after the injection in the patient of a radiopharmaceutical based on a β^+ emitter. Generally, these radioisotopes should have a relatively short half-life compared to those used for radiotherapy, which can be included in a range from minutes to few days maximum, depending on how fast the radiotracer can reach the target *in vivo*. Furthermore since the positron energy determines the range in the tissue, such radioisotopes should ideally have a low positron energy in order to give PET images with a better spatial resolution (Conti and Eriksson, 2016). In **Table 1** below is reported a list of the most common radioisotopes that can be used for the labelling of biomolecules in order to be used as radiopharmaceuticals for PET diagnostic.

Radioisotope	Half-life	Emission	Maximum $\beta^{+/-}$ Energy [MeV]
^{68}Ga	67.8 min	EC, β^+	1.9
^{18}F	109.7 min	EC, β^+	0.6
^{44}Sc	4.0 h	EC, β^+	1.5
^{64}Cu	12.7 h	EC, β^+	0.7
^{89}Zr	78.4 h	EC, β^+	0.9

Table 1: Main radioisotopes used for the labeling of biomolecules for Positron Emission Tomography with specific physical-chemical properties.

These radioisotopes can be incorporated in the radiotracer mainly via complexation reaction with a bifunctional chelator (Price and Orvig, 2014; Sneddon and Cornelissen, 2021) except for ^{18}F where the most common radiolabeling reaction is still based on substitution reactions that require harsh conditions not always suitable with sensitive biomolecules (Zhang *et al.*, 2020). This problem can be overcome by the use of a relatively new methodology based on the complexation of an $[^{18}\text{F}]\text{AlF}$ species previously formed (McBride *et al.*, 2009).

In general, PET and SPECT exploit different physical processes, hence, they are performed with different instruments and they have a different economic impact on clinics: the number of worldwide installed devices is approximately 10-times higher for SPECT compared to PET scanners, also due to the reduced price and the higher availability of appropriate $^{99\text{m}}\text{Tc}$ -radiotracer. Anyhow, “the development of PET and associated fluorinated agents led to an almost complete stop of SPECT research programs and new $^{99\text{m}}\text{Tc}$ labelled molecules are quite rare.” (Zimmermann, 2013).

1.2 Tumor targeting protein-based tracers

PET technique required the use of a radioactive tracer, a pharmaceutical molecule radiolabelled with a radioisotope, in order to visualise a tumor lesion in the human body. The most common tracer for the diagnosis of tumor in early stages, or monitor of therapy outcome, is the [^{18}F]FDG, a “radioactive sugar” that cannot distinguish between different types of cancer (e.g. between a naïve tumor and possible metastasis) (McCarthy *et al.*, 2020). To overcome the problem of poor specificity of [^{18}F]FDG and improve the final outcome of the PET scans, more specific tumor-targeting agents are necessary.

Molecular imaging is the perfect strategy to improve the clinical management of cancers and non-cancerous diseases, since it takes advantage of natural and biological mechanisms where very specific bonds are formed between a ligand and a receptor *in vivo*. Antibody-derived molecular imaging probes have been helpful in visualizing expression of tumor targets and in investigating the pharmacokinetics of therapeutic monoclonal antibodies in living subjects via PET imaging, where its application has distinct advantages in terms of image quality, spatial resolution, and quantification (Rahmim and Zaidi, 2008). In this context, we can more precisely talk about immuno-positron emission tomography (immunoPET or iPET), a technique where the extraordinary targeting specificity of antibodies and antibody-derivatives meets the great sensitivity and resolution of PET (Knowles and Wu, 2012). The concept of immunoPET was manifested more than two decades ago (Philpott *et al.*, 1995; Goldenberg and Nabi, 1999) but its development rapidly accelerated in recent years with the increasing approval of therapeutic antibodies, and the more widespread production of long half-life radionuclides (Wei *et al.*, 2020). Nowadays, the clinical application of immunoPET imaging is constantly increasing in parallel with many additional applications in preclinical models such as the implementation of the detection of immune cell subsets, activation and inhibitory biomarkers, tracking of adoptively transferred cellular therapeutics that can further increase the number of tracers translated to the clinic (Wu and Pandit-Taskar, 2022).

1. INTRODUCTION

An iPET tracer should be composed by a target-specific molecule that can be opportunely labelled with a radioisotope matching its half-life in the blood pool (Chakravarty *et al.*, 2014). As represented in **Figure 2**, a tracer is mainly formed by three separate units: a radioactive isotope (either complexed by a chelator or incorporated in a prosthetic group) can allow the visualization of the target tissue via PET *in vivo*. A biological active vector can drive the tracer to the target tissue in the body, and a linker in between is necessary to separate and connect the two parts.

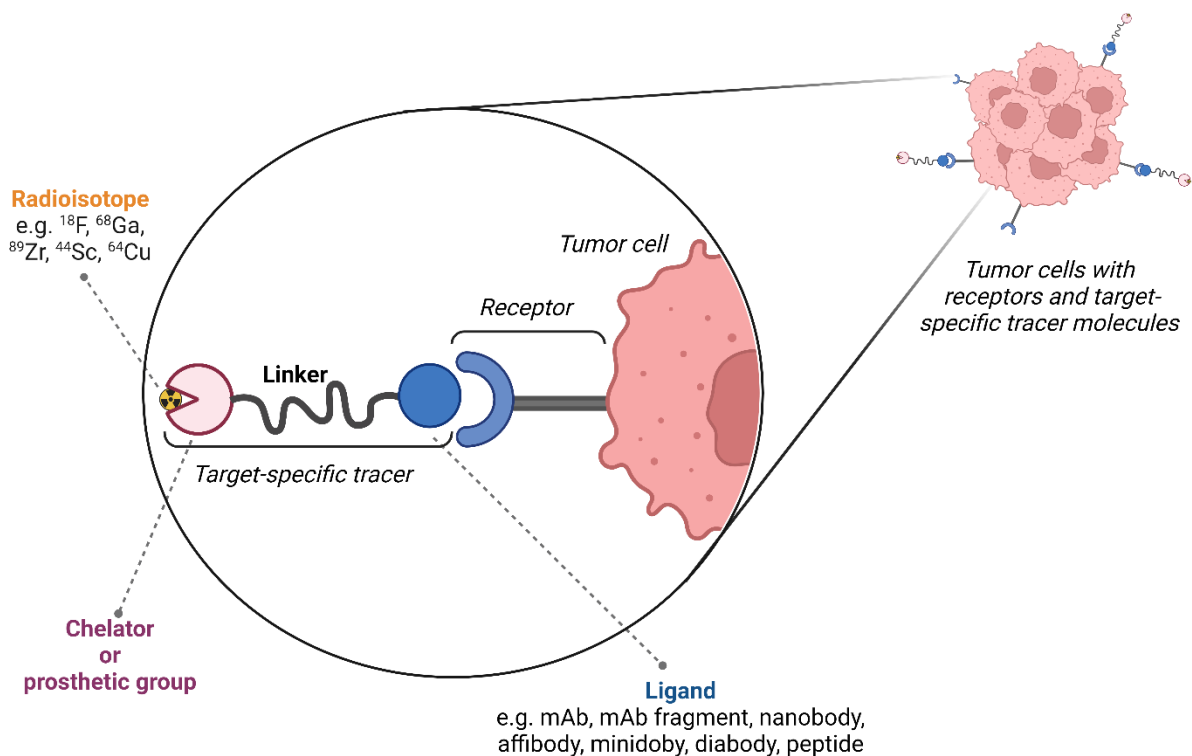


Figure 2: Schematic representation of a tracer where the tumor cell with a specific receptor is the target of the tracer. The molecule is selectively binding the tumor cell due to the specific ligand-receptor affinity. After the Ligand vector, moving to left, a linker is required to separate the target-specific site to the radioactive part of the molecule: a linker is, for example, an aliphatic carbon chain, a PEG chain or any other adequate chemical structure. Finally, as showed in figure, a chelator or a prosthetic group is present bearing the radioisotope of choice. Figure created with BioRender.com.

The linker can have various nature based on the application of the tracer e.g. PEG chain, PAS chain, more or less complex aliphatic chain, and it can be used to modify the pharmacokinetic

1. INTRODUCTION

of the radiotracer *in vivo* (Schlapschy *et al.*, 2013; Guillou *et al.*, 2021; Z. Zhou *et al.*, 2021) or simply reduce the steric hindrance and guarantee the successful completion of the tasks of both units (Chomet *et al.*, 2020; Klasen *et al.*, 2021).

If the tracer consists in a protein-based probe, while planning its labelling, a mandatory requirement is that the reaction is conducted in mild conditions, explained below, in order to keep the protein intact. Different parameters have to be taken into account, for example, an important one is the control of the reaction temperature that often cannot be above 37°C but also no harsh bases and/or acids should be used and, in general, the reaction should be conducted in a water-based buffer at mild pH values (4.5-7.5). These conditions are generally satisfied for most of the radiolabelling reactions where a bifunctional chelator is involved (Vaughn *et al.*, 2020; Feiner *et al.*, 2021; Sneddon and Cornelissen, 2021). In a preferable direct labelling procedure the chelator is firstly conjugated to the protein with a site-specific or random approach (Chigoho *et al.*, 2021), and then the conjugated derivative is labelled with the selected radioisotope. Depending on the blood circulation of the protein of choice, different kind of radioisotopes can be chosen based on their half-life. For the most common ones, such as ^{68}Ga , ^{64}Cu , ^{44}Sc and ^{89}Zr , bifunctional chelators are already available in the literature allowing this kind of labelling approach (Higashikawa *et al.*, 2014; Fersing *et al.*, 2019; Chomet *et al.*, 2021; Ghiani *et al.*, 2021). The research in this field is quite wide, and it is increasing especially because the interest on these radioisotopes is growing since more derivative PET agents have approached the clinical translation in the past decades. Based on the relatively short half-life of ^{18}F (109.7min) and the good spatial resolution of the resulting PET images, this radioisotope is very important for the radiolabelling of protein-based probes characterized by a relatively fast blood circulation and low molecular weight (10-50kDa). Unfortunately, from the chemically point of view many radiofluorination techniques are conducted via substitutions reactions that require high temperatures to happen, hence an indirect labelling approach is required when this is applied to protein-based probe. The procedure leads to a very time consuming and multistep labelling strategies where first, a prosthetic group is ^{18}F -fluorinated

1. INTRODUCTION

at high temperature, and then this radioactive moiety is conjugated to the protein of interested. During this process, the scientist is challenging the decay of the radioisotope, with the inevitable result of a final low overall radiochemical yield (radioisotope incorporation) compared to a direct labelling reaction based on the use of a bifunctional chelator. Here's the unmet need of developing new radiolabelling technique to allow direct radiofluorination of temperature sensitive molecules in mild conditions and at room temperature. A very elegant approach is based on the complexation by bifunctional chelators of adducts formed by interaction between aluminium and fluorine-18 ($[^{18}\text{F}]\text{AlF}$). Unfortunately, the gold standard chelator for such methodology (NOTA chelator), even if it allows the complexation of the $[^{18}\text{F}]\text{AlF}$ (hence the radiofluorination) in mild conditions, it still requires high temperatures to obtain reasonable radiochemical yields (McBride *et al.*, 2009). Hence there is still the need to fill this gap (Archibald and Allott, 2021).

1.3 Antibody-derivatives vectors

Cancer treatment is heading for more personalized imaging and therapy approaches, and thus the necessity of novel agents. This need can be satisfied by a variety of constructs derived from antibodies, use of which is hugely expanding in recent years in parallel to iPET imaging (Figure 3). Examples of such ligand molecules are proteins like antibodies and antibodies derivatives (e.g. antibody fragments, minibodies, diabodies, nanobodies, affibodies) with a relatively fast *in vivo* blood circulation that varies in a range from few hours up to days.

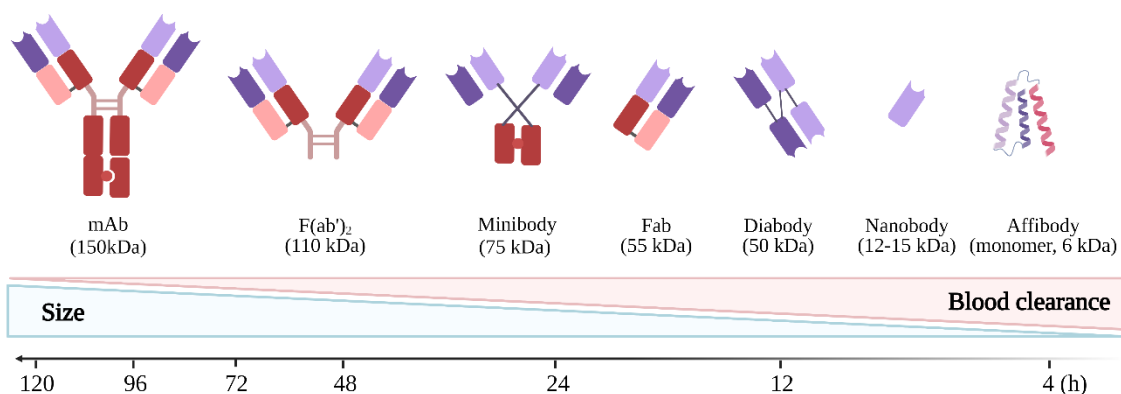


Figure 3. Schematic representation of protein-based constructs used for immunoPET. The image is pointing out how the molecular weight (MW) of the different antibody-derived probes influences their blood pool clearance, which impacts on the selection of the right radioisotope for immunoPET imaging. Figure created with BioRender.com.

The structural and functional nature of antibodies allows for the production of smaller antigen binding fragments, such as fragment antigen binding (Fab)', the single chain fragment variable (scFv), single-domain antibodies, through molecular cloning, antibody engineering, and even enzymatic methods (Bates and Power, 2019). These can be opportunely functionalized in order to be successively labelled with the radioisotope of interest to perform immunoPET (Morais and Ma, 2018; Jackson *et al.*, 2020). Plenty of preclinical data are so far persuasive showing increased performances in term of specificity and detection of early stage tumors,

1. INTRODUCTION

highlighting that antibody-based molecular imaging tracers will play an important future role in the diagnosis and management of cancer and other diseases (Olafsen and Wu, 2010).

Affibody molecules are engineered proteins of 58 aminoacids folded into three alpha helices. They mimic monoclonal antibodies and antibody fragments with their high affinity and selectivity, however, they are much smaller and chemically robust proteins being able to tolerate higher temperatures and more extreme pH values (Fu *et al.*, 2018). The 6-7 kDa size, their inertness to harsh conditions and high affinity (nanomolar range) make them excellent candidates to have a central role in molecular imaging (Löfblom *et al.*, 2010). ^{18}F and ^{68}Ga are the two positron emitting nuclides of high interest for the clinical translation of affibody molecules since their half-lives are sufficient for imaging some hours after injection, and this is compatible with their rapid pharmacokinetics (Tolmachev and Orlova, 2020).

Nanobodies, the variable domains of heavy chain camelid antibodies (VHHs), are a small antigen-binding derivatives with molecular weight around 15 kDa, high affinity, strong stability, low immunogenicity, fast clearance, and strong tissue penetration (Salvador, Vilaplana and Marco, 2019). With regards of their application in immunoPET, their short circulatory half-life have allowed the use of a range of isotopes with short half-lives for imaging, as well as longer-lived isotopes for the labelling of a broad group of tumors and non-cancerous targets (Rashidian and Ploegh, 2020; Berland *et al.*, 2021). Their use in preclinical studies is exponentially increasing (Harmand *et al.*, 2021) and first clinical trials are already ongoing as shown in **Table 2**.

In **Table 2** are reported the main protein-based constructs used in iPET with the respective radioisotopes used so far for their labelling.

Construct	Size (kDa)	Blood clearance (h)	Radioisotope	Clinical trials
Affibody	6	0.5-4	$^{68}\text{Ga}/^{18}\text{F}/^{44}\text{Sc}/^{64}\text{Cu}$	^{68}Ga -labelled compounds (Sandström <i>et al.</i> , 2016; N. Zhou <i>et al.</i> , 2021; Miao <i>et al.</i> , 2022)
Nanobody	12-15	0.5-4	$^{68}\text{Ga}/^{18}\text{F}$	^{68}Ga -labelled compound (Keyaerts <i>et al.</i> , 2016; Wang <i>et al.</i> , 2022)
Diabody	50	up to 24	$^{68}\text{Ga}/^{18}\text{F}/^{64}\text{Cu}/^{124}\text{I}$	^{124}I -labelled compound (Scott <i>et al.</i> , 2020)
Fab fragment	55	up to 24	$^{68}\text{Ga}/^{18}\text{F}/^{89}\text{Zr}$	^{89}Zr -labelled compound (Richter <i>et al.</i> , 2020) and ^{68}Ga -labelled compound (Rathore <i>et al.</i> , 2022)
Minibody	75	up to 48	^{89}Zr	(Pandit-Taskar <i>et al.</i> , 2020; Vlachostergios <i>et al.</i> , 2022)
F(ab') ₂ fragment	110	up to 48	^{89}Zr	n. a.
mAb	150-180	up to 120	$^{89}\text{Zr}/^{64}\text{Cu}$	(Jauw <i>et al.</i> , 2017; Ulaner <i>et al.</i> , 2017; Bensch <i>et al.</i> , 2018; Krishnan <i>et al.</i> , 2020; Verhoeff <i>et al.</i> , 2022)

Table 2. List of main protein-based constructs with relative characteristics and appropriate isotopes used for their labelling. Clinical trials are reported when applicable.

An increasing number of radiopharmaceuticals at the preclinical study stage present potential to be translated to the clinic in near future (Krasniqi *et al.*, 2018; Oroujeni *et al.*, 2018; Xavier *et al.*, 2019; Rubins *et al.*, 2021) exponentially increasing the use of iPET in the clinics.

1.4 T cells tracking

The fight against cancer is becoming more and more efficient since cancer therapy is increasingly expanding towards new approaches. Immunotherapy consist in a therapy approach in fast development nowadays due to high response in melanoma and lung cancer patients. There is the necessity to monitor the efficacy of the cure by using selective imaging methodologies in order to promptly change therapy when not effective. Since at the base of immunotherapy there is the correct functionality of T cells, it is important to develop new tools to track their migration and expansion *in vivo*. Here's where a variety of immune-imaging tools are available and many researches are focused on the development of even further new specific imaging tracers (Wei *et al.*, 2018; Li *et al.*, 2022).

T cells can be labelled directly or indirectly with radiopharmaceuticals. The direct labelling approach consists in the *ex-vivo* labelling of cells isolated by the blood of the patients with an agent that remains trapped inside the cytoplasm. These labelled cells are re-injected in the subject, and their *in vivo* distribution and accumulation can be followed by nuclear imaging. The indirect labelling is instead based on the *in vivo* targeting of specific antigens expressed by selected T cells or to the use of reporter genes (Galli *et al.*, 2021). In these circumstances a target-specific tracer will be directed to a receptor of activated lymphocytes ideally without altering their functionality as shown in **Figure 4** below.

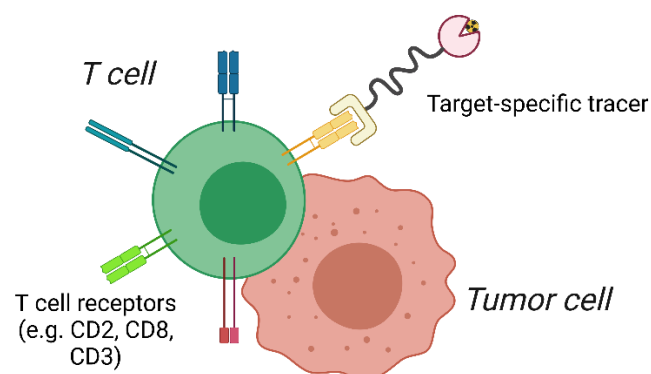


Figure 4. Representation of *in vivo* T cells tracking. The activity of tumor-reactive T cells can be investigated *in vivo* by immunoPET imaging via intravenous injection of target-specific tracers that bind designated receptors expressed on the T cells. Figure created with BioRender.com.

1. INTRODUCTION

Depending on the selected target, T cells visualization *in vivo* can be provided by several constructs labelled with the appropriate radioisotopes matching their blood clearance. This is the case for example, of the antibody antiCD3 used to visualize cytotoxic T-lymphocyte infiltration in preclinical models of colorectal cancer (Larimer *et al.*, 2016), or of the two F(ab')₂ antibody fragments antiCD2 and antiCD7 used to monitor the T central memory cells infiltration and T-cell anti-tumor efficacy in tumor myeloma preclinical models (Mayer *et al.*, 2018). Furthermore, in order to increase the pharmacokinetics of probes in the context of immunoPET, bivalent minibodies (75 kDa) have also found an application as target-specific tools. The radiolabelled minibody ⁸⁹Zr-Df-IAB22M2C consents to perform safe PET imaging in patients with different metastatic solid tumor treated with immunotherapy and turn out to be a good candidate to predict early response to the cure by visualizing the whole-body biodistribution of CD8⁺ leukocytes in tumors and reference tissues (Farwell *et al.*, 2021). Nanobodies also represent a perfect tool for tracking of T cells, and indeed their use in the ImmunoPET application has been increased in the past decay. So far, CD8 seems to be most attractive target for nanobody-based radiotracers. For example, a CD8 specific ⁸⁹Zr-labelled nanobody-based tracer was used to track the presence of intratumoral CD8⁺ T cells in the immunotherapy-susceptible B16 melanoma model in response to checkpoint blockade (Rashidian *et al.*, 2017). More recently, a group of nanobodies were studied to be used as an attractive non-invasive tool to discriminate between both systemic and tumor-infiltrating CD8⁺ T lymphocytes. Among them, a nanobody was selected for the development of the tracer [⁶⁸Ga]Ga-NOTA-SNA006, to track human CD8⁺ T cells and CD8⁺ tumors in different mice models, showing great potential for immunotherapy monitoring and efficacy evaluation (Zhao *et al.*, 2021). Recently a pilot study on three CD8⁺ lung cancer patients confirmed the results previously reported in the preclinical studies presenting the [⁶⁸Ga]Ga-NOTA-SNA006 as a specific tool for CD8⁺ T cells tracking and CD8⁺ tumor visualization (Wang *et al.*, 2022)

2 METHODOLOGY

This chapter wants to give an overview and explain in detail the two main radiolabelling procedures taken in consideration in this thesis. Both of them are based on innovative optimized protocols as described in the two manuscripts reported here.

2.1 ^{89}Zr radiochemistry

2.1.1 ^{89}Zr production and properties

Zirconium-89 (^{89}Zr) is a second row transition metal that, due to its quite long half-life (78.4 h), has played a preeminent role in the development of new radiotracers for immunoPET with conventional full-size monoclonal antibodies (IgG) and their derivatives fragments. This kind of targeting vectors normally require long periods (up to days) to fully accumulate at the target site *in vivo* and, therefore, radionuclides with long half-life such as ^{89}Zr are required. The relatively long half-life of this radionuclide makes its transportation possible internationally: zirconium-89 is commercially available as ^{89}Zr -oxalate by few suppliers worldwide, and it is produced in cyclotrons following the nuclear reaction $^{89}\text{Y}(p,n)^{89}\text{Zr}$, by bombarding a solid ^{89}Y target (Dabkowski *et al.*, 2015). Its decay is partially due to positron emission (23%) and partially to electron capture (77%) to $^{89\text{m}}\text{Y}$ that rapidly convert to the stable ^{89}Y via γ emission of 909 keV (Chomet, van Dongen and Vugts, 2021). An optimized cyclotron production using a sputtered yttrium target showed a remarkable increase in the RCY (radiochemical yield) of a DFO-trastuzumab tracer (>98%) compared to the RCY when the radionuclide is produced with a “standard” target (Queern *et al.*, 2017). Since its average positron energy of 395 keV is relatively low, ^{89}Zr is an ideal candidate for high-resolution PET imaging of slow-accumulating biomolecules. In addition, since its half-life is much longer than those of ^{68}Ga , ^{18}F or ^{44}Sc , zirconium-89 is more suitable for days-long diagnoses, and it is also easier to transport from an external site of production when a cyclotron is not readily available at the scanning site. Since its production is already available as a GMP grade, the future of this radionuclide in clinical application with long biological half-life molecules is bright. As soon as the interest of

the nuclear medicine society grows, new sites will probably initiate the production, leading to costs drop down, and it will become very competitive with other existing PET radionuclides (Zimmermann, 2013).

2.1.2 ^{89}Zr radiolabelling

Zirconium(IV) has an ionic radius of 84 pm and most commonly tends to have a coordination number of 8 (Price, Greenman and Stasiuk, 2016; Sneddon and Cornelissen, 2021). In water it forms salts and adducts that are poorly soluble, except at very high or low pH values: this behavior might make it problematic to handle (Ekberg *et al.*, 2004), mostly during complexation labelling procedures with chelators. To overcome this issue ^{89}Zr is generally supplied as a solution of ^{89}Zr -oxalate and only afterwards the pH is brought to a neutral value using buffers such as HEPES buffer. Briefly, an optimal protocol for the labelling reactions sees a selected ratio of precursor (in water or specific buffer) reacting with ^{89}Zr , being this one dissolved in a total of 100 μL oxalic acid 1M (eventually adjusted with oxalic acid 1M if too concentrated when received from the supplier). The ^{89}Zr -oxalate solution is first neutralized with 45 μL of Na_2CO_3 2M and incubated for 3 min at room temperature, and then 155 μL of HEPES (pH = 7.0) are added. The precursor is then added to the solution and the pH adjusted with 350 μL of HEPES buffer to pH = 7.0. The solution is then incubated at the required temperature (normally 37°C) for a specific amount of time in order to guarantee the complexation reaction. The radiochemical yield is then calculated via radio-TLC and/or radio-HPLC, and eventually a purification step is then performed, when required, in order to achieve a good radiochemical purity (Yusufi *et al.*, 2017; Mayer *et al.*, 2018; De Rose *et al.*, 2019; Russelli *et al.*, 2021).

Generally, due to its coordination number, the chelators used for the complexation of $[\text{}^{89}\text{Zr}]\text{Zr}^{4+}$ consist of siderophores, *i.e.* low-molecular-weight compounds with a high affinity towards iron(III) that results to have similar properties in terms of guest atom. Hydroxamates are the coordinating groups of these species, and thus the coordinating groups of the majority of ^{89}Zr dedicated chelators. However, other chelating systems are also available in the literature and will be described more in details as follow and partially reported in **Figure 5**.

2. METHODOLOGY

Among these ligands, deferoxamine B (DFO) has been the chelator of choice (including human trials) (Dijkers *et al.*, 2010) because of the apparent good *in vivo* stability of its complexes. However, later studies have highlighted accumulation of radiometal in bones (Abou, Ku and Smith-Jones, 2011; Zeglis and Lewis, 2015) and liver (Holland *et al.*, 2010; Abou, Ku and Smith-Jones, 2011) upon administration of ^{89}Zr -based agents. This has been mainly correlated with an instability of $[\text{}^{89}\text{Zr}]\text{Zr-DFO}$ rising from the hexa- (Patra *et al.*, 2014; Zeglis and Lewis, 2015) or heptadentate (Racow *et al.*, 2019; Holland, 2020) complex formed that does not saturate the coordination sphere of the ion. In order to overcome such problem, an elongated version of DFO, namely DFO* has been proposed showing improved radiolabelling yield as well as an increased *in vivo* stability (Patra *et al.*, 2014). Several derivatives of DFO* (**Figure 5a**) have been tested to increase the water solubility, with the OXO-DFO* turning out to be a valid improvement to the previously reported chelators (Brandt *et al.*, 2020). Recently a further development has been done by Sarbisheh and colleagues by the introduction of the so called DFO2, a new dodecadentate version of the DFO chelator that seems to improve the ^{89}Zr -complex stability and leaves the door open for possible theranostic applications (Sarbisheh *et al.*, 2020).

Poly-hydroxamates have been exploited in a number of potential ligands for $[\text{}^{89}\text{Zr}]\text{Zr}^{4+}$: for example, a series of octadentate poly-hydroxamates, either linear or cyclic were developed and investigated (Guérard, Lee and Brechbiel, 2014; Zhai *et al.*, 2015; Boros *et al.*, 2016; Rousseau *et al.*, 2017; Summer *et al.*, 2020; Klasen *et al.*, 2021; Russelli *et al.*, 2021), showing that a spacer of 7 carbon atoms between the hydroxamic moieties leads to better results in terms of stability and radiochemical yield (Guérard, Lee and Brechbiel, 2014). Noteworthy are the works based on the chelators AAZTHAG-C₅-OH (Russelli *et al.*, 2021), core of these thesis, and Hy₃ADA (Klasen *et al.*, 2021) (**Figure 5b**) developed independently, and based on the 6-amino-1,4-diazepane scaffold bearing hydroxamate pendant arms with different lengths. These promising results indicate that the combination of a rigid scaffold with more flexible pendant arms with an adequate length, and functionalized with hydroxamate groups, is indeed

2. METHODOLOGY

a good strategy. Worth of mention are also the derivatives of Fusarine C (FSC) (Zhai *et al.*, 2015) and Desferrichrome (DSC) (Adams, Wilson and Boros, 2017) that have shown promising results (**Figure 5b**), even though these species were affected by poor solubility in aqueous milieus.

Poly-hydroxypyridinones have also been used as effective chelating agents for Zr(IV) (Buchwalder *et al.*, 2017, 2019; Cusnir *et al.*, 2017): the ligand HOPO has been demonstrated to bind ^{89}Zr efficiently and under mild conditions (Deri *et al.*, 2014), similarly to CP256 (Ma *et al.*, 2015). Of particular interest are the molecular architectures of the di-macrocyclic terephthalamide ligands 1 and 2, capable to chelate zirconium-89 quickly under mild conditions, at low concentrations and with quantitative RCYs (Pandya *et al.*, 2015). Finally, several polyaminocarboxylate macrocycles have been also successfully investigated as scaffolds for ^{89}Zr -complexes including not only octadentate DOTA (Pandya *et al.*, 2017), DOTAM (Pandya *et al.*, 2017), DOTP (Pandya *et al.*, 2017) and TRITA (Pandya *et al.*, 2020) but also heptadentate PCTA (Pandya *et al.*, 2020) and even hexadentate NOTA (Pandya *et al.*, 2020). These studies leads to conclude that not only the saturation of the coordination sphere of the metal ion but also the size of the cage play an important role in the stability of the complex. The chemical structures of this last group of selected non-hydroxamate chelators for Zr(IV) are shown in **Figure 5c**.

2. METHODOLOGY

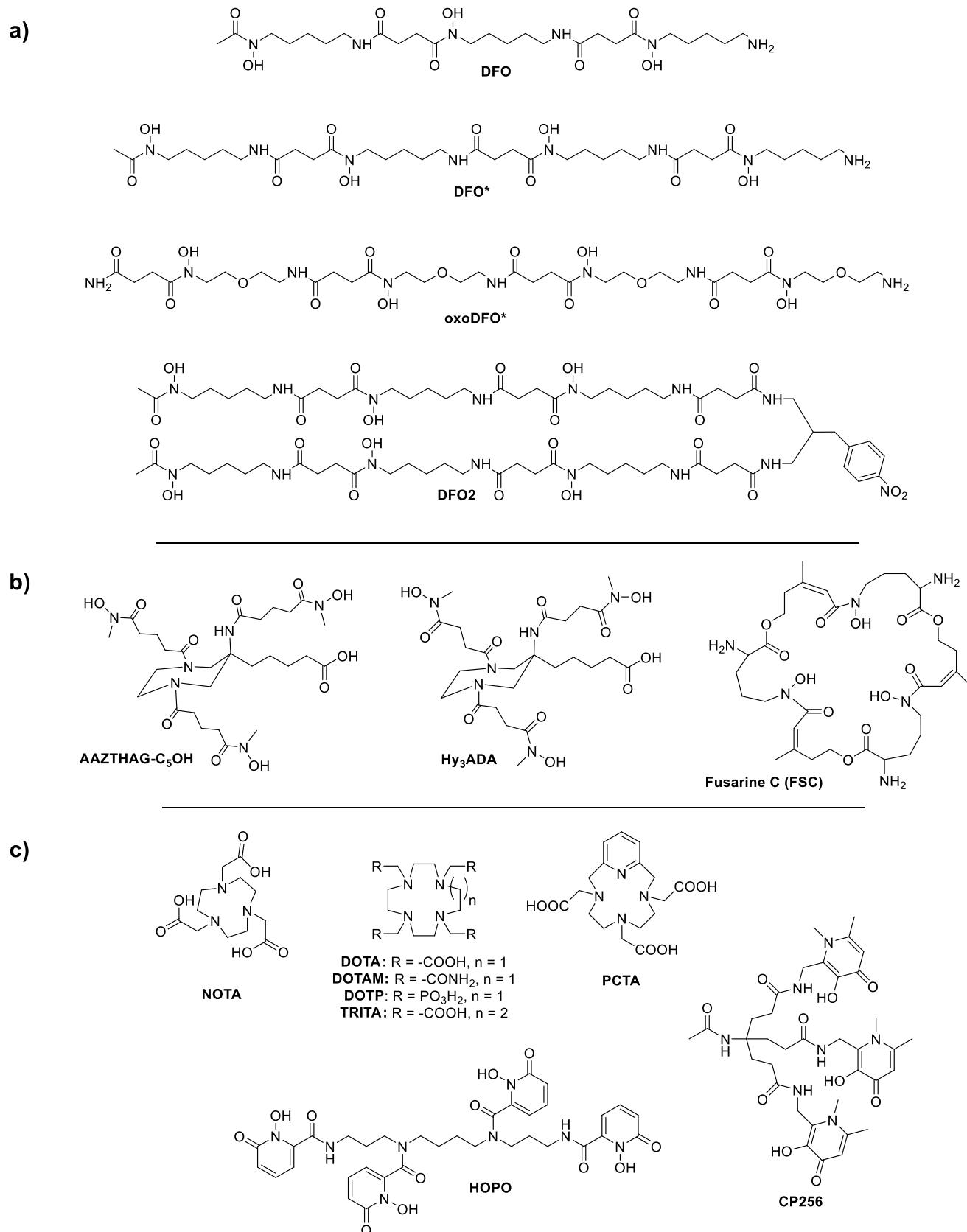


Figure 5. Structures of chelators for the complexation of ⁸⁹Zr. a) DFO and its derivatives. b) Other hydroxamate-based chelators. c) Non-hydroxamate chelators.

2.2 [¹⁸F]AIF radiochemistry

Numerous PET tracers are ¹⁸F labelled due to the main chemical and physical properties of this radioisotope. This subchapter will describe them in detail starting from the production, touching upon the standard ¹⁸F labelling methodology and reaching, finally, the alternative and promising [¹⁸F]AIF method as the second scientific paper of this thesis is based on.

2.2.1 ¹⁸F production and properties

¹⁸F is probably the most widely employed radioisotope in diagnostic nuclear medicine, since [¹⁸F]FDG is daily used as a screening tracer to recognize early stage tumors and metastasis but also to monitor the response to treatments or even to image infectious and inflammatory diseases (Almuhaideb, Papathanasiou and Bomanji, 2011; Fuccio *et al.*, 2013; Hess *et al.*, 2014; Caresia Aroztegui *et al.*, 2017). The broad application of ¹⁸F lies in the fact that this radioisotope can easily be produced in high amounts (5-10 Ci) (Vallabhajosula, 2009), on-site, with a cyclotron via the ¹⁸O(p,n)¹⁸F nuclear reaction by irradiating enriched [¹⁸O]water with 16.5 MeV protons in a niobium target. ¹⁸F decays with ~97% β⁺-emission, a maximum positron energy of 635 keV and a short range in tissues (max. 2.4 mm) (Vallabhajosula, 2009): this property, in addition to its short half-life, make it a perfect candidate for diagnostic applications, since an extended irradiation of patients can be avoided while still guaranteeing high resolution PET images acquisition. The 109.8 min half-life (t_{1/2}) makes this radioisotope suitable not only for on-site applications but also for transportation from the production site to nearby PET medical centres, thus expanding its use. From the radiochemistry point of view, the t_{1/2} is long enough to allow multistep labelling reactions leading to the development of hundreds of radiotracers, using different radiofluorination approaches (McBride *et al.*, 2009; Jacobson, Kiesewetter and Chen, 2014; Gower-Fry *et al.*, 2021). In particular, radiofluorinations are commonly performed via aliphatic and aromatic nucleophilic substitution with a radioactive ¹⁸F isotope on a chosen halides or sulfonates molecule designed to facilitate this chemical mechanism (Cole *et al.*, 2014). Since, as per chemical definition, these reactions normally happened with the aid of high temperatures and/or harsh conditions, they cannot be a valid

2. METHODOLOGY

methodology for the radiofluorination of proteins and sensitive biomolecules. For this reason starting from 2009, thanks to McBride and colleagues (McBride *et al.*, 2009) a new methodology has been tested as alternative to nucleophilic substitutions, taking advantage of the strong bond between an aluminium atom and the ^{18}F nuclide, where the aluminium is afterward complexed by a proper chelator. When the chelator NOTA (2,2',2''-(1,4,7-triazacyclononane-1,4,7-triyl)triacetic acid) is used, the main limit of this reaction is represented by the need of high temperature, and indeed the second work reported in this thesis was meant to present an approach directed to overcome this limitation by introducing new chelators that offer good performances even at lower temperature. Both the two radiofluorination approaches are explained in further details in the following pages.

2.2.2 ^{18}F labelling via prosthetic group

Since the half-life of ^{18}F is long enough to allow multistep labelling reactions but also short enough to avoid extended irradiation of patients, in the last decades several radiotracers based on ^{18}F have been developed (Campbell *et al.*, 2017). Fluorine-18 incorporation into large biomolecules can be achieved by either a direct or an indirect labelling approach. Typically, the direct preparation of ^{18}F -labelled radiotracers involved the attachment of ^{18}F to a carbon in the organic structure of the radiotracer, often requiring a basic pH and high temperatures. Although there are example of direct fluorine-18 labelling of peptides, proteins labelling is typically performed using indirect radiolabelling methods (Höhne *et al.*, 2008; Mu *et al.*, 2008; Becaud *et al.*, 2009). In this approach, a small molecule containing a suitable functional group is radiolabelled by conventional nucleophilic substitution chemistry using [^{18}F] fluorine, and only successively conjugated in soft conditions to the protein of interest. This approach is clearly limited to the use of bifunctional moieties that can guarantee a fast conjugation to the proteins in order to save time and hence, increase the final RCY of the tracer. The most widely used prosthetic groups are the N-succinimidyl-4- [^{18}F]fluorobenzoate ([^{18}F]SFB) for the conjugation with amine functionalities (Wüst *et al.*, 2003; Vaidyanathan and Zalutsky, 2006; Li *et al.*, 2008; Vaidyanathan *et al.*, 2016), and ^{18}F -N-[2](4-Fluorobenzamido)

2. METHODOLOGY

ethyl]-maleimide ($[^{18}\text{F}]\text{FBEM}$) for conjugation to thiols on cysteine residues (Gao *et al.*, 2011; Kiesewetter *et al.*, 2011; Wang *et al.*, 2012). An innovative method to perform room temperature ^{18}F -fluorinations is based on isotopic exchange (IE) of ^{19}F with ^{18}F on organosilicon-based fluoride acceptor (SiFA) (Bernard-Gauthier *et al.*, 2014) but since the use of organic solvents and basic pH values is still involved, this approach cannot be used for the direct labelling of antibody-based molecules. However, while each of these methods has certain advantages, the long procedure time and relatively harsh conditions used (pH, organic solvents, reaction temperature) have limited their applications for clinical purposes. Therefore, the requirement of faster and direct labelling methods of proteins boosted the research of new strategies based on the fluoride anion complexation/coordination chemistry and thus, the formation of an ^{18}F -group-13 element bond, *i.e.* boron, aluminium and gallium (Chansaenpak, Vabre and Gabbai, 2016).

2.2.3 $[^{18}\text{F}]\text{AlF}$ labelling via complexation

The $[^{18}\text{F}][\text{AlF}]^{2+}$ species combines the radiochemical properties of the broadly used radionuclide fluorine-18 and the ionic nature of Al^{3+} , introducing the possibility to perform coordination chemistry reactions with this very important positron emitter that, as already mentioned, until a decade ago could only be introduced in molecules via covalent bond through substitutions reactions. In fact, the aluminium-fluoride bond is stronger than 60 other metal-fluoride bonds (e.g. $\text{Al-F} > \text{Ga-F}, \text{Sc-F}, \text{Si-F}$) (bond energy of 670 kJ/mol) (Martin, 1996), and it is very stable *in vivo*, making small amounts of aluminium fluoride chelate compatible with biological systems (Li Liang, 2003).

This two steps labelling methodology sees the formation of the aluminium fluoride as first step, starting from a reaction between a solution of AlCl_3 in the presence of a solution of $[^{18}\text{F}]\text{F}^-$ at pH 4-5. The pH condition is a crucial factor. It is important to control the acidity of the reaction environment, in order to avoid the formation of different species, e.g. insoluble aluminium hydroxide (Bruce Martin, 1988; McBride, Sharkey and Goldenberg, 2013) that cannot otherwise be complexed by the appropriate chelator in the next step. The chelation can be

2. METHODOLOGY

then carried out by just adding a suitable ligand, usually leading to a thermodynamically and kinetically stable complex (Smith *et al.*, 2011; Farkas *et al.*, 2015) ideally with good radiochemical yields, in a short time-lapse, at low temperature and in general mild conditions. Due to the fact that aluminium(III) forms octahedral complexes but one position is already occupied by the fluoride atom, an optimal chelator should preferably be pentadentate. As shown in **Figure 6**, good examples of suitable chelators are the NOTA and NODAGA ligands that allow a strong coordination of the Al ion (McBride *et al.*, 2009; Da Pieve *et al.*, 2020). On the other hand, the third carboxylate pendant arm tends to displace the fluoride, thus lowering the radiochemical yields (D'Souza *et al.*, 2011; Shetty *et al.*, 2011). NODA has proven successful for a stable chelation but the high temperatures and low pH required to achieve a satisfying RCY can be problematic in the presence of a conjugated targeting vector such as a polypeptide, an antibody or a protein (Da Pieve *et al.*, 2016). This driven the researchers in the field to look for possible alternatives. A complete and detailed review published by Archibald and Allott summarizes all the efficient chelators developed so far for the complexation of [¹⁸F]aluminium-fluoride including their main properties (Archibald and Allott, 2021). Cleeren *et al.* designed and synthesised a group of new acyclic ligands (Cleeren *et al.*, 2016, 2017) among which a rigid CD3A-derivative (named RESCA and now commercially available) can complex [¹⁸F][AlF]²⁺ at room temperature, and whose resulting product is more stable *in vivo* than the respective one for the NODA chelator. In this new class of ligands, the cage resulted to be significantly different compared to the NOTA and NODA-derivative and furthermore phenolic groups are introduced to give better performances. A further improvement has been recently obtained by using 2-aminomethylpiperidine derivatives functionalized with carboxylate or mixed carboxylate/hydroxybenzyl pendant arms (Martinelli *et al.*, 2021). In particular, the [¹⁸F]AlF-AMPDA-HB complex can be prepared at room temperature and with good radiochemical yield in a broad range of pH values (even at physiological conditions), and it turns out to be more stable *in vivo* than the reported CD3A-derivatives (Russelli *et al.*, 2020). As showed in the "Summary and Outlooks" chapter

2. METHODOLOGY

(unpublished data) the chelator turned out to be a good candidate not only to radiolabel heat sensitive protein derivatives, but also for the labelling of small peptides such as, for example, the tumor cell-penetration peptide (TPP) used to image the Hsp70 protein (Stangl *et al.*, 2018).

Figure 6 shows the chemical structures of the most relevant chelators for $[^{18}\text{F}][\text{AlF}]^{2+}$ available in literature so far.

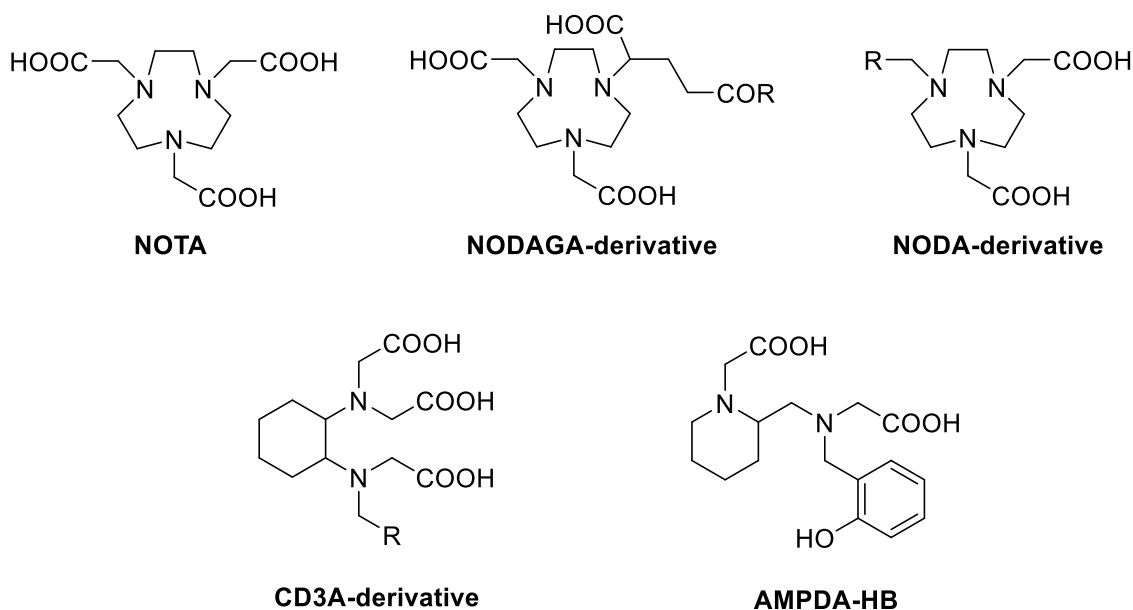


Figure 6. Structures of main chelators for the complexation of $[^{18}\text{F}][\text{AlF}]^{2+}$.

3 OBJECTIVES

In nuclear medicine, and in particular in PET diagnostics, the exploitation of biological protein-ligand complexes can be an excellent solution to satisfy the need of more personalized tracers to detect early stage tumors or meticulously follow up the efficiency of a cancer therapy. Indeed, even though [^{18}F]FDG remains the most routinely used PET radiopharmaceutical, the literature concerning new protein-based tracers is increasing exponentially in the past decades. This is due to the fact that biological processes are extremely specific, giving for one selected protein a precise target in the human body. Once the target identifying a particular biological process connected to a tumor, an inflammatory process or other diseases is selected, different tracers can be developed to specifically visualize that target *in vivo*. The following step then, will be the selection of the most suitable protein within a broad range of biomolecules that would be suitable for a potential future clinical translation. Of course, in order to finalize the development of a new immunoPET tracer, the selection of the right radioisotope plays a fundamental role, with its half-life being the appropriate one to match the tracer blood half-life and to allow the *in vivo* visualization of the target. The last but not less important piece of the puzzle would then be the choice of an effective radiolabelling methodology that can lead to a successful iPET tracer development.

The aim of this doctorate thesis was to find alternative and innovative solutions to labelled newly selected proteins using novel chelators for the complexation of appropriate radioisotopes. In order to do this, the focus was mainly on ^{89}Zr and ^{18}F nuclides. Concerning the ^{89}Zr complexation, a new chelator was developed to increase the stability *in vivo* and to provide a possible good alternative to the gold standard, but still not impeccable, DFO chelator. Secondary, the labelling of ^{18}F was actually made by using a very innovative approach, the [^{18}F]AIF methodology, based on the complexation of the aluminium atom of the [^{18}F]AIF species. This approach might expand the labelling of temperature sensitive proteins with ^{18}F , limited until now due to the harsh conditions of traditional radiofluorination methodologies, and opening the doors for higher resolution images due to the use of ^{18}F and

3. OBJECTIVES

very specific protein-based tracers for imaging of specific biological processes *in vivo*. As a proof-of-concept different kind of proteins were also tested for the validation of the two novel chelators, generating a bunch of new radiopharmaceuticals that, after a further optimization and study, could potentially be translated into clinical application in the incoming years.

4 RESULTS

Below are reported the two publications relevant for this thesis. A graphical abstract is included for each publication followed by a brief summary of the paper. More information can be found in the original version of the papers (see **Appendix I** and **II**).

4.1 A Semi Rigid Novel Hydroxamate AMPED-Based Ligand for ^{89}Zr PET Imaging

Russelli L*, De Rose F, Leone L, Reder S, Schwaiger M, D'Alessandria C, Tei L.. *Molecules*. 2021 Sep 25;26(19):5819. doi: 10.3390/molecules26195819. PMID: 34641362; PMCID: PMC8512011.

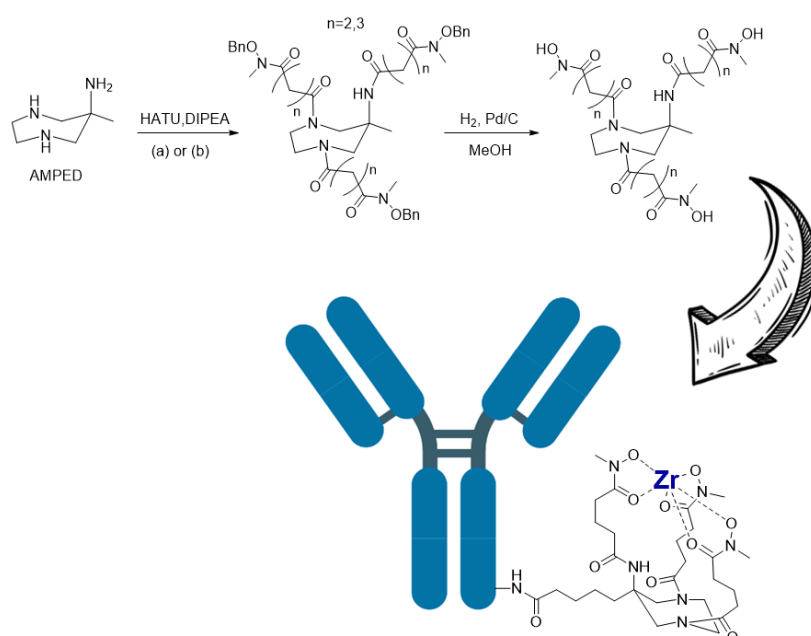


Figure 7. Graphical abstract of “A Semi Rigid Novel Hydroxamate AMPED-Based Ligand for ^{89}Zr PET Imaging”. The image briefly shows the synthetic route leading to the chelators AAZTHAS and AAZTHAG from which the functionalized AAZTHAG chelator was then synthesised, conjugated to an antibody and labelled successfully with ^{89}Zr . (a) 5-((benzyloxy)(methyl)amino)-2,5-dioxopentanoic acid ($n = 2$), (b) 6-((benzyloxy)(methyl)amino)-2,6-dioxohexanoic acid ($n = 3$).

In this paper a new chelator and its bifunctional derivative for ^{89}Zr labelling and PET-imaging were designed, synthesized, characterized, and investigated. The project started with a preliminary study where we synthesized two hexadentate chelators named AAZTHAS and AAZTHAG, based on the seven-membered heterocycle AMPED (6-amino-6-methylperhydro-

4. RESULTS

1,4-diazepine) aiming to increase the rigidity of the ^{89}Zr -complex by using N-methyl-N-(hydroxy)succinamide or N-methyl-N-(hydroxy)glutaramide pendant arms attached to the cyclic structure. N-methylhydroxamate groups are the donor groups chosen to coordinate efficiently ^{89}Zr . Both the two chelators were labelled with ^{89}Zr as explained before in Methodology (paragraph 2.1 - ^{89}Zr radiochemistry) and after *in vitro* stability tests, the best among the two was selected to continue the study. The chelator AAZTHAG, with longer arms, resulted to be the best complexing agent for ^{89}Zr presenting a stability of $86.4 \pm 5.5\%$ in human serum (HS) for at least 72 h. In order to investigate the stability and biodistribution of the resulted ^{89}Zr -complex *in vivo*, small animal PET/CT static scans were acquired at different time points post injection (up to 24 h). *Ex vivo* organ distribution studies were then carried out in healthy nude mice ($n = 3$): mice were sacrificed at the end of the 24h time point scan and selected organs were taken and the activity was measured with a γ -counter. High stability *in vivo*, with low accumulation of free ^{89}Zr in bones and kidneys, was measured. Therefore, this promising results was followed by the synthesis of an activated ester functionalized version of AAZTHAG to allow the conjugation with biomolecules such as antibodies. As a proof-of-concept, the bifunctional chelator was then conjugated to the human anti-HER2 monoclonal antibody Trastuzumab (Tz). Finally, the conjugated product was labelled using an already standardized protocol used in our group, and the resulted ^{89}Zr -labelled compound was characterized via radio-HPLC and SDS-PAGE followed by autoradiography. Moreover, further *in vitro* stability tests were performed incubating the product in different solutions to assess its integrity for at least 4 days.

Overall, L.R. was responsible for all the methodology, data analysis and paper writing. More in particular, L.R. carried out all the synthesis and characterisation of the three chelators mentioned in the paper with the support and supervision of L.L.. The conjugation reaction together with all the labelling reactions and *in vitro* experiments were performed as well by L.R. with the help and supervision of F.D.R.. The *in vivo* experiments were executed by L.R. together with the support of S.R..

4.2 Room Temperature Al¹⁸F Labeling of 2-Aminomethylpiperidine-Based Chelators for PET Imaging

Russelli L*, Martinelli J*, De Rose F, Reder S, Herz M, Schwaiger M, Weber W, Tei L, D'Alessandria C.. *ChemMedChem*. 2020 Feb 5;15(3):284-292. doi: 10.1002/cmdc.201900652. Epub 2020 Jan 7. PMID: 31830368.

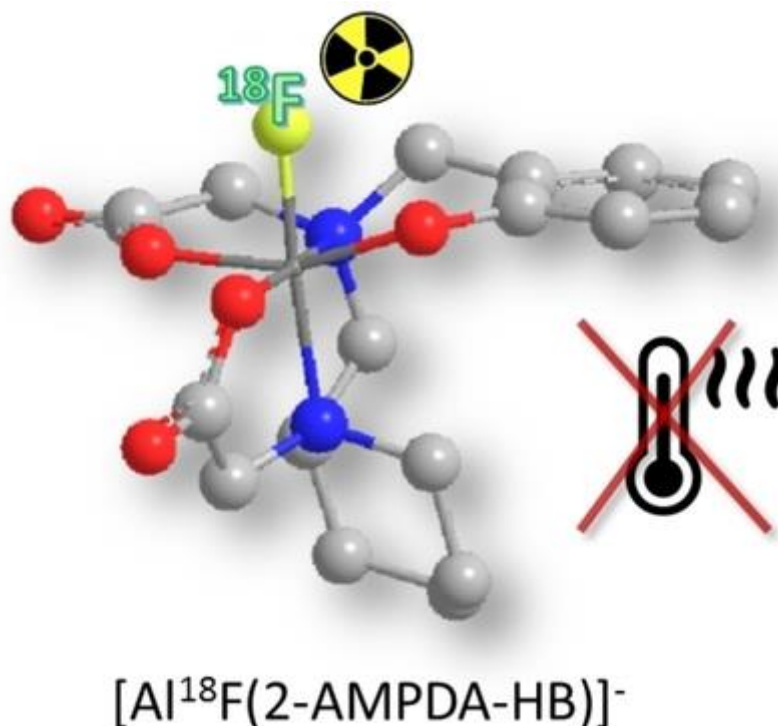


Figure 8. Graphical abstract of “Room Temperature Al¹⁸F Labeling of 2-Aminomethylpiperidine-Based Chelators for PET Imaging”. The picture represents a simulated 3D structure of the compound $[Al^{18}F(2-AMPDA-HB)]^-$ after a radiofluorination reaction conducted at room temperature. The aluminium atom is bonded to the ¹⁸F and is also coordinated by the pending arms of the chelator as well as nitrogen atoms of the main structure.

Positron emission tomography (PET) is a non-invasive molecular imaging technology that is constantly expanding, with a high demand for specific antibody-derived imaging probes. The use of tracers based on temperature-sensitive molecules (i. e. Fab, svFc, nanobodies) is increasing and with it the demand for new methodologies for their labelling in mild condition and low temperature (Cleeren *et al.*, 2018). This led us designing a class of new chelators based on the structure of 2-aminomethylpiperidine (AMP) with acetic and/or hydroxybenzyl pendant arms named 2-AMPTA, NHB-2-AMPDA and 2-AMPDA-HB, which were investigated as such for $[^{18}F][AlF]^{2+}$ -core chelation efficiency. The $[^{18}F]AlF$ methodology as explain above

4. RESULTS

(paragraph 2.2 – [^{18}F]AIF radiochemistry) is an easy and simply alternative to the standard nucleophilic substitutions used to directly radiofluorinate biomolecules (McBride *et al.*, 2009). All the three chelators were characterized by HPLC-MS analysis and NMR spectroscopy as well as their cold counterpart. In this work, the labelling procedure was first optimized based on previous published protocols (Cleeren *et al.*, 2016) and then the [^{18}F]AIF labelling reactions were performed with all the three compounds under various conditions (pH/temperature/time). The radiolabelled chelates were purified via simple cartridge purification, to obtain a high radiochemical purity complexes, and the resulted pure compounds were then characterized by radio-TLC and radio-HPLC. The stability of labelled chelates was investigated up to 240 min in human serum (HS), EDTA 5mM, PBS and 0.9% NaCl solutions. Among the three compounds one of them gave superior results, and its good *in vitro* stability led us to asses also the *in vivo* stability of [$\text{Al}^{18}\text{F}(2\text{-AMPDA-HB})^-$] in healthy nude mice (n=6). Overall, radiochemical yields between 55% and 81% were obtained at pH 5 and room temperature. High stability in HS was measured for [$\text{Al}^{18}\text{F}(2\text{-AMPDA-HB})^-$], with 90% of ^{18}F complexed after 120 min. High stability *in vivo*, rapid hepatobiliary and renal excretion, with low accumulation of free ^{18}F in bones were measured. Thus, this new ^{18}F [AIF]-chelator may have a great impact on immuno-PET radiopharmacy, by facilitating the development of new fluorine-18-labelled heat-sensitive biomolecules.

The paper is a first shared author between L.R. and J.M.. Overall, J.M. was responsible for all the organic synthesis and cold compounds characterization while L.R. performed the labelling reactions and all the subsequent experiments inherent the ^{18}F -labelled compounds. The *in vivo* experiments were accomplished by L.R. together with the help of S.R.. L.R. and J.M. worked on the data analysis and paper writing.

5 SUMMARY AND OUTLOOKS

The labelling of target-specific molecules in order to develop new and always more specific PET tracers plays a fundamental role that can have a huge impact on the ultimate physician reading of the PET scans. Organic and radio chemistry are the sciences focused on the design of new PET tracer, and they get an even more central role when the tracer is protein-based, since a mandatory requirement is that all the reactions are conducted in mild conditions in order to keep the protein intact and its functionalities unaltered. Based on the structure of a PET tracer, the research in this field can be, for example, focused on the development of new labelling techniques (Sarbisheh *et al.*, 2020; Archibald and Allott, 2021; Chomet, Van Dongen and Vugts, 2021; Feiner *et al.*, 2021; Sneddon and Cornelissen, 2021) or on the study of new ligands for the targeting of naïve receptors (Yusufi *et al.*, 2017; Mayer *et al.*, 2018; De Rose *et al.*, 2019; Varasteh *et al.*, 2021; Quigley *et al.*, 2022). The necessity to rethink the labelling approach by designing and developing new labelling strategies, that can fit with the bio-ligand of choice, was the strong motivation that lead to the publication of the works discussed in these thesis.

5.1 A Semi Rigid Novel Hydroxamate AMPED-Based Ligand for ^{89}Zr PET Imaging

New ligands for ^{89}Zr for iPET imaging were conceptually designed, synthesised, and characterized, in particular, two non-functionalized chelators (AAZTHAS and AAZTHAG) and one functionalized (AAZTHAG- $\text{C}_5\text{-OH}$) for conjugation to biomolecules. In a preliminary study conducted on AAZTHAS and AAZTHAG the labelling capabilities of the two chelators were investigated as well as the stability *in vitro* of the resulting ^{89}Zr -complexes. More precisely, the influence of the length of the pendant arms was investigated showing that a longer arm can retain more firmly the metal ion in the host cage. This results were surprisingly confirmed by another paper published in parallel to ours, where a functionalized version of what it's here called AAZTHAS was synthesised and studied (Klasen *et al.*, 2021). The AAZTHAG chelator

5. SUMMARY AND OUTLOOKS

showed indeed best performances, and therefore the stability of the resulting [⁸⁹Zr]Zr-AAZTHAG complex was validated *in vivo* and its biodistribution studied in healthy athymic nude mice, showing low accumulation in bones and in significant organs.

The functionalized chelator called AAZTHAG-C₅-OH, was successively synthesized based on the structure of the AAZTHAG chelator and, as proof-of-concept, it was subsequently conjugated to the mAb Trastuzumab targeting the HER2 receptor. The conjugation reaction protocol was optimized with the aim to increase both reaction and labelling yield, preserving the integrity of the protein by avoiding strong reaction conditions. Labelling tests were then carried out and the stability *in vitro* assessed showing promising results. In the near future *in vivo* experiments in mice bearing breast cancer cells HER2⁺ should be performed in order to evaluate the unchanged binding capability of the mAb towards this specific target and the stability and biodistribution of the tracer. PET images would also be acquired at different time points to select the best time window that gives the higher tumour uptake of the tracer and permit a clear visualisation of the malignancy.

Moreover, future work can be directed towards two main lines: 1) the conjugation reaction to the biomolecule might be facilitated by modifying the functional group of AAZTHAG-C₅-OH from a carboxylic acid (-COOH) to an isothiocyanate group (-NCS). The introduction of this functional group could reduce the time of the conjugation step and would be a valid alternative for the conjugation of chelators to mAbs (Perk *et al.*, 2010)(Mendler *et al.*, 2015)(Price and Orvig, 2014). 2) Another modification that could be applied to the ligand is the introduction of a fourth pendant arm leading to an octadentate version of the AAZTHAG chelator that could be, together with the use of the cyclic diazepine core, the key step to produce a highly stable complex (Patra *et al.*, 2014). For this purpose, a new synthetic strategy must be planned.

5.2 Room Temperature Al¹⁸F Labeling of 2-Aminomethylpiperidine-Based Chelators for PET Imaging

Here a series of chelator for the complexation of [¹⁸F]AlF at room temperature was designed and synthesised. The products were deeply characterized as well as their resulting “hot” and “cold” complexes. All the chelators where firstly characterized via HPLC-MS and NMR, then cold complexes with [¹⁹F]AlF were also characterized with the same modalities. The labelling reactions with [¹⁸F]AlF were performed and optimized as well as the purification step that led to pure compounds with high RCP (>99%). Following *in vitro* and *in vivo* stability tests in nude mice permitted the selection of one chelator, among the others, presenting better performances in terms of radiochemical yields and *in vitro* stability. The next step was the development of two functionalised versions of the selected chelator, so called 2-AMPDA-HB, in order to allow the conjugation of the chelator to any kind of vector needed and, in particular to heat-sensitive molecules. As a proof-of concept, the chelator was conjugated to three different constructs: an antibody fragment F(ab') from a rat monoclonal antibody anti-Galectin-3 (produced by enzymatic digestion of the full-size mAb), a nanobody targeting the CD2 receptor and a peptide commercially available (unpublished data). More precisely, an N-hydroxysuccinimide ester (-NHS ester) and a malimide (-mal) derivatives were synthesised and characterized by HPLC-MS and NMR at the University of Piemonte Orientale by Prof. Lorenzo Tei and Dr. Jonathan Martinelli.

The 2-AMPDA-HB-NHS derivate was then handed over to the Nuclear Medicine Department of the Klinikum Rechts der Isar were the conjugation to the antiCD2-sdAb (and a non-targeting control sdAb, R3B23, which targets 5T2 multiple myeloma (MM) cell-produced M-protein) and the Fab fragment via amide bond to lysine residues was performed.

Next, the 2-AMPDA-HB-mal derivate was further conjugated to a tumor cell-penetration peptide (TPP) (Stangl *et al.*, 2018) via a cysteine residue. The product was then purified by preparative HPLC, characterized and transferred to our department for radiofluorinations and preliminary experiments.

5. SUMMARY AND OUTLOOKS

All the radioactive and non-radioactive products were characterized by several techniques such as SDS-page with or without autoradiography, HPLC and/or radio-HPLC, radio-TLC, MS (for the sdAb compounds). The labelling reactions with $[^{18}\text{F}]\text{AIF}$ were optimized and standardized giving a RCY up to 50% for the nanobody-based products, up to 28% for the Fab-based one and 22% for the peptide tracer. After the stability of the compounds was assessed *in vitro*, preliminary studies in mice models bearing different tumours expressing specific receptors accordingly to the tracers used were performed. More in detail, mice bearing Jurkat tumor cells expressing the CD2 receptor where used to test the $[^{18}\text{F}]\text{AIF-2-AMPDA-HB-antiCD2-sdAb}$ (**Figure 9a**) and mice bearing 4T1 breast cancer cells expressing Hsp70, the target of $[^{18}\text{F}]\text{AIF-2-AMPDA-HB-TPP}$ (**Figure 9b**) were used.

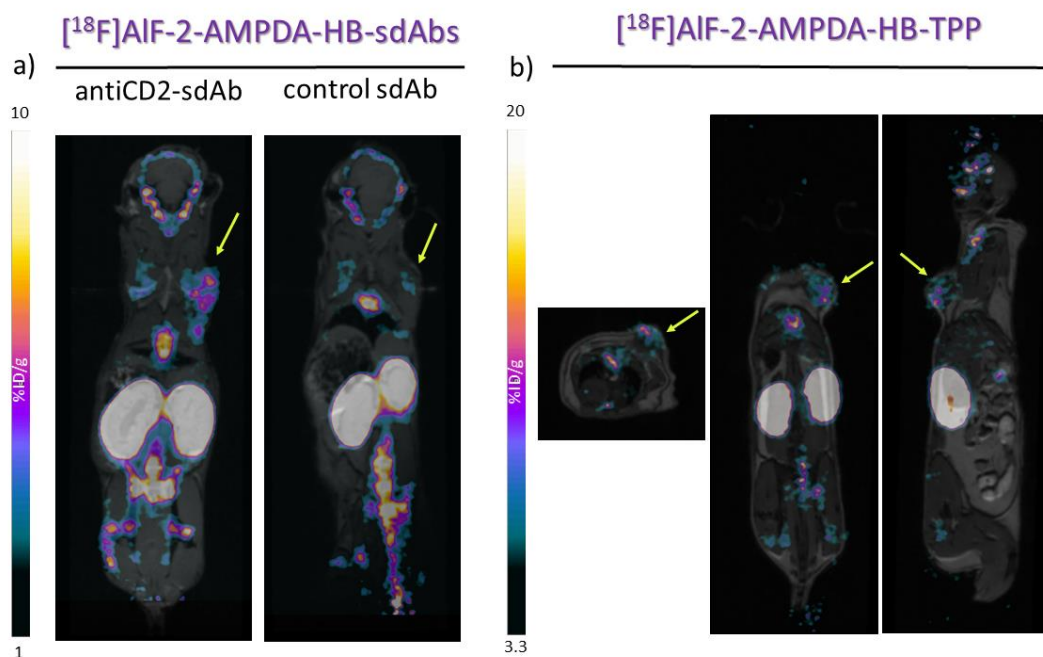


Figure 9. Animals PET-MR images. First proof-of-concept *in vivo* PET-MR imaging of a) $[^{18}\text{F}]\text{AIF-2-AMPDA-HB-sdAbs}$ and b) $[^{18}\text{F}]\text{AIF-2-AMPDA-HB-TPP}$ showing a good stability *in vivo* of the functionalized version of the studied chelator 2-AMPDA-HB. The scale is expressed as %ID/g.

The preliminary results show a good behaviour of the functionalized chelator *in vivo* with a good accumulation in the tumour area and slow or absent accumulation in relevant organs

5. SUMMARY AND OUTLOOKS

compared to similar chelators, such as the gold standard NOTA chelator (Hu *et al.*, 2022) and the recently developed RESCA chelator (Cleeren *et al.*, 2017). More *in vivo* experiments should be performed to confirm the promising preliminary data and to test the tracer [¹⁸F]AIF-2-AMPDA-HB-antiGal3-F(ab') on mice bearing thyroid cancer cells expressing Galectin-3 (e.g. FRO82-1) (De Rose *et al.*, 2019). In addition, future projects also include the synthesis of a specific functionalized version of the chelator to perform e.g. click chemistry reaction *in vivo*, application that would be one of the many possible uses of the 2-AMPDA-HB chelator.

6 REPRINT PERMISSIONS








All manuscripts were reproduced by permission of the corresponding journals. The detailed bibliographic data of the respective articles can be found in **Chapter 4: Results**. Original publications can be found in **Chapter 11: Appendix**.

6.1 Publication on “Molecules” journal

Russelli L*, De Rose F, Leone L, Reder S, Schwaiger M, D'Alessandria C, Tei L. A Semi Rigid Novel Hydroxamate AMPED-Based Ligand for ^{89}Zr PET Imaging. *Molecules*. 2021 Sep 25;26(19):5819. doi: 10.3390/molecules26195819. PMID: 34641362; PMCID: PMC8512011.

Open Access Article

A Semi Rigid Novel Hydroxamate AMPED-Based Ligand for ^{89}Zr PET Imaging

by  Lisa Russelli ¹ ,  Francesco De Rose ¹ ,  Loredana Leone ² ,  Sybille Reder ¹ ,
 Markus Schwaiger ¹ ,  Calogero D'Alessandria ^{1,*†}  and  Lorenzo Tei ^{2,*†} 

¹ Department of Nuclear Medicine, Klinikum Rechts der Isar TU München, Ismaningerstraße 22, 81675 Munich, Germany

² Department of Science and Technological Innovation, Università del Piemonte Orientale, Viale T. Michel 11, 15121 Alessandria, Italy

* Authors to whom correspondence should be addressed.

† Join senior authors.

Academic Editors: António Paulo, Filipa Fernandes Mendes and João D. G. Correia

Molecules **2021**, *26*(19), 5819; <https://doi.org/10.3390/molecules26195819>

Received: 30 July 2021 / Revised: 16 September 2021 / Accepted: 20 September 2021 / Published: 25 September 2021

(This article belongs to the Special Issue *New Advances in Radiopharmaceutical Sciences: Chemistry and Applications*)

[View Full-Text](#)

[Download PDF](#)

[Browse Figures](#)


[Citation Export](#)

Abstract

In this work, we designed, developed, characterized, and investigated a new chelator and its bifunctional derivative for ^{89}Zr labeling and PET-imaging. In a preliminary study, we synthesized two hexadentate chelators named AAZTHAS and AAZTHAG, based on the seven-membered heterocycle AMPED (6-amino-6-methylperhydro-1,4-diazepine) with the aim to increase the rigidity of the ^{89}Zr complex by using *N*-methyl-*N*-(hydroxy)succinamide or *N*-methyl-*N*-(hydroxy)glutaramide pendant arms attached to the cyclic structure. *N*-methylhydroxamate groups are the donor groups chosen to efficiently coordinate ^{89}Zr . After in vitro stability tests, we selected the chelator with longer arms, AAZTHAG, as the best complexing agent for ^{89}Zr presenting a stability of $86.4 \pm 5.5\%$ in human serum (HS) for at least 72 h. Small animal PET/CT static scans acquired at different time points (up to 24 h) and ex vivo organ distribution studies were then carried out in healthy nude mice ($n = 3$) to investigate the stability and biodistribution in vivo of this new ^{89}Zr -based complex. High stability in vivo, with low accumulation of free ^{89}Zr in bones and kidneys, was measured. Furthermore, an activated ester functionalized version of AAZTHAG was synthesized to allow the conjugation with biomolecules such as antibodies. The bifunctional chelator was then conjugated to the human anti-HER2 monoclonal antibody Trastuzumab (Tz) as a proof of principle test of conjugation to biologically active molecules. The final ^{89}Zr labeled compound was characterized via radio-HPLC and SDS-PAGE followed by autoradiography, and its stability in different solutions was assessed for at least 4 days. [View Full-Text](#)

Keywords: zirconium-89; polydentate chelators; hydroxamates; PET-imaging; labeling

[► Show Figures](#)

 This is an open access article distributed under the [Creative Commons Attribution License](#) which permits unrestricted use, distribution, and reproduction in any medium, provided the original work is properly cited

6.2 Publication on “ChemMedChem” journal

Russelli L*, Martinelli J*, De Rose F, Reder S, Herz M, Schwaiger M, Weber W, Tei L, D'Alessandria C. Room Temperature Al¹⁸F Labeling of 2-Aminomethylpiperidine-Based Chelators for PET Imaging. ChemMedChem. 2020 Feb 5;15(3):284-292. doi: 10.1002/cmdc.201900652. Epub 2020 Jan 7. PMID: 31830368.

JOHN WILEY AND SONS LICENSE
TERMS AND CONDITIONS
Jul 18, 2022

This Agreement between Ms. Lisa Russelli ("You") and John Wiley and Sons ("John Wiley and Sons") consists of your license details and the terms and conditions provided by John Wiley and Sons and Copyright Clearance Center.

License Number	5351870273514
License date	Jul 18, 2022
Licensed Content Publisher	John Wiley and Sons
Licensed Content Publication	ChemMedChem
Licensed Content Title	Room Temperature Al ¹⁸ F Labeling of 2-Aminomethylpiperidine-Based Chelators for PET Imaging
Licensed Content Author	Calogero D'Alessandria, Lorenzo Tei, Wolfgang Weber, et al
Licensed Content Date	Jan 7, 2020
Licensed Content Volume	15
Licensed Content Issue	3
Licensed Content Pages	9
Type of use	Dissertation/Thesis
Requestor type	Author of this Wiley article
Format	Print and electronic
Portion	Full article
Will you be translating?	No
Title	Development of innovative chelators for the synthesis of ⁸⁹ Zr and [¹⁸ F]AIF protein-based PET tracers.
Institution name	Klinikum rechts der Isar der TUM
Expected presentation date	Jul 2022
Requestor Location	Ms. Lisa Russelli Ismaningerstrasse 22 Nuklearmedizin Munich, Bayern 81675 Germany Attn: Lisa Russelli
Publisher Tax ID	EU826007151
Total	0.00 EUR
Terms and Conditions	

7 ABBREVIATIONS

Ab	Antibody
CD	Cluster of differentiation
CT	Computer tomography
Da	Dalton
DFO	Deferoxamine B
EC	Electron capture
EDTA	Ethylenediaminetetraacetic acid
Fab	Fragment antigen-binding
[¹⁸ F]FDG	¹⁸ F-Fluorodeoxyglucose
GMP	Good manufacturing practice
HEPES	2-[4-(2-hydroxyethyl)piperazin-1-yl]ethanesulfonic acid
HPLC	High performance liquid chromatography
HS	Human serum
IE	Isotopic exchange
iPET	immunoPET
mAb	Monoclonal antibody
MeV	Megaelectronvolt
MRI	Magnetic resonance imaging
MS	Mass spectrometry
Nb	Nanobody
NMR	Nuclear magnetic resonance
NODA	1,4,7-triazacyclononane-diacetic acid
NOTA	1,4,7-triazacyclononane-triacetic acid

7. ABBREVIATIONS

p.i.	Post injection
PBS	Phosphate-buffered saline
PAS	Pro, Ala and Ser polypeptide chain
PEG	Polyethylene glycol
PET	Positron imaging tomography
RCP	Radiochemical purity
RCY	Radiochemical yield
RESCA	Restrained complexing agent
ROI	Region of interest
sdAb	Single domain antibody
SDS page	Sodium dodecyl sulphate - Polyacrylamide gel electrophoresis
SPECT	Single-photon emission computed tomography
SUV	Standardize uptake value
TLC	Thin layer chromatography
TPP	Tumor cell-penetration peptide
Tz	Trastuzumab
%ID/g	Percent of injected dose per gram

8 LIST OF PUBLICATIONS

- Gosmann D*, **Russelli L***, Weber WA, Schwaiger M, Krackhardt AM, D'Alessandria C. Promise and challenges of clinical non-invasive T-cell tracking in the era of cancer immunotherapy. *EJNMMI Res.* 2022 Jan 31;12(1):5.
- **Russelli L***, De Rose F, Leone L, Reder S, Schwaiger M, D'Alessandria C, Tei L. A Semi Rigid Novel Hydroxamate AMPED-Based Ligand for ⁸⁹Zr PET Imaging. *Molecules.* 2021 Sep 25;26(19):5819.
- **Russelli L***, Martinelli J*, De Rose F, Reder S, Herz M, Schwaiger M, Weber W, Tei L, D'Alessandria C. Room Temperature Al¹⁸F Labeling of 2-Aminomethylpiperidine-Based Chelators for PET Imaging. *ChemMedChem.* 2020 Feb 5;15(3):284-292.
- Mayer KE, Mall S, Yusufi N, Gosmann D, Steiger K, **Russelli L**, Bianchi HO, Audehm S, Wagner R, Bräunlein E, Stelzl A, Bassermann F, Weichert W, Weber W, Schwaiger M, D'Alessandria C, Krackhardt AM. T-cell functionality testing is highly relevant to developing novel immuno-tracers monitoring T cells in the context of immunotherapies and revealed CD7 as an attractive target. *Theranostics.* 2018 Nov 28;8(21):6070-6087.

9 ACKNOWLEDGEMENTS

The past four years gave me the possibility to grow immensely as scientist and researcher. For this, I want to thank Prof. Dr. Wolfgang Weber for being my first supervisor and giving me the opportunity to pursue my doctorate at the Department of Nuclear Medicine. My sincere gratitude goes to my mentor, Dr. Calogero D'Alessandria, that supported me since I was a master student and gave me the chance to conduce a high level research during my PhD within the SFB824 network. Thank you for the patient, guidance and all the opportunities I've got in the past 5 years in your lab. Furthermore, I would like to thank Prof. Dr. Gabriele Multhoff for being my second advisor and support my project with a stimulating collaboration.

Lots of gratitude goes to Prof. Dr. Angela Krackhardt and Dario Gosmann for all the immunological knowledge I was able to learn from them. It has been a pleasure to collaborate within the C10 SFB824 project until now. Looking forward to what the future will bring us!

I am glad to have got the chance to continue working together with Prof. Lorenzo Tei and Dr. Jonathan Martinelli whom I want to thank for the close and successful collaboration.

I would like to thank Dr. Francesco De Rose for have been first, an inspiring teacher, and second a great colleague during my time at Nuclear Medicine. Thanks to Sybille Reder, Markus Mittelhäuser and Hannes Rolbieski for the excellent work and support in performing PET/CT scans within the *in vivo* animal experiments. Many thanks to Birgit Blechert and Dr. Elisabeth Bliemsrieder for organizational and technical support in the labs of the Nuclear Medicine department as well as during the animal experiments. A big thank to the entire Nuclear Medicine department, to present and past colleagues.

Finally, I would like to express my gratefulness to my beloved family and to my friends here in Munich and the furthest ones in Italy, for their sustenance and care over the course of this exciting yet exhausting journey.

Ad maiora!

10 REFERENCES

- Abou, D. S., Ku, T. and Smith-Jones, P. M. (2011) 'In vivo biodistribution and accumulation of ^{89}Zr in mice', *Nuclear Medicine and Biology*, 38(5), pp. 675–681. doi: <https://doi.org/10.1016/j.nucmedbio.2010.12.011>.
- Adams, C. J., Wilson, J. J. and Boros, E. (2017) 'Multifunctional Desferrichrome Analogues as Versatile $^{89}\text{Zr(IV)}$ Chelators for ImmunoPET Probe Development', *Molecular Pharmaceutics*. American Chemical Society, 14(8), pp. 2831–2842. doi: 10.1021/acs.molpharmaceut.7b00343.
- Almuhaideb, A., Papathanasiou, N. and Bomanji, J. (2011) '18F-FDG PET/CT imaging in oncology.', *Annals of Saudi medicine*. Ann Saudi Med, 31(1), pp. 3–13. doi: 10.4103/0256-4947.75771.
- Archibald, S. J. and Allott, L. (2021) 'The aluminium-[18F]fluoride revolution: simple radiochemistry with a big impact for radiolabelled biomolecules', *EJNMMI Radiopharmacy and Chemistry*, 6(1). doi: 10.1186/s41181-021-00141-0.
- Bates, A. and Power, C. A. (2019) 'David vs. Goliath: The Structure, Function, and Clinical Prospects of Antibody Fragments', *Antibodies 2019, Vol. 8, Page 28*. Multidisciplinary Digital Publishing Institute, 8(2), p. 28. doi: 10.3390/ANTIB8020028.
- Becaud, J. *et al.* (2009) 'Direct One-Step 18 F-Labeling of Peptides via Nucleophilic Aromatic Substitution', *Bioconjugate Chemistry*, 20(12), pp. 2254–2261. doi: 10.1021/bc900240z.
- Bensch, F. *et al.* (2018) '89Zr-atezolizumab imaging as a non-invasive approach to assess clinical response to PD-L1 blockade in cancer', *Nature Medicine 2018 24:12*. Nature Publishing Group, 24(12), pp. 1852–1858. doi: 10.1038/s41591-018-0255-8.
- Berland, L. *et al.* (2021) 'Nanobodies for Medical Imaging: About Ready for Prime Time?', *Biomolecules 2021, Vol. 11, Page 637*. Multidisciplinary Digital Publishing Institute, 11(5), p. 637. doi: 10.3390/BIOM11050637.
- Bernard-Gauthier, V. *et al.* (2014) '18F-Labeled Silicon-Based Fluoride Acceptors: Potential Opportunities for Novel Positron Emitting Radiopharmaceuticals', *BioMed Research International*. Hindawi Limited, 2014. doi: 10.1155/2014/454503.
- Beyer, T. *et al.* (2000) 'A Combined PET/CT Scanner for Clinical Oncology', *Journal of Nuclear Medicine*, 41(8).
- Bockisch, A. *et al.* (2009) 'Hybrid imaging by SPECT/CT and PET/CT: proven outcomes in cancer imaging', *Seminars in nuclear medicine*. Semin Nucl Med, 39(4), pp. 276–289. doi: 10.1053/J.SEMNUCLMED.2009.03.003.
- Boros, E. *et al.* (2016) 'Macrocyclic-Based Hydroxamate Ligands for Complexation and Immunoconjugation of ^{89}Zr for Positron Emission Tomography (PET) Imaging', *ChemPlusChem*, 81(3), pp. 274–281. doi: 10.1002/cplu.201600003.
- Brandt, M. *et al.* (2020) 'Radiolabelling of the octadentate chelators DFO* and oxoDFO* with zirconium-89 and gallium-68', *JBIC Journal of Biological Inorganic Chemistry*, 25(5), pp. 789–796. doi: 10.1007/s00775-020-01800-4.
- Bruce Martin, R. (1988) 'Ternary hydroxide complexes in neutral solutions of Al^{3+} and F^- ', *Biochemical and Biophysical Research Communications*, 155(3), pp. 1194–1200. doi: [https://doi.org/10.1016/S0006-291X\(88\)81266-X](https://doi.org/10.1016/S0006-291X(88)81266-X).
- Buchwalder, C. *et al.* (2017) 'A new tetrapodal 3-hydroxy-4-pyridinone ligand for complexation of ^{89}Zr for positron emission tomography (PET) imaging', *Dalton Transactions*. The Royal Society of Chemistry, 46(29), pp. 9654–9663. doi: 10.1039/C7DT02196H.

10. REFERENCES

- Buchwalder, C. *et al.* (2019) 'Evaluation of the Tetrakis(3-Hydroxy-4-Pyridinone) Ligand THPN with Zirconium(IV): Thermodynamic Solution Studies, Bifunctionalization, and in Vivo Assessment of Macromolecular ^{89}Zr -THPN-Conjugates', *Inorganic Chemistry*. American Chemical Society, 58(21), pp. 14667–14681. doi: 10.1021/acs.inorgchem.9b02350.
- Campbell, M. G. *et al.* (2017) 'Bridging the gaps in F PET tracer development', *Nature chemistry*. Nature Publishing Group, 9(1), pp. 1–3. doi: 10.1038/nchem.2693.
- Caresia Aroztegui, A. P. *et al.* (2017) '18F-FDG PET/CT in breast cancer: Evidence-based recommendations in initial staging.', *Tumour biology : the journal of the International Society for Oncodevelopmental Biology and Medicine*. Tumour Biol, 39(10), p. 1010428317728285. doi: 10.1177/1010428317728285.
- Chakravarty, R. *et al.* (2014) 'Matching the decay half-life with the biological half-life: ImmunoPET imaging with (44)Sc-labeled cetuximab Fab fragment', *Bioconjugate chemistry*. Bioconjug Chem, 25(12), pp. 2197–2204. doi: 10.1021/BC500415X.
- Chansaenpak, K., Vabre, B. and Gabbai, F. P. (2016) '[18F]-Group 13 fluoride derivatives as radiotracers for positron emission tomography', *Chem. Soc. Rev.*, 45, pp. 954–971. doi: 10.1039/c5cs00687b.
- Cherry, S. R., Sorenson, J. A. and Phelps, M. E. (2012) *Chapter 18 - Positron Emission Tomography*. 4th edn, *Physics in Nuclear Medicine*. 4th edn. Available at: <https://www.elsevier.com/books/physics-in-nuclear-medicine/cherry/978-1-4160-5198-5>.
- Chigoho, D. M. *et al.* (2021) 'Site-Specific Radiolabeling of a Human PD-L1 Nanobody via Maleimide-Cysteine Chemistry', *Pharmaceuticals (Basel, Switzerland)*. Pharmaceuticals (Basel), 14(6). doi: 10.3390/PH14060550.
- Chomet, M. *et al.* (2020) 'Head-to-head comparison of DFO* and DFO chelators: selection of the best candidate for clinical ^{89}Zr -immuno-PET', *European Journal of Nuclear Medicine and Molecular Imaging*. European Journal of Nuclear Medicine and Molecular Imaging, pp. 694–707. doi: 10.1007/s00259-020-05002-7.
- Chomet, M. *et al.* (2021) 'Head-to-head comparison of DFO* and DFO chelators: selection of the best candidate for clinical ^{89}Zr -immuno-PET', *European Journal of Nuclear Medicine and Molecular Imaging*. European Journal of Nuclear Medicine and Molecular Imaging, 48(3), pp. 694–707. doi: 10.1007/s00259-020-05002-7.
- Chomet, M., Van Dongen, G. A. M. S. and Vugts, D. J. (2021) 'State of the Art in Radiolabeling of Antibodies with Common and Uncommon Radiometals for Preclinical and Clinical Immuno-PET', *Bioconjugate Chemistry*. doi: 10.1021/acs.bioconjchem.1c00136.
- Chomet, M., van Dongen, G. and Vugts, D. J. (2021) 'State of the Art in Radiolabeling of Antibodies with Common and Uncommon Radiometals for Preclinical and Clinical Immuno-PET', *Bioconjug Chem*. 2021/05/12. doi: 10.1021/acs.bioconjchem.1c00136.
- Cleeren, F. *et al.* (2016) 'New Chelators for Low Temperature Al18F-Labeling of Biomolecules', *Bioconjugate Chemistry*, 27(3), pp. 790–798. doi: 10.1021/acs.bioconjchem.6b00012.
- Cleeren, F. *et al.* (2017) 'Al18F-labeling of heat-sensitive biomolecules for positron emission tomography imaging', *Theranostics*, 7(11), pp. 2924–2939. doi: 10.7150/thno.20094.
- Cleeren, F. *et al.* (2018) 'Direct fluorine-18 labeling of heat-sensitive biomolecules for positron emission tomography imaging using the Al18F-RESCA method', *Nature Protocols*. Springer US, 13(10), pp. 2330–2347. doi: 10.1038/s41596-018-0040-7.
- Cole, E. *et al.* (2014) 'Radiosyntheses using fluorine-18: the art and science of late stage fluorination',

10. REFERENCES

- Current topics in medicinal chemistry*. *Curr Top Med Chem*, 14(7), pp. 875–900. doi: 10.2174/1568026614666140202205035.
- Conti, M. and Eriksson, L. (2016) 'Physics of pure and non-pure positron emitters for PET: a review and a discussion', *EJNMMI Physics*. Springer, 3(1). doi: 10.1186/S40658-016-0144-5.
- Crişan, G. *et al.* (2022) 'Radiopharmaceuticals for PET and SPECT Imaging: A Literature Review over the Last Decade', *International journal of molecular sciences*. *Int J Mol Sci*, 23(9). doi: 10.3390/IJMS23095023.
- Cusnir, R. *et al.* (2017) 'Hydroxypyridinone Chelators: From Iron Scavenging to Radiopharmaceuticals for PET Imaging with Gallium-68', *International journal of molecular sciences*. MDPI, 18(1), p. 116. doi: 10.3390/ijms18010116.
- D'Souza, C. A. *et al.* (2011) 'High-Yielding Aqueous ¹⁸F-Labeling of Peptides via Al ¹⁸F Chelation', *Bioconjugate Chemistry*, 22(9), pp. 1793–1803. doi: 10.1021/bc200175c.
- Dabkowski, A. M. *et al.* (2015) 'Optimization of cyclotron production for radiometal of zirconium 89', *Acta Physica Polonica A*, 127(5), pp. 1479–1482. doi: 10.12693/APhysPolA.127.1479.
- Delso, G. *et al.* (2011) 'Performance measurements of the Siemens mMR integrated whole-body PET/MR scanner', *Journal of nuclear medicine : official publication, Society of Nuclear Medicine*. *J Nucl Med*, 52(12), pp. 1914–1922. doi: 10.2967/JNUMED.111.092726.
- Deri, M. A. *et al.* (2014) 'Alternative Chelator for ⁸⁹Zr Radiopharmaceuticals: Radiolabeling and Evaluation of 3,4,3-(LI-1,2-HOPO)', *Journal of Medicinal Chemistry*. American Chemical Society, 57(11), pp. 4849–4860. doi: 10.1021/jm500389b.
- Dijkers, E. C. *et al.* (2010) 'Biodistribution of ⁸⁹Zr-trastuzumab and PET Imaging of HER2-Positive Lesions in Patients With Metastatic Breast Cancer', *Clinical Pharmacology & Therapeutics*. John Wiley & Sons, Ltd, 87(5), pp. 586–592. doi: <https://doi.org/10.1038/clpt.2010.12>.
- Ekberg, C. *et al.* (2004) 'Studies on the Hydrolytic Behavior of Zirconium(IV)', *Journal of Solution Chemistry*, 33(1), pp. 47–79. doi: 10.1023/B:JOSL.0000026645.41309.d3.
- Even-Sapir, E. *et al.* (2001) 'The New Technology of Combined Transmission and Emission Tomography in Evaluation of Endocrine Neoplasms', *THE JOURNAL OF NUCLEAR MEDICINE* •, 42(7).
- Farkas, E. *et al.* (2015) 'Equilibrium and dissociation kinetics of the [Al(NOTA)] complex (NOTA = 1,4,7-triazacyclononane-1,4,7-triacetate)', *Reaction Kinetics, Mechanisms and Catalysis*, 116(1), pp. 19–33. doi: 10.1007/s11144-015-0892-6.
- Farwell, M. D. *et al.* (2021) 'CD8-targeted PET Imaging of Tumor Infiltrating T cells in Patients with Cancer: A Phase I First-in-Human Study of ⁸⁹Zr-Df-IAB22M2C, a Radiolabeled anti-CD8 Minibody', *Journal of nuclear medicine : official publication, Society of Nuclear Medicine*. *J Nucl Med*, p. jnumed.121.262485. doi: 10.2967/JNUMED.121.262485.
- Feiner, I. V. J. *et al.* (2021) 'The Race for Hydroxamate-Based Zirconium-89 Chelators', *Cancers*. *Cancers (Basel)*, 13(17). doi: 10.3390/CANCERS13174466.
- Fersing, C. *et al.* (2019) 'A Comprehensive Review of Non-Covalent Radiofluorination Approaches Using Aluminum [¹⁸F]fluoride: Will [¹⁸F]AlF Replace ⁶⁸Ga for Metal Chelate Labeling?', *Molecules*, 24(16), p. 2866. doi: 10.3390/molecules24162866.
- Fu, R. *et al.* (2018) 'Antibody Fragment and Affibody ImmunoPET Imaging Agents: Radiolabelling Strategies and Applications', *ChemMedChem*. John Wiley & Sons, Ltd, 13(23), pp. 2466–2478. doi: 10.1002/CMDC.201800624.
- Fuccio, C. *et al.* (2013) '¹⁸F-FDG-PET/CT in malignant mesothelioma', *Biomedicine & Pharmacotherapy*, 67(6), pp. 539–542. doi: 10.1016/j.biopha.2013.01.008.

10. REFERENCES

- Galli, F. *et al.* (2021) 'Immune cell labelling and tracking: implications for adoptive cell transfer therapies', *EJNMMI Radiopharmacy and Chemistry*. Springer, 6(1). doi: 10.1186/S41181-020-00116-7.
- Gao, H. *et al.* (2011) 'PET of Insulinoma Using 18 F-FBEM-EM3106B, a New GLP-1 Analogue', *Molecular Pharmaceutics*, 8, pp. 1775–1782. doi: 10.1021/mp200141x.
- Ghiani, S. *et al.* (2021) 'Synthesis, radiolabeling, and pre-clinical evaluation of [44Sc]Sc-AAZTA conjugate PSMA inhibitor, a new tracer for high-efficiency imaging of prostate cancer', *European Journal of Nuclear Medicine and Molecular Imaging*. European Journal of Nuclear Medicine and Molecular Imaging. doi: 10.1007/s00259-020-05130-0.
- Goldenberg, D. M. and Nabi, H. A. (1999) 'Breast cancer imaging with radiolabeled antibodies', *Seminars in nuclear medicine*. Semin Nucl Med, 29(1), pp. 41–48. doi: 10.1016/S0001-2998(99)80028-2.
- Gower-Fry, L. *et al.* (2021) 'Recent advances in the clinical translation of silicon fluoride acceptor (SiFA)18F-radiopharmaceuticals', *Pharmaceuticals*, 14(7). doi: 10.3390/ph14070701.
- Guérard, F., Lee, Y.-S. and Brechbiel, M. W. (2014) 'Rational design, synthesis, and evaluation of tetrahydroxamic acid chelators for stable complexation of zirconium(IV)', *Chemistry (Weinheim an der Bergstrasse, Germany)*. 2014/04/16, 20(19), pp. 5584–5591. doi: 10.1002/chem.201304115.
- Guillou, A. *et al.* (2021) 'The Influence of a Polyethylene Glycol Linker on the Metabolism and Pharmacokinetics of a 89 Zr-Radiolabeled Antibody', *Bioconjugate chemistry*. Bioconjug Chem, 32(7), pp. 1263–1275. doi: 10.1021/ACS.BIOCONJCHEM.1C00172.
- Harmand, T. J. *et al.* (2021) 'Nanobodies as in vivo, non-invasive, imaging agents', *RSC Chemical Biology*. RSC, 2(3), pp. 685–701. doi: 10.1039/D1CB00023C.
- Hess, S. *et al.* (2014) 'FDG-PET/CT in Infectious and Inflammatory Diseases', *PET Clinics*. PET Clin, 9(4), pp. 497–519. doi: 10.1016/j.cpet.2014.07.002.
- Higashikawa, K. *et al.* (2014) '64Cu-DOTA-Anti-CTLA-4 mAb Enabled PET Visualization of CTLA-4 on the T-Cell Infiltrating Tumor Tissues', *PLoS ONE*. Edited by G. Multhoff. European Journal of Nuclear Medicine and Molecular Imaging, 9(11), p. e109866. doi: 10.1371/journal.pone.0109866.
- Höhne, A. *et al.* (2008) 'Synthesis, 18 F-Labeling, and in Vitro and in Vivo Studies of Bombesin Peptides Modified with Silicon-Based Building Blocks', *Bioconjugate Chemistry*, 19(9), pp. 1871–1879. doi: 10.1002/anie.200705854.
- Holland, J. P. *et al.* (2010) '89Zr-DFO-J591 for immunoPET of prostate-specific membrane antigen expression in vivo', *Journal of nuclear medicine: official publication, Society of Nuclear Medicine*. 2010/07/21, 51(8), pp. 1293–1300. doi: 10.2967/jnumed.110.076174.
- Holland, J. P. (2020) 'Predicting the Thermodynamic Stability of Zirconium Radiotracers', *Inorganic Chemistry*. American Chemical Society, 59(3), pp. 2070–2082. doi: 10.1021/acs.inorgchem.9b03515.
- Hu, K. *et al.* (2022) 'Preclinical evaluation and pilot clinical study of [18F]AlF-labeled FAPI-tracer for PET imaging of cancer associated fibroblasts', *Acta Pharmaceutica Sinica B*. Elsevier, 12(2), pp. 867–875. doi: 10.1016/J.APSB.2021.09.032.
- Jackson, J. A. *et al.* (2020) 'Bioconjugates of Chelators with Peptides and Proteins in Nuclear Medicine: Historical Importance, Current Innovations, and Future Challenges', *Bioconjugate chemistry*. Bioconjug Chem, 31(3), pp. 483–491. doi: 10.1021/ACS.BIOCONJCHEM.0C00015.
- Jacobson, O., Kiesewetter, D. O. and Chen, X. (2014) 'Fluorine-18 Radiochemistry, Labeling Strategies

10. REFERENCES

- and Synthetic Routes', *Bioconjugate Chemistry*. American Chemical Society, 26(1), pp. 1–18. doi: 10.1021/BC500475E.
- Jauw, Y. W. S. *et al.* (2017) 'Performance of 89Zr-Labeled-Rituximab-PET as an Imaging Biomarker to Assess CD20 Targeting: A Pilot Study in Patients with Relapsed/Refractory Diffuse Large B Cell Lymphoma', *PloS one*. PLoS One, 12(1). doi: 10.1371/JOURNAL.PONE.0169828.
- Keyaerts, M. *et al.* (2016) 'Phase i study of 68Ga-HER2-Nanobody for PET/CT assessment of HER2 expression in breast carcinoma', *Journal of Nuclear Medicine*, 57(1), pp. 27–33. doi: 10.2967/jnumed.115.162024.
- Kiesewetter, D. O. *et al.* (2011) 'Automated radiochemical synthesis of [18 F] FBEM : A thiol reactive synthon for radiofluorination of peptides and proteins This publication', *Applied Radiation and Isotopes*. Elsevier, 69(2), pp. 410–414. doi: 10.1016/j.apradiso.2010.09.023.
- Kinahan, P. E. and Fletcher, J. W. (2010) 'PET/CT Standardized Uptake Values (SUVs) in Clinical Practice and Assessing Response to Therapy', *Seminars in ultrasound, CT, and MR*. NIH Public Access, 31(6), p. 496. doi: 10.1053/J.SULT.2010.10.001.
- Klasen, B. *et al.* (2021) 'Development and in vitro evaluation of new bifunctional 89Zr-chelators based on the 6-amino-1,4-diazepane scaffold for immuno-PET applications', *Nuclear Medicine and Biology*. Elsevier Inc., 102–103, pp. 12–23. doi: 10.1016/j.nucmedbio.2021.06.007.
- Knowles, S. M. and Wu, A. M. (2012) 'Advances in immuno-positron emission tomography: antibodies for molecular imaging in oncology', *Journal of clinical oncology : official journal of the American Society of Clinical Oncology*. J Clin Oncol, 30(31), pp. 3884–3892. doi: 10.1200/JCO.2012.42.4887.
- Krasniqi, A. *et al.* (2018) 'Same-Day Imaging Using Small Proteins: Clinical Experience and Translational Prospects in Oncology', *Journal of nuclear medicine : official publication, Society of Nuclear Medicine*. J Nucl Med, 59(6), pp. 885–891. doi: 10.2967/JNUMED.117.199901.
- Krishnan, A. *et al.* (2020) 'Identifying CD38+ cells in patients with multiple myeloma: first-in-human imaging using copper-64-labeled daratumumab', *Blood advances*. Blood Adv, 4(20), pp. 5194–5202. doi: 10.1182/BLOODADVANCES.2020002603.
- Larimer, B. M. *et al.* (2016) 'Quantitative CD3 PET imaging predicts tumor growth response to anti-CTLA-4 therapy', *Journal of Nuclear Medicine*, 57(10), pp. 1607–1611. doi: 10.2967/jnumed.116.173930.
- Li, C. *et al.* (2022) 'Visualizing T-Cell Responses: The T-Cell PET Imaging Toolbox', *Journal of nuclear medicine : official publication, Society of Nuclear Medicine*. J Nucl Med, 63(2), pp. 183–188. doi: 10.2967/JNUMED.121.261976.
- Li Liang (2003) 'The biochemistry and physiology of metallic fluoride: Action, mechanism, and implications.', *Crit Rev Oral Biol Med*, 14(2), pp. 100–114.
- Li, Z. *et al.* (2008) 'The Synthesis of 18 F-FDS and Its Potential Application in Molecular Imaging', *Molecular Imaging and Biology*, 10, pp. 92–98. doi: 10.1007/s11307-007-0125-0.
- Löfblom, J. *et al.* (2010) 'Affibody molecules: engineered proteins for therapeutic, diagnostic and biotechnological applications', *FEBS letters*. FEBS Lett, 584(12), pp. 2670–2680. doi: 10.1016/J.FEBSLET.2010.04.014.
- Ma, M. T. *et al.* (2015) 'Tripodal tris(hydroxypyridinone) ligands for immunoconjugate PET imaging with 89Zr4+: comparison with desferrioxamine-B', *Dalton Transactions*. The Royal Society of Chemistry, 44(11), pp. 4884–4900. doi: 10.1039/C4DT02978J.
- Martin, R. B. (1996) 'Ternary complexes of A13 + and F- with a third ligand', *Coord. Chem. Rev.*, 141,

- pp. 23–32.
- Martinelli, J. *et al.* (2021) 'Semi-Rigid (Aminomethyl) Piperidine-Based Pentadentate Ligands for Mn(II) Complexation', *Molecules*. doi: 10.3390/molecules26195993.
- Maurer, A. H. (2008) 'Combined imaging modalities: PET/CT and SPECT/CT', *Health physics*. *Health Phys*, 95(5), pp. 571–576. doi: 10.1097/01.HP.0000334064.46217.20.
- Mayer, K. E. *et al.* (2018) 'T-cell functionality testing is highly relevant to developing novel immunotracers monitoring T cells in the context of immunotherapies and revealed CD7 as an attractive target', *Theranostics*, 8(21), pp. 6070–6087. doi: 10.7150/thno.27275.
- McBride, W. J. *et al.* (2009) 'A Novel Method of 18F Radiolabeling for PET', *Journal of Nuclear Medicine*, 50(6), pp. 991–998. doi: 10.2967/jnumed.108.060418.
- McBride, W. J., Sharkey, R. M. and Goldenberg, D. M. (2013) 'Radiofluorination using aluminum-fluoride (Al18F)', *EJNMMI Research*, 3(1), p. 36. doi: 10.1186/2191-219X-3-36.
- McCarthy, C. E. *et al.* (2020) 'In vivo Imaging Technologies to Monitor the Immune System', *Frontiers in Immunology*, 11(June), pp. 1–21. doi: 10.3389/fimmu.2020.01067.
- Mendler, C. T. *et al.* (2015) '89Zr-Labeled Versus 124I-Labeled HER2 Fab with Optimized Plasma Half-Life for High-Contrast Tumor Imaging In Vivo', *Journal of Nuclear Medicine*, 56(7), pp. 1112–1118. doi: 10.2967/jnumed.114.149690.
- Miao, H. *et al.* (2022) 'Application of a Novel 68 Ga-HER2 Affibody PET/CT Imaging in Breast Cancer Patients', *Frontiers in oncology*. *Front Oncol*, 12. doi: 10.3389/FONC.2022.894767.
- Morais, M. and Ma, M. T. (2018) 'Site-specific chelator-antibody conjugation for PET and SPECT imaging with radiometals', *Drug Discov Today Technol.* 2018/12/17, 30, pp. 91–104. doi: 10.1016/j.ddtec.2018.10.002.
- Mu, L. *et al.* (2008) 'Silicon-Based Building Blocks for One-Step 18 F-Radiolabeling of Peptides for PET Imaging', *Anal. Biochem.*, 47, pp. 4922–4925. doi: 10.1002/anie.200705854.
- Olafsen, T. and Wu, A. M. (2010) 'Novel Antibody Vectors for Imaging', *Seminars in nuclear medicine*. NIH Public Access, 40(3), p. 167. doi: 10.1053/J.SEMNUCLMED.2009.12.005.
- Oroujeni, M. *et al.* (2018) 'Preclinical Evaluation of [68Ga]Ga-DFO-ZEGFR:2377: A Promising Affibody-Based Probe for Noninvasive PET Imaging of EGFR Expression in Tumors.', *Cells*. *Cells*, 7(9), p. 141. doi: 10.3390/cells7090141.
- Pandit-Taskar, N. *et al.* (2020) 'First-in-Humans Imaging with 89 Zr-Df-IAB22M2C Anti-CD8 Minibody in Patients with Solid Malignancies: Preliminary Pharmacokinetics, Biodistribution, and Lesion Targeting', *Journal of nuclear medicine : official publication, Society of Nuclear Medicine*. *J Nucl Med*, 61(4), pp. 512–519. doi: 10.2967/JNUMED.119.229781.
- Pandya, D. N. *et al.* (2015) 'Di-macrocylic terephthalamide ligands as chelators for the PET radionuclide zirconium-89', *Chemical Communications*. The Royal Society of Chemistry, 51(12), pp. 2301–2303. doi: 10.1039/c4cc09256b.
- Pandya, D. N. *et al.* (2017) 'Zirconium tetraazamacrocycle complexes display extraordinary stability and provide a new strategy for zirconium-89-based radiopharmaceutical development', *Chemical Science*. The Royal Society of Chemistry, 8(3), pp. 2309–2314. doi: 10.1039/C6SC04128K.
- Pandya, D. N. *et al.* (2020) 'Polyazamacrocycle Ligands Facilitate 89Zr Radiochemistry and Yield 89Zr Complexes with Remarkable Stability', *Inorganic Chemistry*. American Chemical Society, 59(23), pp. 17473–17487. doi: 10.1021/acs.inorgchem.0c02722.
- Patra, M. *et al.* (2014) 'An octadentate bifunctional chelating agent for the development of stable

10. REFERENCES

- zirconium-89 based molecular imaging probes', *Chem. Commun.* The Royal Society of Chemistry, 50(78), pp. 11523–11525. doi: 10.1039/C4CC05558F.
- Perk, L. R. *et al.* (2010) 'P-Isothiocyanatobenzyl-desferrioxamine: A new bifunctional chelate for facile radiolabeling of monoclonal antibodies with zirconium-89 for immuno-PET imaging', *European Journal of Nuclear Medicine and Molecular Imaging*, 37(2), pp. 250–259. doi: 10.1007/s00259-009-1263-1.
- Philpott, G. W. *et al.* (1995) 'RadioimmunoPET: detection of colorectal carcinoma with positron-emitting copper-64-labeled monoclonal antibody.', *Journal of Nuclear Medicine: Official Publication, Society of Nuclear Medicine*, 36(10), pp. 1818–1824. Available at: <https://europepmc.org/article/med/7562049> (Accessed: 29 June 2022).
- Pichler, B. J. *et al.* (2010) 'PET/MRI: paving the way for the next generation of clinical multimodality imaging applications', *Journal of nuclear medicine: official publication, Society of Nuclear Medicine*. *J Nucl Med*, 51(3), pp. 333–336. doi: 10.2967/JNUMED.109.061853.
- Da Pieve, C. *et al.* (2016) 'Efficient [18F]AIF Radiolabeling of ZHER3:8698 Affibody Molecule for Imaging of HER3 Positive Tumors', *Bioconjugate Chemistry*. American Chemical Society, 27(8), pp. 1839–1849. doi: 10.1021/acs.bioconjchem.6b00259.
- Da Pieve, C. *et al.* (2020) 'Thiol-Reactive PODS-Bearing Bifunctional Chelators for the Development of EGFR-Targeting [18F]AIF-Affibody Conjugates', *Molecules*. doi: 10.3390/molecules25071562.
- Price, E. W. and Orvig, C. (2014) 'Matching chelators to radiometals for radiopharmaceuticals', *Chem Soc Rev*. 2013/11/01, 43(1), pp. 260–290. doi: 10.1039/c3cs60304k.
- Price, T. W., Greenman, J. and Stasiuk, G. J. (2016) 'Current advances in ligand design for inorganic positron emission tomography tracers 68Ga, 64Cu, 89Zr and 44Sc', *Dalton Transactions*. The Royal Society of Chemistry, 45(40), pp. 15702–15724.
- Queern, S. L. *et al.* (2017) 'Production of Zr-89 using sputtered yttrium coin targets 89 Zr using sputtered yttrium coin targets', *Nuclear medicine and biology*. *Nucl Med Biol*, 50, pp. 11–16. doi: 10.1016/J.NUCMEDBIO.2017.03.004.
- Quigley, N. G. *et al.* (2022) 'PET/CT imaging of head-and-neck and pancreatic cancer in humans by targeting the "Cancer Integrin" $\alpha\beta 6$ with Ga-68-Trivehexin', *European journal of nuclear medicine and molecular imaging*. *Eur J Nucl Med Mol Imaging*, 49(4), pp. 1136–1147. doi: 10.1007/S00259-021-05559-X.
- Racow, E. E. *et al.* (2019) 'General Approach to Direct Measurement of the Hydration State of Coordination Complexes in the Gas Phase: Variable Temperature Mass Spectrometry', *Journal of the American Chemical Society*. American Chemical Society, 141(37), pp. 14650–14660. doi: 10.1021/jacs.9b05874.
- Rahmim, A. and Zaidi, H. (2008) 'PET versus SPECT: strengths, limitations and challenges', *Nuclear Medicine Communications*, 29(3), pp. 193–207.
- Rashidian, M. *et al.* (2017) 'Predicting the response to CTLA-4 blockade by longitudinal noninvasive monitoring of CD8 T cells', *Journal of Experimental Medicine*, 214(8), pp. 2243–2255. doi: 10.1084/jem.20161950.
- Rashidian, M. and Ploegh, H. (2020) 'Nanobodies as non-invasive imaging tools', *Immuno-oncology technology*. *Immuno-oncol Technol*, 7, pp. 2–14. doi: 10.1016/J.IOTECH.2020.07.001.
- Rathore, Y. *et al.* (2022) 'Development 68Ga trastuzumab Fab and bioevaluation by PET imaging in HER2/neu expressing breast cancer patients', *Nuclear medicine communications*. *Nucl Med Commun*, 43(4), pp. 458–467. doi: 10.1097/MNM.0000000000001521.

10. REFERENCES

- Richter, A. *et al.* (2020) 'First In-Human Medical Imaging with a PASylated 89 Zr-Labeled Anti-HER2 Fab-Fragment in a Patient with Metastatic Breast Cancer', *Nuclear medicine and molecular imaging*. Nucl Med Mol Imaging, 54(2), pp. 114–119. doi: 10.1007/S13139-020-00638-7.
- De Rose, F. *et al.* (2019) 'Galectin-3 targeting in thyroid orthotopic tumors opens new ways to characterize thyroid cancer', *Journal of Nuclear Medicine*, 60(6), pp. 770–776. doi: 10.2967/jnumed.118.219105.
- Rousseau, J. *et al.* (2017) 'Design, synthesis and evaluation of novel bifunctional tetrahydroxamate chelators for PET imaging of 89Zr-labeled antibodies', *Bioorganic & Medicinal Chemistry Letters*, 27(4), pp. 708–712. doi: <https://doi.org/10.1016/j.bmcl.2017.01.052>.
- Rubins, D. J. *et al.* (2021) 'In Vivo Evaluation and Dosimetry Estimate for a High Affinity Affibody PET Tracer Targeting PD-L1', *Molecular imaging and biology*. Mol Imaging Biol, 23(2), pp. 241–249. doi: 10.1007/S11307-020-01544-2.
- Russelli, L. *et al.* (2020) 'Room Temperature Al18F Labeling of 2-Aminomethylpiperidine-Based Chelators for PET Imaging', *ChemMedChem*, 15(3), pp. 284–292. doi: 10.1002/cmdc.201900652.
- Russelli, L. *et al.* (2021) 'A Semi Rigid Novel Hydroxamate AMPED-Based Ligand for 89Zr PET Imaging', *Molecules*, 26(19), p. 5819. doi: 10.3390/molecules26195819.
- Salvador, J. P., Vilaplana, L. and Marco, M. P. (2019) 'Nanobody: outstanding features for diagnostic and therapeutic applications', *Analytical and Bioanalytical Chemistry*. Analytical and Bioanalytical Chemistry, 411(9), pp. 1703–1713. doi: 10.1007/s00216-019-01633-4.
- Sandström, M. *et al.* (2016) 'Biodistribution and Radiation Dosimetry of the Anti-HER2 Affibody Molecule 68Ga-ABY-025 in Breast Cancer Patients', *Journal of nuclear medicine : official publication, Society of Nuclear Medicine*. J Nucl Med, 57(6), pp. 867–871. doi: 10.2967/JNUMED.115.169342.
- Sarbisheh, E. K. *et al.* (2020) 'A High-Denticity Chelator Based on Desferrioxamine for Enhanced Coordination of Zirconium-89', *Inorganic Chemistry*. American Chemical Society, 59(16), pp. 11715–11727. doi: 10.1021/ACS.INORGCHEM.0C01629.
- Sarikaya, I. *et al.* (2021) 'Visual versus semiquantitative analysis of 18 F- fluorodeoxyglucose-positron emission tomography brain images in patients with dementia', *World journal of nuclear medicine*. World J Nucl Med, 20(1), pp. 82–89. doi: 10.4103/WJNM.WJNM_53_18.
- Sauter, A. W. *et al.* (2010) 'Combined PET/MRI: one step further in multimodality imaging', *Trends in molecular medicine*. Trends Mol Med, 16(11), pp. 508–515. doi: 10.1016/J.MOLMED.2010.08.003.
- Schlapschy, M. *et al.* (2013) 'PASylation: a biological alternative to PEGylation for extending the plasma half-life of pharmaceutically active proteins', *Protein engineering, design & selection : PEDS*. Protein Eng Des Sel, 26(8), pp. 489–501. doi: 10.1093/PROTEIN/GZT023.
- Scott, A. M. *et al.* (2020) 'First clinical study of a pegylated diabody 124 I-labeled PEG-AVP0458 in patients with tumor-associated glycoprotein 72 positive cancers', *Theranostics*. Theranostics, 10(25), pp. 11404–11415. doi: 10.7150/THNO.49422.
- Shetty, D. *et al.* (2011) 'Stable aluminium fluoride chelates with triazacyclononane derivatives proved by X-ray crystallography and 18F-labeling study', *Chemical Communications*, 47(34), pp. 9732–9734. doi: 10.1039/c1cc13151f.
- Smith, G. E. *et al.* (2011) 'Inorganic approaches for radiolabelling biomolecules with fluorine-18 for imaging with Positron Emission Tomography', *Dalton Transactions*, 40(23), pp. 6196–6205.
- Sneddon, D. and Cornelissen, B. (2021) 'Emerging chelators for nuclear imaging', *Current Opinion in*

10. REFERENCES

- Chemical Biology*, 63, pp. 152–162. doi: 10.1016/j.cbpa.2021.03.001.
- Stangl, S. *et al.* (2018) 'Preclinical evaluation of the Hsp70 peptide tracer TPP-PEg24-DFO[89Zr] for tumor-specific PET/CT imaging', *Cancer Research*, 78(21), pp. 6268–6281. doi: 10.1158/0008-5472.CAN-18-0707.
- Summer, D. *et al.* (2020) 'Hybrid Imaging Agents for Pretargeting Applications Based on Fusarinine C—Proof of Concept', *Molecules*. doi: 10.3390/molecules25092123.
- Thie, J. A. (2004) 'Understanding the Standardized Uptake Value, Its Methods, and Implications for Usage', *Journal of Nuclear Medicine*, 45(9).
- Tolmachev, V. and Orlova, A. (2020) 'Affibody molecules as targeting vectors for PET imaging', *Cancers*, 12(3). doi: 10.3390/cancers12030651.
- Townsend, D. W. (2008) 'Dual-modality imaging: Combining anatomy and function', *Journal of Nuclear Medicine*, 49(6), pp. 938–955. doi: 10.2967/JNUMED.108.051276.
- Turkington, T. G. (2001) 'Introduction to PET Instrumentation', *Journal of Nuclear Medicine Technology*, 29(1).
- Turkington, T. G. (2011) *PET imaging basics*, in *Clinical PET-CT in Radiology*. Springer.
- Ulaner, G. A. *et al.* (2017) 'First-in-human HER2-targeted imaging using 89Zr-pertuzumab PET/CT: Dosimetry and clinical application in patients with breast cancer', *Journal of Nuclear Medicine*. Society of Nuclear Medicine, 59(6), pp. 900–906. doi: 10.2967/JNUMED.117.202010.
- Vaidyanathan, G. *et al.* (2016) 'Biomolecular Chemistry', *Organic & Biomolecular Chemistry*. Royal Society of Chemistry, 14, pp. 1261–1271. doi: 10.1039/c5ob02258d.
- Vaidyanathan, G. and Zalutsky, M. R. (2006) 'Synthesis of N -succinimidyl 4- [18 F] fluorobenzoate , an agent for labeling proteins and peptides with 18 F', *Nature Protocols*, 1(4), pp. 1655–1661. doi: 10.1038/nprot.2006.264.
- Vallabhajosula, S. (2009) *Molecular Imaging: PET and SPECT scanners*, *Molecular Imaging: Radiopharmaceuticals for PET and SPECT*. Berlin, Heidelberg: Springer Berlin Heidelberg. doi: 10.1007/978-3-540-76735-0.
- Varasteh, Z. *et al.* (2021) 'Imaging atherosclerotic plaques by targeting Galectin-3 and activated macrophages using (89Zr)-DFO- Galectin3-F(ab')₂ mAb', *Theranostics*, 11(4), pp. 1864–1876. doi: 10.7150/thno.50247.
- Vaughn, B. A. *et al.* (2020) 'Chelation with a twist: a bifunctional chelator to enable room temperature radiolabeling and targeted PET imaging with scandium-44', *Chemical Science*. The Royal Society of Chemistry, 11(2), pp. 333–342. doi: 10.1039/C9SC04655K.
- Verhoeff, S. R. *et al.* (2022) '89 Zr-DFO-durvalumab PET/CT prior to durvalumab treatment in patients with recurrent or metastatic head and neck cancer', *Journal of nuclear medicine : official publication, Society of Nuclear Medicine*. J Nucl Med, p. jnumed.121.263470. doi: 10.2967/JNUMED.121.263470.
- Vlachostergios, P. J. *et al.* (2022) 'Pilot study of the diagnostic utility of 89 Zr-df-IAB2M and 68 Ga-PSMA-11 PET imaging and multiparametric MRI in localized prostate cancer', *The Prostate*. Prostate, 82(4), pp. 483–492. doi: 10.1002/PROS.24294.
- Wang, H. *et al.* (2012) 'Meta-analysis of the diagnostic performance of [F] FDG-PET and PET / CT in renal cell carcinoma', *Cancer Imaging*, 12, pp. 464–474. doi: 10.1102/1470-7330.2012.0042.
- Wang, Y. *et al.* (2022) 'Pilot study of a novel nanobody 68 Ga-NODAGA-SNA006 for instant PET imaging of CD8 + T cells', *European journal of nuclear medicine and molecular imaging*. Eur J Nucl Med Mol Imaging. doi: 10.1007/S00259-022-05903-9.

10. REFERENCES

- Wei, W. *et al.* (2018) 'Noninvasive PET Imaging of T cells', *Trends in Cancer*. Cell Press, 4(5), pp. 359–373. doi: 10.1016/j.trecan.2018.03.009.
- Wei, W. *et al.* (2020) 'ImmunoPET: Concept, Design, and Applications', *Chemical Reviews*. American Chemical Society, 120(8), pp. 3787–3851. doi: 10.1021/ACS.CHEMREV.9B00738/ASSET/IMAGES/LARGE/CR9B00738_0032.JPEG.
- Wu, A. M. and Pandit-Taskar, N. (2022) 'ImmunoPET: harnessing antibodies for imaging immune cells', *Molecular Imaging and Biology*. Springer Science and Business Media Deutschland GmbH, 24(2), pp. 181–197. doi: 10.1007/S11307-021-01652-7/FIGURES/5.
- Wüst, F. *et al.* (2003) 'Radiolabelling of isopeptide N e - (g -glutamyl) - l -lysine by conjugation with N -succinimidyl-4- [18 F] fluorobenzoate', *Applied Radiation and Isotopes*, 59, pp. 43–48. doi: 10.1016/S0969-8043(03)00161-1.
- Xavier, C. *et al.* (2019) 'Clinical Translation of [68Ga]Ga-NOTA-anti-MMR-sdAb for PET/CT Imaging of Protumorigenic Macrophages', *Molecular Imaging and Biology*. Molecular Imaging and Biology, 21(5), pp. 898–906. doi: 10.1007/s11307-018-01302-5.
- Yusufi, N. *et al.* (2017) 'In-depth characterization of a TCR-specific tracer for sensitive detection of tumor-directed transgenic T cells by immuno-PET', *Theranostics*, 7(9), pp. 2402–2416. doi: 10.7150/thno.17994.
- Zeglis, B. M. and Lewis, J. S. (2015) 'The bioconjugation and radiosynthesis of 89Zr-DFO-labeled antibodies', *Journal of visualized experiments : JoVE*. MyJove Corporation, (96), p. 52521. doi: 10.3791/52521.
- Zhai, C. *et al.* (2015) 'Novel Bifunctional Cyclic Chelator for 89Zr Labeling–Radiolabeling and Targeting Properties of RGD Conjugates', *Molecular Pharmaceutics*. American Chemical Society, 12(6), pp. 2142–2150. doi: 10.1021/acs.molpharmaceut.5b00128.
- Zhang, M. *et al.* (2020) 'Research progress of 18F labeled small molecule positron emission tomography (PET) imaging agents', *European Journal of Medicinal Chemistry*. Elsevier Masson s.r.l., 205. doi: 10.1016/J.EJMECH.2020.112629.
- Zhao, H. *et al.* (2021) 'ImmunoPET imaging of human CD8+ T cells with novel 68Ga-labeled nanobody companion diagnostic agents', *Journal of Nanobiotechnology*. BioMed Central, 19(1), pp. 1–11. doi: 10.1186/s12951-021-00785-9.
- Zhou, N. *et al.* (2021) 'Impact of 68 Ga-NOTA-MAL-MZHER2 PET imaging in advanced gastric cancer patients and therapeutic response monitoring', *European journal of nuclear medicine and molecular imaging*. Eur J Nucl Med Mol Imaging, 48(1), pp. 161–175. doi: 10.1007/S00259-020-04898-5.
- Zhou, Z. *et al.* (2021) 'Site-Specific and Residualizing Linker for 18 F Labeling with Enhanced Renal Clearance: Application to an Anti-HER2 Single-Domain Antibody Fragment', *Journal of nuclear medicine : official publication, Society of Nuclear Medicine*. J Nucl Med, 62(11), pp. 1624–1630. doi: 10.2967/JNUMED.120.261446.
- Zimmermann, R. G. (2013) 'Why are investors not interested in my radiotracer? The industrial and regulatory constraints in the development of radiopharmaceuticals', *Nuclear medicine and biology*. Nucl Med Biol, 40(2), pp. 155–166. doi: 10.1016/J.NUCMEDBIO.2012.10.012.

11 APPENDIX

Appendix I

Russelli L*, De Rose F, Leone L, Reder S, Schwaiger M, D'Alessandria C, Tei L. A Semi Rigid Novel Hydroxamate AMPED-Based Ligand for ^{89}Zr PET Imaging. *Molecules*. 2021 Sep 25;26(19):5819.

Appendix II

Russelli L*, Martinelli J*, De Rose F, Reder S, Herz M, Schwaiger M, Weber W, Tei L, D'Alessandria C. Room Temperature Al^{18}F Labeling of 2-Aminomethylpiperidine-Based Chelators for PET Imaging. *ChemMedChem*. 2020 Feb 5;15(3):284-292.

APPENDIX I

Russelli L*, De Rose F, Leone L, Reder S, Schwaiger M, D'Alessandria C, Tei L. A Semi Rigid Novel Hydroxamate AMPED-Based Ligand for ^{89}Zr PET Imaging. *Molecules*. 2021 Sep 25;26(19):5819.

Article

A Semi Rigid Novel Hydroxamate AMPED-Based Ligand for ^{89}Zr PET Imaging

Lisa Russelli ¹, Francesco De Rose ¹, Loredana Leone ², Sybille Reder ¹, Markus Schwaiger ¹, Calogero D'Alessandria ^{1,*} and Lorenzo Tei ^{2,*}

¹ Department of Nuclear Medicine, Klinikum Rechts der Isar TU München, Ismaningerstraße 22, 81675 Munich, Germany; lisa.russelli@tum.de (L.R.); francesco.de-rose@tum.de (F.D.R.); sybille.reder@mri.tum.de (S.R.); markus.schwaiger@tum.de (M.S.)

² Department of Science and Technological Innovation, Università del Piemonte Orientale, Viale T. Michel 11, 15121 Alessandria, Italy; loredana.leone@uniupo.it

* Correspondence: calogero.dalessandria@tum.de (C.D.); lorenzo.tei@uniupo.it (L.T.)

† Join senior authors.

Abstract: In this work, we designed, developed, characterized, and investigated a new chelator and its bifunctional derivative for ^{89}Zr labeling and PET-imaging. In a preliminary study, we synthesized two hexadentate chelators named AAZTHAS and AAZTHAG, based on the seven-membered heterocycle AMPED (6-amino-6-methylperhydro-1,4-diazepine) with the aim to increase the rigidity of the ^{89}Zr complex by using *N*-methyl-*N*-(hydroxy)succinamide or *N*-methyl-*N*-(hydroxy)glutaramide pendant arms attached to the cyclic structure. *N*-methylhydroxamate groups are the donor groups chosen to efficiently coordinate ^{89}Zr . After in vitro stability tests, we selected the chelator with longer arms, AAZTHAG, as the best complexing agent for ^{89}Zr presenting a stability of $86.4 \pm 5.5\%$ in human serum (HS) for at least 72 h. Small animal PET/CT static scans acquired at different time points (up to 24 h) and ex vivo organ distribution studies were then carried out in healthy nude mice ($n = 3$) to investigate the stability and biodistribution in vivo of this new ^{89}Zr -based complex. High stability in vivo, with low accumulation of free ^{89}Zr in bones and kidneys, was measured. Furthermore, an activated ester functionalized version of AAZTHAG was synthesized to allow the conjugation with biomolecules such as antibodies. The bifunctional chelator was then conjugated to the human anti-HER2 monoclonal antibody Trastuzumab (Tz) as a proof of principle test of conjugation to biologically active molecules. The final ^{89}Zr labeled compound was characterized via radio-HPLC and SDS-PAGE followed by autoradiography, and its stability in different solutions was assessed for at least 4 days.

Keywords: zirconium-89; polydentate chelators; hydroxamates; PET-imaging; labeling



Citation: Russelli, L.; De Rose, F.; Leone, L.; Reder, S.; Schwaiger, M.; D'Alessandria, C.; Tei, L. A Semi Rigid Novel Hydroxamate AMPED-Based Ligand for ^{89}Zr PET Imaging. *Molecules* **2021**, *26*, 5819. <https://doi.org/10.3390/molecules26195819>

Academic Editors: António Paulo, Filipa Fernandes Mendes and João D. G. Correia

Received: 30 July 2021

Accepted: 20 September 2021

Published: 25 September 2021

Publisher's Note: MDPI stays neutral with regard to jurisdictional claims in published maps and institutional affiliations.



Copyright: © 2021 by the authors. Licensee MDPI, Basel, Switzerland. This article is an open access article distributed under the terms and conditions of the Creative Commons Attribution (CC BY) license (<https://creativecommons.org/licenses/by/4.0/>).

1. Introduction

A rapidly expanding number of radionuclides with a variety of half-lives, emission types, and energies for the application of radionuclide imaging are routinely produced. When choosing the most suitable radionuclide for a certain application, one should not only consider the decay properties and availability of the radionuclide, but it is also of great importance that the physical half-life of the radionuclide matches the biological half-life of the vector molecule [1,2]. This biological half-life can be in the range of minutes (small organic molecules), hours (peptides, antibody fragments), or even days (full-size monoclonal antibodies). Longer-lived radioisotopes should be selected when an extended time is required to achieve optimal target-to-background ratios, expressed as the ratio between the accumulation of the radiotracer in the target tissue and the accumulation in muscle (as background organ). For diagnostic purposes, a radionuclide with relatively limited energy (100–200 KeV) and a high average path (typical γ rays) that can be detected by a detector near the patient is required. After the decay, the nuclide should lead to a low

activity isotope that can be easily eliminated from the organism. Radioisotopes such as ^{68}Ga , ^{18}F , ^{64}Cu , ^{44}Sc , or ^{89}Zr reflect these characteristics. One of the most important aspects of the development of metal-based PET probes is achieving a stable complexation of the radiometal to avoid its release in the blood pool, and to allow the delivery to a specific target in the body guaranteeing good diagnostic results. The study and development of new chelating ligands for commonly used radioisotopes is nowadays more focused on a series of cyclic, cross-bridged, and acyclic ligands that can lead to more stable and inert complexes with ^{68}Ga , ^{44}Sc , ^{89}Zr , and ^{64}Cu [3]. The well-known AAZTA chelator has already proven to be an interesting ligand for several metal ions due to the thermodynamically stable complexes formed with it [4,5]. In the past years, AAZTA-like derivatives have been synthesized for the successful complexation of ^{68}Ga such as the recent PIDAZTA chelator and the CyAAZTA chelator [6,7]. Moreover, AAZTA was also used for preclinical PET application based on ^{44}Sc radioisotope demonstrating the suitability of this chelating agent for the preparation of Sc-based radiopharmaceuticals [8,9]. Zirconium-89 (^{89}Zr) is a second-row transition metal, and its potential application in PET imaging with ^{89}Zr -based antibodies tracers was first demonstrated in 1992 [10]. Due to its long half-life ($t_{1/2} = 78.4$ h), the development of new radiotracers based on ^{89}Zr has increased in recent years. In particular, zirconium-89 perfectly supports the development of radiotracers for immuno-PET that utilize immunoglobulin G (IgG) antibodies as targeting vectors, which require long periods (days to weeks) to fully accumulate at the target site in vivo [11]. Due to the fact that immunoPET has become the method of choice for imaging not only tumors but also immune cells, immune checkpoints, and inflammatory processes, the radiochemistry of Zr-89 and complexation strategies to use this radioisotope has driven the design and development of new chelators [12]. The main oxidation state of zirconium in aqueous solutions is +4 and for this reason, Zr(IV) (ionic radius = 0.84 Å) can be classified as a hard Lewis acid, and it is ideally complexed by hard Lewis bases, e.g., oxygen donor groups [13]. Since this tetravalent cation usually forms 6- and 8-coordinate complexes, nowadays the development of new ligands for ^{89}Zr is based on the use of hexa and octadentate chelators with hydroxamate functional groups. The hydroxamate moiety is one of the best bidentate chelating groups forming a five-membered chelating ring around hard metal ions such as Zr^{4+} or Fe^{3+} . From potentiometric studies, it was demonstrated that *N*-methylhydroxamate derivatives show improved coordination abilities to form stable Zr(IV)-complexes. Considering the similarities of Zr(IV) with Fe(III), the development of ^{89}Zr chelators is commonly based on the natural complexes of Fe(III) [14]. Siderophores are high-affinity natural Fe(III)-chelating compounds designed to transport iron across cell membranes: they are amongst the strongest soluble Fe(III) binding agents known containing catecholates, hydroxamates, or (α -hydroxy-) carboxylates donor groups [15,16]. Thus, in the past years, new chelators for ^{89}Zr have been developed containing hydroxamates, catecholates, and hydroxypyridinones coordinating groups [17]. Antibody radiolabeling with ^{89}Zr is typically performed using the Desferrioxamine B (DFO) chelator, an FDA approved siderophore bearing three hydroxamate groups involved in the coordination of the metal [18]. However, the high flexibility of this linear chelator accounts for the inadequate stability of the ^{89}Zr -DFO complex and has pushed the development of novel chelators based on macrocyclic structures able to form more inert complexes [19,20]. Moreover, since Zr(IV) can accommodate up to eight donors in its coordination sphere and DFO occupies only six coordination sites, octadentate non-macrocyclic chelators have also been designed and developed [21–23]. In particular, the octadentate version of the DFO chelator, the so-called DFO*, has been developed. Two different functionalized versions of this chelator were synthesized, conjugated with a monoclonal antibody, and tested in vivo showing a lower ^{89}Zr bone uptake over the DFO conjugate [24]. Nowadays, the development of radiotracers for PET imaging is focused on the use of antibodies or antibodies fragments as carriers. Working with antibodies or their derivatives requests to take into account several issues: (i) antibodies are often pH-sensitive as well as heat-sensitive biomolecules; therefore, all reaction steps must be carried out in a reasonable pH range (4–9) and at controlled

temperatures (e.g., 25, 37 °C), to prevent both the formation of irreversible c-structure tetramers and denaturing of the antibody; (ii) during the radiolabeling reactions, due to the sensitivity of antibodies to acidic pH values, it is necessary to work with neutralized solutions prior to radiolabeling [25]; (iii) the radiometal complex has to be stable enough over the time to achieve accumulation of the probe within the target tissue and allowing internalization after binding to the target antigen. In that case, a positron emitter is needed that residualizes in the target cell after internalization, like in the case of ^{89}Zr , to enable imaging at optimal contrast. In this study, we synthesized and characterized two hexadentate AMPED-based ligands for ^{89}Zr complexation investigating their in vitro and in vivo stability. A functionalized derivative of the most promising one was also synthesized and characterized to allow the conjugation with a humanized antibody and the subsequent ^{89}Zr labeling. The stability of the radiolabeled immunoconjugate was then tested in vitro.

2. Results and Discussion

2.1. Ligand Synthesis

In this work, we developed two hexadentate chelators for zirconium-89 starting from the heterocyclic structure of the triamine AMPED by insertion of three bidentate *N*-methylhydroxamate coordinating groups. The 6-amino-6-methyl-1,4-diazepine (AMPED) scaffold was synthesized using the established protocol via the double nitro-Mannich reaction between *N,N*-dibenzylethylenediamine, formaldehyde, and nitroethane, followed by simultaneous hydrogenation of the nitro group and hydrogenolysis of the benzyl moieties with H_2 and Pd/C [4]. The pendant arm was synthesized following a reported procedure starting from *O*-benzyl-hydroxylamine [26]. Briefly, *O*-benzyl-hydroxylamine was protected with benzyl chloroformate, *N*-methylated with methyl iodide, deprotected at the nitrogen with hydrobromic acid (33% in AcOH), and finally acylated by succinic or glutaric anhydride to form the C4 or C5 carbon chains, respectively. The two different pendant arms were then coupled to the AMPED cycle by forming amide bonds using HATU (1-[Bis(dimethylamino)methylene]-1*H*-1,2,3-triazolo[4,5-*b*]pyridinium 3-oxide hexafluorophosphate) activator and DIPEA (*N,N*-diisopropylethylamine) to obtain *O*-benzyl protected AAZTHAS and AAZTHAG ligands as shown in Figure 1. AAZTHAS and AAZTHAG differ for the length of the spacers between the AMPED scaffold and the *N*-methylhydroxamate groups (succinic and glutaric moieties, respectively), based on previous studies where only a succinic spacer was used between the tetraazacyclotetradecane scaffold and the *N*-methylhydroxamate donors [20]. Furthermore, a recent paper by Klasen et al. reported a functionalized version of the chelator called AAZTHAS with the shorter spacer between the chelating units and the AMPED scaffold, showing a lower stability in human serum and PBS even when conjugated to a mAb [27]. As already mentioned in the introduction, the choice of a cyclic-based structure to hold the hydroxamate pendant arms relies on the higher rigidity given by this kind of scaffold to the final complex. In fact, it is reported in the literature that AMPED-based ligands are able to form stable complexes with various metal ions, being a good alternative for the development of tracers for PET imaging [8]. The final chelators were then obtained after hydrogenolysis of the *O*-benzyl groups. Labeling with ^{89}Zr and stability tests in different solutions and human serum (Table 1) showed that ^{89}Zr -AAZTHAG is more stable than ^{89}Zr -AAZTHAS, therefore, the bifunctional AAZTHAG-C₅-OH chelator bearing a tetrafluorophenol (TFP) activated ester to allow the conjugation with biomolecules via amide linkage was then synthesized. The higher stability of the tracer with longer arms highlights the quality of our design and confirms what was reported by Klasen et al. [27].

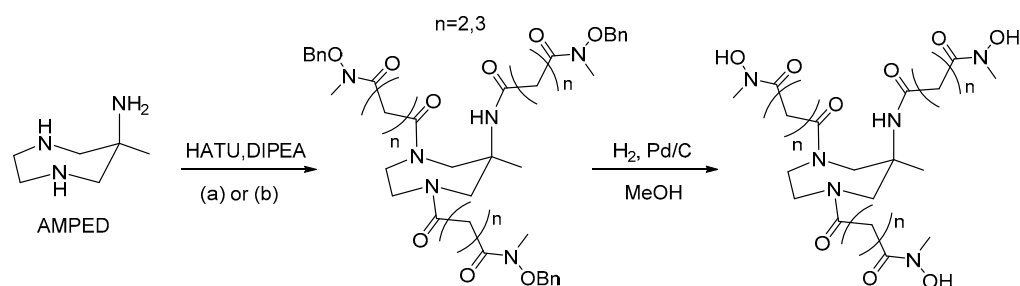


Figure 1. Brief synthesis scheme of AAZTHAS and AAZTHAG chelators. (a) 5-((benzyloxy)(methyl)amino)-2,5-dioxopentanoic acid ($n = 2$), (b) 6-((benzyloxy)(methyl)amino)-2,6-dioxohexanoic acid ($n = 3$).

Table 1. In vitro stability analysis of ^{89}Zr -AAZTHAS, ^{89}Zr -AAZTHAG and ^{89}Zr -AAZTHAG- C_5 -Tz. All the complexes were incubated at 37 °C in formulation buffer (3 mM gentisic acid + 0.25 M NaOAc, pH = 5.5), human serum and EDTA 50 mM solution. Two μL of each radiolabeled complex were spotted onto: (a) a thin-layer chromatography strip (TLC) eluted using elution solution 2; ^{89}Zr -AAZTHAS/ ^{89}Zr -AAZTHAG migrate along the TLC strip ($R_f = 0.9$), while free ^{89}Zr remains at the origin ($R_f = 0.0$); (b) an instant thin-layer chromatography strip (iTLC) eluted using elution solution 1; free ^{89}Zr migrates along the iTLC strip ($R_f = 0.9$), while ^{89}Zr -AAZTHAG- C_5 -Tz remains at the origin ($R_f = 0.0$). Data are expressed as % of ^{89}Zr complexed over total activity measured (^{89}Zr complexed + free ^{89}Zr).

^{89}Zr Tracer	Incubation Solution	Day 0	Day 1	Day 2	Day 3	Day 4
AAZTHAS	Formulation buffer	71.0	63.3	62.3	41.4	n.a. ¹
	HS	71.0	76.8	59.2		n.a.
	EDTA	15.1	1.0	1.6	1.5	n.a.
AAZTHAG	Formulation buffer	91.5 ± 10.6	83.0 ± 6.5	78.1 ± 13.8	73.0 ± 5.2	n.a.
	HS	92.0 ± 11.3	77.7 ± 18.6	76.9 ± 15.4	86.4 ± 5.5	n.a.
	EDTA	30.6 ± 30.3	4.4 ± 3.9	2.4 ± 0.1	3.2 ± 2.6	n.a.
AAZTHAG- C_5 -Tz	Formulation buffer	n.a.	100.0	99.6	99.5	98.8
	HS	n.a.	99.5	98.0	96.0	95.4
	EDTA	n.a.	22.3	20.0	18.6	8

¹ Not applicable.

2.2. Production of AAZTHAG- C_5 -Tz

Briefly, the AMPED scaffold bearing the three *N*-hydroxy-*N*-methylglutaramide pendant arms and an activated pentanoic acid group in 6-position of the cycle was synthesized with the aim to conjugate it to the biological carriers. The 6-position of the functional group is either due to easier synthetic access, as the cyclization was carried out using methyl 6-nitrohexanoate, or due to stereochemical and steric considerations, since the groups placed in this position should prevent any steric influence with the metal and retain the symmetry of the ligand avoiding the generation of stereocentres. Thus, the synthesis of the 6-methylpentanoate-AMPED derivative was performed as reported by Manzoni and colleagues, and then the amino groups were acylated by the *N*-(benzyloxy)-*N*-methylglutaric acid moieties using HATU activator and DIPEA as discussed earlier for the synthesis of AAZTHAG [28]. The final AAZTHAG- C_5 -OH ligand was obtained after LiOH mediated hydrolysis of the methyl ester followed by hydrogenolysis of the *O*-benzyl groups and semi-preparative HPLC-MS purification. The conjugation of the ligand to the $-\text{NH}_2$ groups of Lys residues of the antibody requires the activation of the carboxylic acid group. We choose to activate it by forming a tetrafluorophenol ester using

TFP and EDC (1-ethyl-3-(3-dimethylaminopropyl)carbodiimide), as TFP is more stable than *N*-hydroxysuccinimide group in basic conditions such as those used for the conjugation reaction to antibodies [29]. Briefly, as shown in Figure 2, it was first necessary to protect the hydroxamate groups of the pendant arms by complexing Fe(III) as already reported for the conjugation of mAbs with ^{89}Zr via a tetrafluorophenol-*N*-succinyl-Fe-desferal ester [30]. Then, the activated ester of the complex, Fe-AAZTHAG-C₅-OTFP, was formed by adding TFP/EDC as activators and conjugated to Trastuzumab (Herceptin[®], Tz) in buffer NaHCO₃ at pH = 9 at different temperatures (37–40 °C), times (30 min up to 24 h) and Ab concentrations (1.0 up to 8.0 mg/mL). The optimal conjugation conditions resulted in a conjugation reaction carried out at 40 °C, for 24 h and with a concentration of Ab of 8.0 mg/mL. These conditions differ from the protocol of Verel et al. since the reaction time is longer and the temperature slightly higher, in agreement with procedures reported by other authors [30]. In general, the yield of the conjugation step could be dependent on several parameters, such as the nature of the protein used, the incubation time, temperature, concentration of protein, concentration of chelator, and organic solvent used. Furthermore, the steric hindrance could play a role in this reaction: a semi-rigid chelator would most likely have a higher steric hindrance than the acyclic desferrioxamine B reported in the protocol from Verel and colleagues, reducing the reaction rate. Thus, in the present case, the reaction conditions were optimized to obtain a good recovery of the immunoconjugated product. Then, Fe(III) was removed from the tracer by transchelation reaction with EDTA at pH 4.4. We optimized this step avoiding the use of concentrated H₂SO₄ by carrying out the acidification with a buffer exchange using a solution of 0.25 M sodium acetate + gentisic acid 3 mM pH = 5.5 (called formulation buffer), and then adding EDTA at a concentration of 67.4 mM, as reported elsewhere [30]. The buffer exchange also allowed the purification of the product from the activated complex. The mixture was purified using PD-10 columns with formulation buffer that contains gentisic acid as a scavenger to avoid the radiolysis effect due to γ radiation, produced by ^{89}Zr decay, and responsible for the oxidation of some protein sites, which might cause degradation of antibody structure with possible impairment of biological functions [31,32].

2.3. Determination of Chelator-to-Protein Ratio

The ratio between numbers of chelators AAZTHAG-C₅-OH per molecule of Tz was measured indirectly via metal loading measurement carried out using ICP-MS. To this purpose, the cold $^{\text{nat}}\text{Zr}$ -AAZTHAG-C₅-Tz was synthesized by reaction of the final chelator-Tz conjugate with $^{\text{nat}}\text{Zr}$ and purified on a PD-10 column. The complex was then subjected to both Bradford assay [A] and ICP-MS measurements [B] to determine protein and metal concentrations, respectively. Average values of $2.51 \pm 0.04 \times 10^{-7}$ M and $9.34 \pm 0.03 \times 10^{-8}$ M were obtained for [A] and [B], respectively. Then, the average number of chelators per Ab calculated as [A]/[B], resulted to be 2.6.

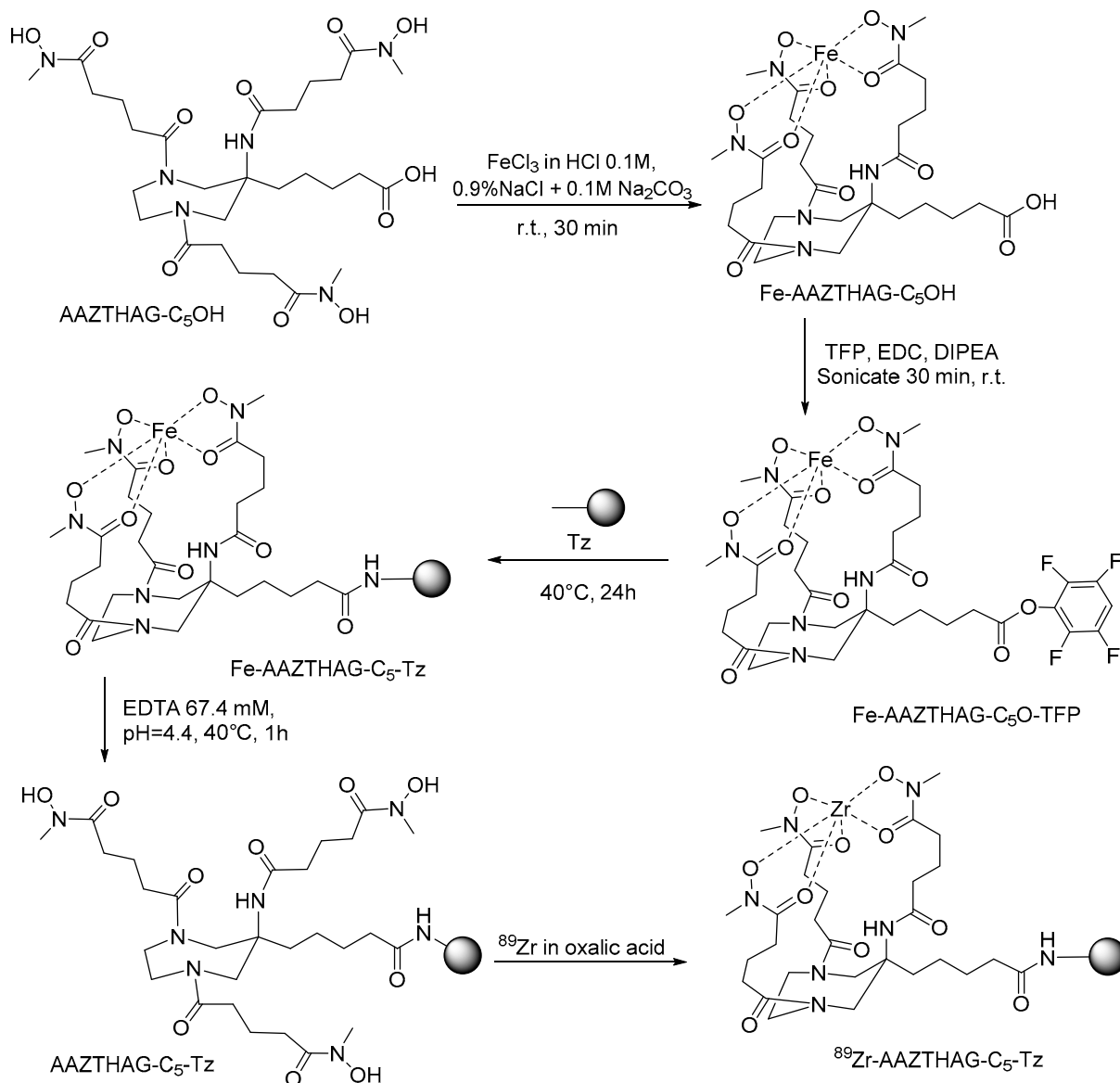


Figure 2. Synthesis scheme of ^{89}Zr -AAZTHAG- C_5 -Tz.

2.4. Radiolabeling and Characterization of AAZTHAG- C_5 -Tz

All labeling reactions were carried out following the procedure reported by Yusufi and colleagues, with slight modifications [33]. The products were then purified by a PD-10 column with formulation buffer as eluent and characterized with SEC-HPLC with γ and UV-VIS detectors. Since the concentration of the antibody can have a significant role during labeling reactions, we optimized the labeling protocol at different concentrations of the immunoconjugated compound. Thus, a radiolabeling yield (RCY) of $60 \pm 15\%$ with a specific activity of $7.1 \pm 2.5 \text{ GBq}/\mu\text{mol}$ was reached using a protein concentration of 8.0 mg/mL. The labeling yield was calculated using the formula:

$$\text{RCY}\% = \frac{\text{final activity } (\mu\text{Ci})}{\text{initial activity } (\mu\text{Ci})} * 100$$

After conjugation, labeling and purification, the product ^{89}Zr -AAZTHAG- C_5 -Tz was analyzed with SEC-radio-HPLC (Figure 3) and compared to Tz to show the successful conjugation and labeling of the tracer.

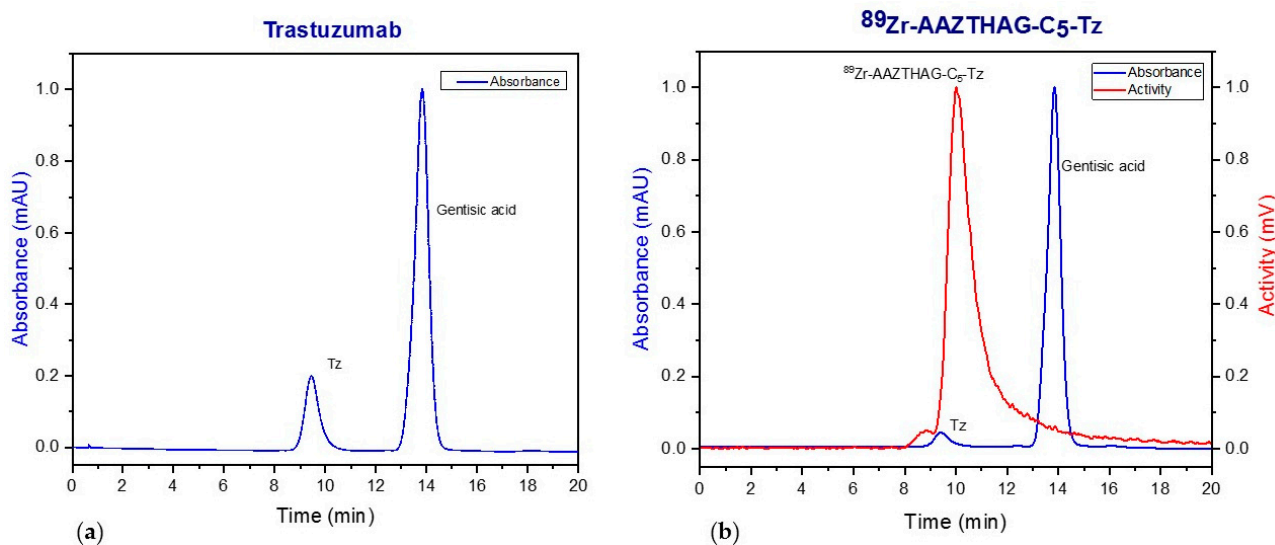


Figure 3. HPLC-SEC chromatogram of (a) Trastuzumab; (b) ⁸⁹Zr-AAZTHAG-C₅-Tz. UV-Vis: $t_r = 9.40$ min; activity: $t_r = 10.00$ min, the peak with $t_r = 13.38$ min is due to Gentisic acid present in the formulation buffer used for the purification of the product. The radioactivity peak has the same retention time as the UV-Vis peak (the small delay between the two peaks is due to the sequential setup of the UV and radioactive detectors), proving that the antibody is conjugated to the ligand and that ⁸⁹Zr is complexed by the ligand-antibody conjugate.

In addition, SDS-PAGE and autoradiography analysis confirmed the integrity of the radiotracer and the association of the radioactivity with the band correspondent to the Trastuzumab (Figure S3).

2.5. In Vitro Stability Studies

Stability studies were performed on ⁸⁹Zr labeled AAZTHAS and AAZTHAG to test the effect of the pendant arm length on complex stability. The stability of the two ⁸⁹Zr-complexes was investigated by radio-TLC after incubation for 72 h at 37 °C in formulation buffer, EDTA 5 mM (1000-fold excess), and human serum (HS). The percentage of ⁸⁹Zr complexed measured in HS and in formulation buffer after 72 h for ⁸⁹Zr-AAZTHAG was $87 \pm 5\%$, and $73 \pm 5\%$, respectively, indicating good in vitro stability of the compound. The stability was higher than that obtained for ⁸⁹Zr-AAZTHAS equal to 46% in HS and 42% in the formulation buffer. These results suggested poor stability of the complex ⁸⁹Zr-AAZTHAS showing a release of the radioisotope; furthermore, the complex tends to precipitate over time probably due to interaction with blood pool proteins. Based on these results, we carried on the study using the glutaramide derivative, since the longer length of the pendant arms resulted in a more stable ⁸⁹Zr-complex.

In human serum, the amount of ⁸⁹Zr associated with ⁸⁹Zr-AAZTHAG after 3 days was $86.4 \pm 5.5\%$. Based on these preliminary results, we also tested the stability of ⁸⁹Zr-AAZTHAG in vivo (see Section 2.6). Then, the stability of the immunoconjugate derivative, ⁸⁹Zr-AAZTHAG-C₅-Tz, was also studied in vitro, showing a high percentage of Zr-89 retained by the complex for at least 4 days of incubation, both in formulation buffer and HS. These findings confirmed that even when functionalized and conjugated to a biomolecule (e.g., mAb) the chelator AAZTHAG can stably complex the Zr-89 isotope, even better than the correspondent non-functionalized version.

2.6. In Vivo Studies with ^{89}Zr -AAZTHAG

Based on the good preliminary in vitro stability results, we investigated the behavior of ^{89}Zr -AAZTHAG in vivo in healthy female nude mice ($n = 3$) by acquiring PET/CT images at six different time points (30 min, 3 h, 6 h, 9 h, 12 h, and 24 h), and mice were then sacrificed 24 h p.i. to perform a biodistribution study. In Figure 4 below are reported the PET/CT images at the six time points, where a hepatobiliary and renal excretion is visible. Moreover, since a very low amount of Zr-89 has been released from the complex, a low signal in bones was visualized during the PET acquisition, indicating good stability in vivo, comparable to other compounds reported in the literature [21].

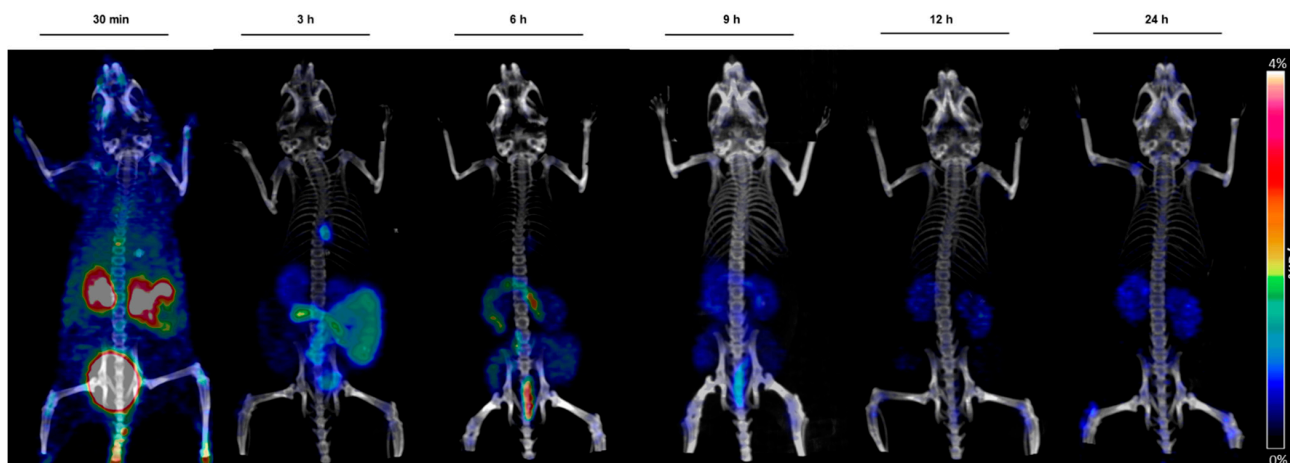


Figure 4. Maximum image projections (MIPs) obtained from static PET/CT scans at different time points. A hepatobiliary and renal excretion is clearly visible as well as a low accumulation in bones and kidneys 24 h p.i. Scale bar: 0–4%ID/g.

From a comparison between the biodistribution data of ^{89}Zr -AAZTHAG and those described by Deri et al., on the HOPO chelator (Figure S4), it can be inferred that ^{89}Zr -AAZTHAG presents higher stability and favorable low accumulation in selected organs such as liver, intestine, heart, muscle, bladder, and kidneys when compared to DFO, and a similar accumulation in femur and kidneys when compared to HOPO [21].

2.7. Ex Vivo Studies

Tracer accumulation results (Figure 5 and Figure S5) show high in vivo stability of the labeled complex ^{89}Zr -AAZTHAG, as demonstrated by the low ^{89}Zr accumulation measured in the femur ($0.193 \pm 0.108\%$ ID/g), kidneys ($0.575 \pm 0.199\%$ ID/g), and other organs at 24 h p.i. These results are comparable to those reported in the literature for in vivo stability studies of desferrioxamine (DFO) and another alternative chelator for Zr-89, the so-called HOPO chelator [21]. According to the PET images, our biodistribution data confirm the fast hepatobiliary/renal excretion of the labeled ligand due to the low molecular weight (558.63 Da) [34]. Although a “naked” and negatively charged ^{89}Zr -chelate complex does not persist in vivo long enough to encounter a challenge to its structural integrity compared to a conjugated version, nevertheless, the results obtained show a stable ^{89}Zr -complex once conjugated with a biomolecule. As already reported above, the functionalized version of this chelator was afterwards synthesized and conjugated to Tz, as a proof of concept. No damage occurred to the structure of the monoclonal antibody Trastuzumab once conjugated and radiolabeled with ^{89}Zr , as confirmed by SDS-PAGE + autoradiography analysis and by stability analysis in vitro over time.

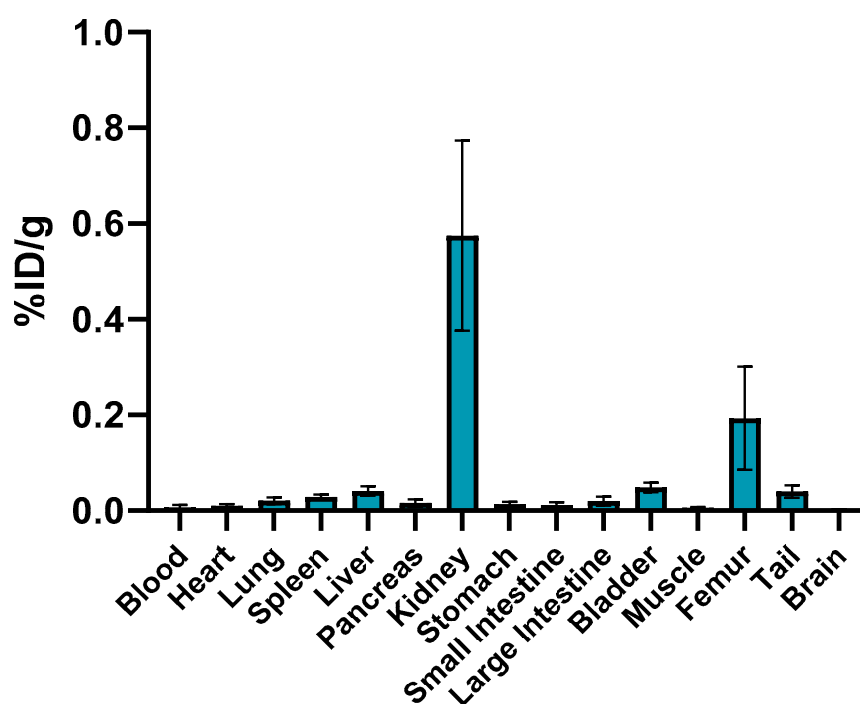


Figure 5. Biodistribution data of ^{89}Zr -AAZTHAG on female healthy nude mice in selected organs measured 24 h p.i. The activity accumulated is reported as percentage of injected dose per gram (%ID/g \pm SD) ($n = 3$).

3. Materials and Methods

3.1. General

All chemicals were purchased from Sigma-Aldrich (Saint Louis, MI, USA) or Alfa Aesar (Heysham, UK) unless otherwise stated and were used without further purification. The ^1H and ^{13}C NMR spectra were recorded using a Bruker Avance III 500 MHz (11.4 T) spectrometer equipped with 5 mm PABBO probes and a BVT-3000 temperature control unit. Chemical shifts δ are reported relative to TMS and were referenced using the residual proton solvent resonances. HPLC analyses and mass spectra were performed on a Waters HPLC-MS system equipped with a Waters 1525 binary pump. Analytical measurements were carried out on a Waters XTerra MS C18 (5 μm 4.6 \times 100 mm) and on a Waters C18 XTerra Prep (5 μm 19 \times 50 mm) for preparative purposes. Electrospray ionization mass spectra (ESI MS) were recorded using an SQD 3100 Mass Detector (Waters), operating in positive or negative ion mode, with 1% *v/v* formic acid in methanol as the carrier solvent. The concentration of Trastuzumab and the immunoconjugated tracer (before labeling) were measured with an IMPLEN NanoPhotometer P330 (IMPLEN). For the purification of the final tracer before and after the labeling reaction, a PD-10 desalting column (Sephadex G-25 resin, GE Healthcare Life Sciences, London, UK) was used using a buffer solution of gentisic acid (2,5-dihydroxybenzoic acid) 3 mM + 0.25 M sodium acetate, pH = 5.5 (formulation buffer) as eluent. The immunoconjugated tracer (before and after labeling) was characterized by a Prominence HPLC system (Shimadzu, Kyoto, Japan) with a Photo Diode Array detector (Shimadzu) and a GABI Star γ detector (Raytest, Straubenhardt, Germany) with an SEC column Yarra 3 μm SEC-3000 (Phenomenex, Torrance, CA, USA) and isocratic elution with a PBS buffer (pH = 6.8) and a flow rate of 1 mL/min. The radiotracer was further characterized by SDS-PAGE in non-reducing conditions loading 20 μg of sample in each well, running the gel for 90 min at 100 V. The gel was stained using Coomassie Blue staining solution, followed by autoradiography measurement performed by exposing the gel to phosphorimaging plates (Fujifilm, Fuji, Tokyo, Japan) for 24 h. Read-out of the plate was performed with a Phosphor-imager (CR35 BIO, Dürr-Biomedical, Miami, FL, USA), and the radioactive signals associated with the bands corresponding to

the intact tracer on the autoradiography images were analyzed using AIDA Image analyzer software. The ^{89}Zr used during the labeling experiments was purchased from Perkin Elmer (Skovlunde, Denmark). The activity during experiments was measured with a Capintec CRC[®] 15 R dose calibrator. Radiochemical yields (RCYs) were determined by radio-TLC using different elution solutions (Elution solution 1: 0.1 M sodium citrate pH = 5; Elution solution 2: ACN/H₂O 7:3) and either TLC silica gel 60 plates (Merck Millipore, Burlington, MA, USA) or instant thin-layer chromatographic stripes (iTLC, Agilent). The stripes were read-out using a radio-TLC-scanner (Bioscan, Eckert and Ziegler, Brussels, Belgium) and data were analyzed by the Bio-Chrom Lite software. PET/CT scans of animals were performed using an Inveon Small Animal PET/CT scanner (Siemens, Knoxville, TN, USA). During ex vivo experiments, the activity accumulation in specific organs was measured using a γ -counter (Perkin Elmer).

3.2. Synthesis of AAZTHAS

The *N*-methyl-*N*-(benzyloxy)succinamide [26] protected arm (102 mg, 0.43 mmol, 4 eq) was dissolved in DMF (2 mL) and DIPEA (77 μL , 0.43 mmol, 4 eq) was added. The mixture was reacted for 5 min and then HATU (164 mg, 0.43 mmol, 4 eq) was added to activate the carboxylic acid. After 15 min, a solution of AMPED [4] (14 mg, 0.11 mmol, 1 eq) in MeOH was added dropwise and the mixture was reacted overnight at room temperature [20]. Then, AcOEt (+HCl 0.1 M) was added to the mixture and after 2 h the product was extracted in the organic phase, separated, dried, and evaporated under vacuum. The mixture was dissolved in MeOH to perform a hydrogenolysis reaction with Pd/C (10%) in an H₂ atmosphere for 4 h under strong stirring. The mixture was then filtered on Celite[®] 500 and washed well with MeOH. The final mixture was then purified with a preparative HPLC-MS with the following method: Flow: 20 mL/min H₂O (+0.1% TFA)/MeOH; 0–3 min: from 5 to 40% B; 3–15 min: from 40 to 80% B; 15–16 min: from 80 to 100% B; 16–20 min: 100% B; 20–21 min from 100 to 5% B. The product (15 mg) was obtained in 27.3% yield. ¹H NMR (Figure S6) (D₂O, 500 MHz) δ (ppm): 1.29 (s, 3H, CH₃-cycle), 2.52–2.72 (m, 3 \times 4H, -CH₂CH₂CONOH), 3.40–3.86 (m, 4 \times 2H, cycle), 3.13 (s, 9H, -CONCH₃). ¹³C NMR (Figure S7) (D₂O, 500 MHz) δ (ppm): 20.88 (CH₃-cycle), 27.13–27.53 (-CH₂CH₂CONOH), 31.3–31.4 (-CH₂CH₂CONOH), 35.9 (-CONCH₃), 48.94 (C-cycle), 46.43–57.97 (cycle), 162.78–163.07 (-NHCOCH₂-), 174.22–174.71 (-CONOH). MS ESI⁺ *m/z*: 516.25 (C₂₁H₃₆N₆O₉ calculated), 517.53 [M + H]⁺ observed.

3.3. Synthesis of AAZTHAG

N-methyl-*N*-(benzyloxy)glutaramide [26] protected arm (106 mg, 0.43 mmol, 4 eq) was dissolved in DMF (2 mL) and DIPEA (77 μL , 0.43 mmol, 4 eq) was added. The mixture was reacted for 5 min and then HATU (164 mg, 0.43 mmol, 4 eq) was added to activate the carboxylic acid. After 15 min, a solution of AMPED [4] (14 mg, 0.11 mmol, 1 eq) in MeOH was added dropwise and the mixture was reacted overnight at room temperature [20]. Then AcOEt (+HCl 0.1 M) was added to the mixture and after 2 h the product was extracted in the organic phase, separated, dried, and evaporated under vacuum. The mixture was dissolved in MeOH to perform a hydrogenolysis reaction with Pd/C (10%) in an H₂ atmosphere for 4 h under strong stirring. The mixture was then filtered on Celite[®] 500 and washed well with MeOH. The final mixture was then purified with a preparative HPLC-MS with the following method: Flow: 20 mL/min H₂O (+0.1% TFA)/MeOH; 0–3 min: from 5 to 40% B; 3–15 min: from 40 to 80% B; 15–16 min: from 80 to 100% B; 16–20 min: 100% B; 20–21 min from 100 to 5% B. The product (13 mg) was obtained in 20% yield. ¹H NMR (Figure S8) (D₂O, 500 MHz) δ (ppm): 1.41 (s, 3H, CH₃-cycle), 1.88 (m, 3 \times 2H -CH₂CH₂CH₂CONOH), 2.45–2.56 (m, 3 \times 4H, -CH₂CH₂CH₂CONOH), 3.28 (s, 9H, -CONCH₃), 3.60–4.20 (m, 4 \times 2H, cycle). ¹³C NMR (Figure S9) (D₂O, 500 MHz) δ (ppm): 20.27 (CH₃-cycle), 20.85–21.55 (-CH₂CH₂CH₂CONOH), 30.78–31.43 (-CH₂CH₂CH₂CONOH), 32.11–32.41 (-CH₂CH₂CH₂CONOH), 36.94 (-CONCH₃), 49.15 (C-

cycle), 46.29–58.30 (cycle), 162.90–163.20 (-NHCOCH₂-), 174.98–175.42 (-CONOH). MS ESI⁺ *m/z*: 558.30 (C₂₄H₄₂N₆O₉ calculated), 559.64 [M + H]⁺ observed.

3.4. Synthesis of AAZTHAG-C₅-Tz

3.4.1. AAZTHAG-C₅OH

The *N*-methyl-*N*-(benzyloxy)glutaramide [26] (88 mg, 0.35 mmol, 4 eq) was dissolved in DMF (1.8 mL) and DIPEA (60 µL, 0.35 mmol, 4 eq) was added. The mixture was reacted for 5 min and then HATU (133 mg, 0.35 mmol, 4 eq) was added to activate the carboxylic acid. After 15 min a solution of the functionalized AMPED [28] (20 mg, 0.087 mmol, 1 eq) in MeOH was added dropwise and the mixture was reacted overnight at room temperature [20]. Then AcOEt (+HCl 0.1 M) was added to the mixture and after 2 h the product was extracted in the organic phase, separated, dried, and evaporated under vacuum to obtain the intermediate compound I1 (Figure S2). The mixture was dissolved in MeOH adding a 5 mM solution of LiOH in MeOH/H₂O and reacted overnight. The pH was adjusted to pH = 3 and the solvent was evaporated under reduced pressure. The product was washed with 10 mL of CH₂Cl₂ (×2), dried, filtered and the solvent was evaporated under reduced pressure to give 42 mg of the intermediate I2 (Figure S2). After hydrogenolysis reaction with Pd/C (10%) in an H₂ atmosphere for 4 h under strong stirring, the final mixture was filtered on Celite[®] 500 and then purified with a preparative HPLC-MS with the following method: Flow: 20 mL/min H₂O (+0.1% TFA)/MeOH; 0–3 min: from 5 to 40% B; 3–15 min: from 40 to 80% B; 15–16 min: from 80 to 100% B; 16–20 min: 100% B; 20–21 min from 100 to 5% B. The product (6 mg) was obtained in 10% yield. ¹H NMR (Figure S10) (D₂O, 500 MHz) δ(ppm): 1.35 (d, 2H, -C_γH₂-), 1.50 (m, 2H -C_δH₂), 1.59 (m, 2H, -C_βH₂-), 2.25 (m, 3 × 2H, -CH₂CH₂CH₂CONOH), 2.41 (m, 2H, -C_αH₂COOH), 2.53 (m, 3 × 4H, -CH₂CH₂CH₂CONOH), 3.25 (s, 3 × 3H, -CONCH₃), 3.38–3.91 (m, 4 × 2H, cycle). ¹³C NMR (Figure S11) (D₂O, 500 MHz) δ (ppm): 20.28 (-C_γH₂-), 22.04 (-CH₂CH₂CH₂CONOH), 24.31 (-C_βH₂-), 30.88 (-CH₂CH₂CH₂CONOH), 31.39–32.4 (-CH₂CH₂CH₂CONOH), 32.84–32.92 (-C_αH₂-), 33.4 (-C_δH₂-), 35.93 (-CONCH₃), 46.48–55.17 (AAZTA cycle), 174.9–175 (-COCH₂CH₂CH₂CONOH), 175.46–176.14 (-CH₂CH₂CH₂CONOH), 178.70 (-COOH). MS ESI⁺ *m/z*: 644.34 (C₂₈H₄₈N₆O₁₁ calculated), 645.73 [M + H]⁺ observed.

3.4.2. AAZTHAG-C₅-OTFP

According to Verel and colleagues [35], 19 µL of a 41 mM solution of AAZTHAG-C₅-OH were mixed with 170 µL of 0.9% NaCl (+0.1 M Na₂CO₃) and to this solution, 6.1 µL of FeCl₃ 140 mM in 0.1% HCl was added to give a final concentration of AAZTHAG-C₅-OH of 4 mM. After 30 min at room temperature under stirring the compound was freeze-dried. 0.78 µmol of the obtained Fe-AAZTHAG-C₅-OH were dissolved in 170 µL of ACN/H₂O and to this solution a 200 mg/mL ACN solution of TFP (17.1 µL, 20.6 µmol, 26.4 eq) and EDC (6.9 mg, 36.1 µmol, 43.3 eq) was added, pH = 5.8–6, carrying out to the formation of a brown-orange precipitate. The mixture was sonicated for 30 min at room temperature, and then the precipitate was washed with ACN/H₂O and dried to obtain the Fe-AAZTHAG-C₅-OTFP.

3.4.3. AAZTHAG-C₅-Tz

The chelator was then conjugated with Trastuzumab (Herceptin[®]) as follows. Briefly, a 21 mg/mL solution of Tz in PBS buffer (pH = 6.8) underwent a buffer exchange with a NaHCO₃ buffer (pH = 9) using a 100 kDa Amicon Ultra 0.5 mL centrifugal filter unit (Merck Millipore). The concentration was then adjusted to 8 mg/mL and afterwards a 5 mM DMSO solution of Fe-AAZTHAG-C₅-OTFP (5 eq) was added. The solution was kept in the dark and allowed to react under soft stirring for 24 h at 40 °C. The final solution underwent an additional buffer exchange step with an Amicon Ultra centrifugal filter (Merck) and formulation buffer (pH = 4.4) and then a 67.4 mM solution of EDTA (50 eq) was added. The demetallation reaction was carried out at 40 °C for 1 h. The product was then purified using a PD-10 column and formulation buffer (pH = 5.5). The antibody

recovery after conjugation (up to 80%) was calculated comparing the initial and final concentration of the carrier species measured with the Nanophotometer as reported below:

$$\text{Ab recovery (\%)} = \frac{[\text{Ab}]_f}{[\text{Ab}]_i} * 100$$

3.5. Radiolabeling Experiments

AAZTHAS, AAZTHAG, and AAZTHAG-C₅-Tz were labeled with ⁸⁹Zr (Perkin Elmer) as reported elsewhere [33] and radiochemical purity (RCY) after PD-10 purification assessed by radio-HPLC and by radio-TLC.

3.5.1. Synthesis of ⁸⁹Zr-AAZTHAS and ⁸⁹Zr-AAZTHAG

The labeling reactions were performed with a ratio of 80 µg of the compound to 1 mCi ⁸⁹Zr in 100 µL oxalic acid 1 M (eventually adjusting the volume with oxalic acid 1 M). The ⁸⁹Zr-oxalate solution was first neutralized with 45 µL of Na₂CO₃ 2M and incubated for 3 min at room temperature, and then 155 µL of HEPES (pH = 7.0) was added. Either AAZTHAS or AAZTHAG was added to the solution and the pH was adjusted with 350 µL of HEPES buffer to pH = 7.0. The solution was incubated at 37 °C for 30 min and RCYs were afterwards calculated by radio-TLC (Elution solution 2). The products were purified using a Sep-Pak Alumina N Plus Light cartridges preconditioned with 5 mL of 0.9% NaCl solution and then eluted with 1.5 mL of 0.9% NaCl solution.

3.5.2. Synthesis of ⁸⁹Zr-AAZTHAG-C₅-Tz

Three different concentrations of the immunoconjugated product (1.0, 2.0, and 5.0 mg/mL) were tested. The labeling reactions were performed with a ratio of 500 µg of AAZTHAG-C₅-Tz to 1 mCi ⁸⁹Zr in 100 µL oxalic acid 1 M (eventually adjusting the volume with oxalic acid 1 M). The ⁸⁹Zr-oxalate solution was first neutralized with 45 µL of Na₂CO₃ 2 M and incubated for 3 min at room temperature, and then 155 µL of HEPES (pH = 7.0) was added. At this point, the AAZTHAG-C₅-Tz was added to the solution and the pH was adjusted with 350 µL of HEPES buffer to pH = 7.0. The solution was incubated at 37 °C for 30 min and the product was purified using a PD-10 desalting column with formulation buffer, collecting the eluate in different fractions of about 700 µL (20 drops). RCY was calculated by radio-TLC (Elution solution 1). The product was then characterized by SEC-HPLC with isocratic elution using PBS buffer (pH = 6.8) as solvent.

3.6. In Vitro Stability Studies

After the purification step and analysis of the radioactive complex via radio-HPLC, the stability assessment of the complex at different time points and in different solutions was carried out. ⁸⁹Zr-AAZTHAS and ⁸⁹Zr-AAZTHAG were dissolved in formulation buffer, EDTA 5 mM, and human serum in 1:5 *v/v* ratio and were incubated at 37 °C up to 96 h. At each time point the stability was evaluated by radio-TLC (Elution solution 2) using TLC silica gel 60 plates (Merck Millipore). ⁸⁹Zr-AAZTHAG-C₅-Tz was dissolved in formulation buffer, EDTA 5 mM and human serum in 1:5 *v/v* ratio and was incubated at 37 °C up to 96 h. At each time point the stability was evaluated by radio-iTLC (Elution solution 1) using an instant thin-layer chromatographic strip (iTLC, Agilent).

3.7. Determination of Chelator-to-Protein Ratio

The metal loading of the conjugate was determined by complexing 0.5 mg of AAZTHAG-C₅-OH with ^{Nat}Zr(IV) (ZrCl₄, 162 µg, 0.9 eq), for 30 min at room temperature. After lyophilization, ^{Nat}Zr-AAZTHAG-C₅-OH was dissolved in 170 µL of ACN/H₂O and to this solution, 17.1 µL of a 200 mg/mL ACN solution of TFP (20.6 µmol, 26.4 eq) and 6.9 mg of EDC (36.1 µmol, 43.3 eq) were added (pH = 5.8–6.0) and carried out until the formation of a brown-orange precipitate. The mixture was sonicated for 30 min at room temperature, and the precipitate was washed with ACN/H₂O and dried to obtain the

^{89}Zr -AAZTHAG- C_5 -OTFP. The product was then conjugated with Trastuzumab. To a NaHCO_3 buffer solution of Tz (pH = 9.0) a 5 mM DMSO solution of ^{89}Zr -AAZTHAG- C_5 -OTFP (5 eq) was added and was reacted at 40 °C for 24 h under soft stirring and kept in the dark. The conjugate was then purified using a PD-10 column and formulation buffer (pH = 5.5) and the collected fractions were then subjected to both a Bradford assay [A] to determine the protein concentration and to ICP-MS measurements [B] to determine the metal concentrations. Regarding ICP-MS experiments, the fractions were digested with HNO_3 (69% *w/w*) for 3 h at 65 °C in an ultrasonic bath. After the completion of the mineralization run and the cooling to room temperature, the content was transferred into a marked flask using HNO_3 1%. Metal quantification was measured by inductively coupled plasma-mass spectrometry (ICP-MS, Thermo Optek X Series 2).

3.8. Animal Studies

3.8.1. In Vivo Studies with ^{89}Zr -AAZTHAG

In order to study the biodistribution and the in vivo stability of the ^{89}Zr -AAZTHAG, 8 weeks old pathogen-free female athymic Nude-Foxn1nu/nu mice (Charles River Laboratories, Sulzfeld, Germany) ($n = 3$) were injected via a catheter in the tail vein with 2.9 ± 0.1 MBq of ^{89}Zr -AAZTHAG in 300 μL NaCl 0.9% solution, and imaged at different time points (30 min, 3 h, 6 h, 9 h, 12 h, 24 h) via PET/CT static acquisition using an Inveon Small Animal PET/CT scanner (Siemens, Knoxville, TN, USA).

3.8.2. Ex Vivo Tracer Accumulation Analysis

Biodistribution studies were also performed to assess the in vivo distribution of the ^{89}Zr -AAZTHAG complex and evaluate its in vivo stability. After sacrifice, the mice by anesthesia, blood, and other selected organs were collected, weighed, and the activity was measured by a γ -counter. The tracer accumulation in selected organs was expressed as a percentage of injected dose per gram of tissue (%ID/g).

4. Conclusions

New pseudo-macrocyclic ligands for ^{89}Zr complexation for PET imaging were synthesized, in particular, two non-functionalized chelators, AAZTHAS and AAZTHAG, and one functionalized for conjugation to biomolecules, AAZTHAG- C_5 -OTFP. All three chelators are based on N-methylhydroxamate coordination groups accordingly to the coordination sphere of Zr^{4+} . Preliminary labeling and in vitro stability studies were performed, focused on testing the effect of the length of the spacer arms in the AAZHTAS and AAZTHAG chelators. The initial hypothesis was that longer pendant arms would better coordinate the Zr-89 isotope, leading to a more stable complex over time. In fact, while the complex ^{89}Zr -AAZTHAS precipitates when incubated in HS, the chelator AAZTHAG formed an ^{89}Zr -complex stable in HS for at least 4 h. Very recent work from Klasen and colleagues, which showed low stability both in PBS and human serum of the functionalized version of AAZTHAS conjugated to a mAb, supports our results [27]. A functionalized version of the AAZTHAG chelator was then synthesized since it was confirmed that a longer spacer arm leads to a more stable ^{89}Zr -complex. The protocol used for the conjugation reaction between the ligand and the antibody was optimized with the aim to increase both reaction and labeling yield, avoiding the biomolecules to be subjected to strong reaction conditions. The optimized procedure allowed to obtain a final RCY of 41% after the labeling reaction of AAZTHAG- C_5 -Tz. Based on the obtained results, future work can be directed towards two main lines: (1) focusing on a direct conjugation approach of the chelator to the biomolecule avoiding the “protection/deprotection” steps consisting of the Fe(III) complexation and EDTA transchelation reactions. This can be obtained, for example, by modifying the functional group from a carboxylic acid to isothiocyanate or maleimide groups. In fact, the introduction of these functional groups could reduce the time of the conjugation/labeling procedure being a valid alternative for the conjugation reaction with mAb [1,18,36]. (2) Another modification that could be applied to the ligand

is the introduction of a fourth pendant arm leading to an octadentate chelator that could be, together with the use of cyclic chelators, the key to produce a highly stable complex as recently reported for the DFO derivative DFO* [2,37] For this purpose, a new synthetic strategy must be planned.

Supplementary Materials: The following are available online. Figure S1: Synthesis scheme of AAZTHAS and AAZTHAG, Figure S2: Synthesis scheme of AAZTHAG-C₅-OH, Figure S3: SDS-PAGE and autoradiography of ⁸⁹Zr-AAZTHAG-C₅-Tz, Figure S4: Comparison between biodistribution data of ⁸⁹Zr-AAZTHAG with ⁸⁹Zr-DFO and ⁸⁹Zr-HOPO, Table S5: Biodistribution data of ⁸⁹Zr-AAZTHAG, Figures S6–S11: ¹H and ¹³C NMR spectra of final ligands.

Author Contributions: Conceptualization, L.T. and C.D.; methodology, L.R., F.D.R. and L.L.; validation, L.R.; formal analysis, L.R.; investigation, L.R., F.D.R., L.L. and S.R.; technical resources, M.S.; data curation, L.R.; writing—original draft preparation, L.R.; writing—review and editing, L.T. and C.D.; supervision, L.T. and C.D.; project administration, L.T. and C.D.; funding acquisition, L.T. and C.D. All authors have read and agreed to the published version of the manuscript.

Funding: This work was partially supported by the DEUTSCHE FORSCHUNGSGEMEINSCHAFT (SFB824 Project C10) granted to C.D. and by the ALEXANDER VON HUMBOLDT FOUNDATION granted to L.T.

Institutional Review Board Statement: All animal experiments were approved by local authorities (animal license: 55.2-1-54-2532-216-15) and handled according to guidelines for the welfare and use of animals in experimental procedures.

Informed Consent Statement: Not applicable.

Data Availability Statement: The data are available on request from the corresponding author.

Acknowledgments: L.R. and C.D. acknowledge Markus Mittelhäuser for technical support during animal injections and PET/CT scans.

Conflicts of Interest: The authors declare no conflict of interest.

Sample Availability: Samples of the compounds are not available from the authors.

References

1. Price, E.W.; Orvig, C. Matching chelators to radiometals for radiopharmaceuticals. *Chem. Soc. Rev.* **2014**, *43*, 260–290. [[CrossRef](#)]
2. Price, T.W.; Greenman, J.; Stasiuk, G.J. Current advances in ligand design for inorganic positron emission tomography tracers ⁶⁸Ga, ⁶⁴Cu, ⁸⁹Zr and ⁴⁴Sc. *Dalt. Trans.* **2016**, *45*, 15702–15724. [[CrossRef](#)]
3. Wadas, T.J.; Wong, E.H.; Weisman, G.R.; Anderson, C.J. Coordinating radiometals of copper, gallium, indium, yttrium, and zirconium for PET and SPECT imaging of disease. *Chem. Rev.* **2010**, *110*, 2858–2902. [[CrossRef](#)]
4. Aime, S.; Calabi, L.; Cavallotti, C.; Gianolio, E.; Giovenzana, G.B.; Losi, P.; Maiocchi, A.; Palmisano, G.; Sisti, M. [Gd-AAZTA]-: A new structural entry for an improved generation of MRI contrast agents. *Inorg. Chem.* **2004**, *43*, 7588–7590. [[CrossRef](#)] [[PubMed](#)]
5. Baranyai, Z.; Uggeri, F.; Maiocchi, A.; Giovenzana, G.B.; Cavallotti, C.; Takács, A.; Tóth, I.; Bányai, I.; Bényei, A.; Brucher, E.; et al. Equilibrium, kinetic and structural studies of AAZTA complexes with Ga³⁺, In³⁺ and Cu²⁺. *Eur. J. Inorg. Chem.* **2013**, 147–162. [[CrossRef](#)]
6. Farkas, E.; Vágner, A.; Negri, R.; Lattuada, L.; Tóth, I.; Colombo, V.; Esteban-Gómez, D.; Platas-Iglesias, C.; Notni, J.; Baranyai, Z.; et al. PIDAZTA: Structurally Constrained Chelators for the Efficient Formation of Stable Gallium-68 Complexes at Physiological pH. *Chem. A Eur. J.* **2019**, *25*, 10698–10709. [[CrossRef](#)]
7. Vágner, A.; D’Alessandria, C.; Gambino, G.; Schwaiger, M.; Aime, S.; Maiocchi, A.; Tóth, I.; Baranyai, Z.; Tei, L. A rigidified AAZTA-like ligand as efficient chelator for ⁶⁸Ga radiopharmaceuticals. *Chem. Sel.* **2016**, *1*, 163–171. [[CrossRef](#)]
8. Nagy, G.; Szikra, D.; Trencsényi, G.; Fekete, A.; Garai, I.; Giani, A.M.; Negri, R.; Masciocchi, N.; Maiocchi, A.; Uggeri, F.; et al. AAZTA: An Ideal Chelating Agent for the Development of ⁴⁴Sc PET Imaging Agents. *Angew. Chemie Int. Ed.* **2017**, *56*, 2118–2122. [[CrossRef](#)] [[PubMed](#)]
9. Ghiani, S.; Hawala, I.; Szikra, D.; Trencsényi, G.; Baranyai, Z.; Nagy, G.; Vágner, A.; Stefania, R.; Pandey, S.; Maiocchi, A. Synthesis, radiolabeling, and pre-clinical evaluation of [⁴⁴Sc]Sc-AAZTA conjugate PSMA inhibitor, a new tracer for high-efficiency imaging of prostate cancer. *Eur. J. Nucl. Med. Mol. Imaging* **2021**. [[CrossRef](#)]
10. Meijs, W.E.; Herscheid, J.D.M.; Haisma, H.J.; Pinedo, H.M. Evaluation of desferal as a bifunctional chelating agent for labeling antibodies with Zr-89. *Int. J. Radiat. Appl. Instrum. Part* **1992**, *43*, 1443–1447. [[CrossRef](#)]
11. Brandt, M.; Cardinale, J.; Aulsebrook, M.L.; Gasser, G.; Mindt, T.L. An overview of PET radiochemistry, part 2: Radiometals. *J. Nucl. Med.* **2018**, *59*, 1500–1506. [[CrossRef](#)]

12. Wei, W.; Rosenkrans, Z.T.; Liu, J.; Huang, G.; Luo, Q.Y.; Cai, W. ImmunoPET: Concept, Design, and Applications. *Chem. Rev.* **2020**, *120*, 3787–3851. [[CrossRef](#)]
13. Shannon, R.D. Revised effective ionic radii and systematic studies of interatomic distances in halides and chalcogenides. *Acta Crystallogr. Sect. A* **1976**, *32*, 751–767. [[CrossRef](#)]
14. Guérard, F.; Lee, Y.-S.; Tripier, R.; Szajek, L.P.; Deschamps, J.R.; Brechbiel, M.W. Investigation of Zr(v) and ⁸⁹Zr(iv) complexation with hydroxamates: Progress towards designing a better chelator than desferrioxamine B for immuno-PET imaging. *Chem. Commun.* **2013**, *49*, 1002–1004. [[CrossRef](#)] [[PubMed](#)]
15. Neilands, J.B. Siderophores: Structure and Function of Microbial Iron Transport Compounds. *J. Biol. Chem.* **1995**, *270*, 26723–26726. [[CrossRef](#)] [[PubMed](#)]
16. Miethke, M.; Marahiel, M.A. Siderophore-Based Iron Acquisition and Pathogen Control. *Microbiol. Mol. Biol. Rev.* **2007**, *71*, 413–451. [[CrossRef](#)] [[PubMed](#)]
17. Gorden, A.E.V.; Xu, J.; Raymond, K.N.; Durbin, P. Rational Design of Sequestering Agents for Plutonium and Other Actinides. *Chem. Rev.* **2003**, *103*, 4207–4282. [[CrossRef](#)] [[PubMed](#)]
18. Perk, L.R.; Vosjan, M.J.W.D.; Visser, G.W.M.; Budde, M.; Jurek, P.; Kiefer, G.E.; Van Dongen, G.A.M.S. P-Isothiocyanatobenzyl-desferrioxamine: A new bifunctional chelate for facile radiolabeling of monoclonal antibodies with zirconium-89 for immuno-PET imaging. *Eur. J. Nucl. Med. Mol. Imaging* **2010**, *37*, 250–259. [[CrossRef](#)]
19. Pandya, D.N.; Bhatt, N.; Yuan, H.; Day, C.S.; Ehrmann, B.M.; Wright, M.; Bierbach, U.; Wadas, T.J. Zirconium tetraazamacrocyclic complexes display extraordinary stability and provide a new strategy for zirconium-89-based radiopharmaceutical development. *Chem. Sci.* **2017**, *8*, 2309–2314. [[CrossRef](#)]
20. Boros, E.; Holland, J.P.; Kenton, N.; Rottle, N.; Caravan, P. Macrocyclic-Based Hydroxamate Ligands for Complexation and Immunoconjugation of ⁸⁹Zirconium for Positron Emission Tomography (PET) Imaging. *ChemPlusChem* **2016**, *81*, 274–281. [[CrossRef](#)] [[PubMed](#)]
21. Deri, M.A.; Ponnala, S.; Zeglis, B.M.; Pohl, G.; Dannenberg, J.J.; Lewis, J.S.; Francesconi, L.C. Alternative Chelator for ⁸⁹Zr Radiopharmaceuticals: Radiolabeling and Evaluation of 3,4,3-(LI-1,2-HOPO). *J. Med. Chem.* **2014**, *57*, 4849–4860. [[CrossRef](#)]
22. Deri, M.A.; Ponnala, S.; Kozlowski, P.; Burton-Pye, B.P.; Cicek, H.T.; Hu, C.; Lewis, J.S.; Francesconi, L.C. P-SCN-Bn-HOPO: A Superior Bifunctional Chelator for ⁸⁹Zr ImmunoPET. *Bioconjug. Chem.* **2015**, *26*, 2579–2591. [[CrossRef](#)]
23. Patra, M.; Bauman, A.; Mari, C.; Fischer, C.A.; Blacque, O.; Häussinger, D.; Gasser, G.; Mindt, T.L. An octadentate bifunctional chelating agent for the development of stable zirconium-89 based molecular imaging probes. *Chem. Commun.* **2014**, *50*, 11523–11525. [[CrossRef](#)] [[PubMed](#)]
24. Chomet, M.; Schreurs, M.; Bolijn, M.J.; Verlaan, M.; Beaino, W.; Brown, K.; Poot, A.J.; Windhorst, A.D.; Gill, H.; Marik, J.; et al. Head-to-head comparison of DFO* and DFO chelators: Selection of the best candidate for clinical ⁸⁹Zr-immuno-PET. *Eur. J. Nucl. Med. Mol. Imaging* **2021**, *48*, 694–707. [[CrossRef](#)] [[PubMed](#)]
25. McInnes, L.E.; Rudd, S.E.; Donnelly, P.S. Copper, gallium and zirconium positron emission tomography imaging agents: The importance of metal ion speciation. *Coord. Chem. Rev.* **2017**, *352*, 499–516. [[CrossRef](#)]
26. Sharma, S.K.; Miller, M.J.; Payne, S.M. Spermexatin and Spermexatol: New Synthetic Spermidine-Based Siderophore Analogues. *J. Med. Chem.* **1989**, *32*, 357–367. [[CrossRef](#)]
27. Klasen, B.; Lemcke, D.; Mindt, T.L.; Gasser, G.; Rösch, F. Development and in vitro evaluation of new bifunctional ⁸⁹Zr-chelators based on the 6-amino-1,4-diazepane scaffold for immuno-PET applications. *Nucl. Med. Biol.* **2021**, *102–103*, 12–23. [[CrossRef](#)]
28. Manzoni, L.; Belvisi, L.; Arosio, D.; Bartolomeo, M.P.; Bianchi, A.; Brioschi, C.; Buonsanti, F.; Cabella, C.; Casagrande, C.; Civera, M.; et al. Synthesis of Gd and ⁶⁸Ga Complexes in Conjugation with a Conformationally Optimized RGD Sequence as Potential MRI and PET Tumor-Imaging Probes. *ChemMedChem* **2012**, *7*, 1084–1093. [[CrossRef](#)] [[PubMed](#)]
29. Lockett, M.R.; Phillips, M.F.; Jarecki, J.L.; Peelen, D.; Smith, L.M. A Tetrafluorophenyl Activated Ester Self-Assembled Monolayer for the Immobilization of Amine-Modified Oligonucleotides. *Langmuir* **2008**, *24*, 69–75. [[CrossRef](#)]
30. Holland, J.P.; Divilov, V.; Bander, N.H.; Smith-Jones, P.M.; Larson, S.M.; Lewis, J.S. ⁸⁹Zr-DFO-591 for immunoPET imaging of prostate-specific membrane antigen (PSMA) expression in vivo. *J. Nucl. Med.* **2010**, *51*, 1293–1300. [[CrossRef](#)]
31. Chakrabarti, M.C.; Le, N.; Paik, C.H.; De Graff, W.G.; Carrasquillo, J.A. Prevention of radiolysis of monoclonal antibody during labeling. *J. Nucl. Med.* **1996**, *37*, 1384–1388. [[PubMed](#)]
32. Liu, S.; Edwards, D.S. Stabilization of ⁹⁰Y-labeled DOTA-biomolecule conjugates using gentisic acid and ascorbic acid. *Bioconjug. Chem.* **2001**, *12*, 554–558. [[CrossRef](#)] [[PubMed](#)]
33. Yusufi, N.; Mall, S.; de Oliveira Bianchi, H.; Steiger, K.; Reder, S.; Klar, R.; Audehm, S.; Mustafa, M.; Nekolla, S.; Peschel, C.; et al. In-depth characterization of a TCR-specific tracer for sensitive detection of tumor-directed transgenic T cells by immuno-PET. *Theranostics* **2017**, *7*, 2402–2416. [[CrossRef](#)]
34. Yang, X.; Gandhi, Y.A.; Duignan, D.B.; Morris, M.E. Prediction of Biliary Excretion in Rats and Humans Using Molecular Weight and Quantitative Structure–Pharmacokinetic Relationships. *AAPS J.* **2009**, *11*. [[CrossRef](#)] [[PubMed](#)]
35. Verel, I.; Visser, G.W.M.; Boellaard, R.; Stigter-van Walsum, M.; Walsum, S.-V.; Snow, G.B.; Van Dongen, G.A.M.S. ⁸⁹Zr Immuno-PET: Comprehensive Procedures for the Production of ⁸⁹Zr-Labeled Monoclonal Antibodies. *J. Nucl. Med.* **2003**, *44*, 1271–1281.

-
36. Mendler, C.T.; Gehring, T.; Wester, H.-J.; Schwaiger, M.; Skerra, A. ⁸⁹Zr-Labeled Versus ¹²⁴I-Labeled HER2 Fab with Optimized Plasma Half-Life for High-Contrast Tumor Imaging In Vivo. *J. Nucl. Med.* **2015**, *56*, 1112–1118. [[CrossRef](#)]
 37. Vugts, D.J.; Klaver, C.; Sewing, C.; Poot, A.J.; Adamzek, K.; Huegli, S.; Mari, C.; Visser, G.W.M.; Valverde, I.E.; Gasser, G.; et al. Comparison of the octadentate bifunctional chelator DFO*-pPhe-NCS and the clinically used hexadentate bifunctional chelator DFO-pPhe-NCS for ⁸⁹Zr-immuno-PET. *Eur. J. Nucl. Med. Mol. Imaging* **2017**, *44*, 286–295. [[CrossRef](#)]

APPENDIX II

Russelli L*, Martinelli J*, De Rose F, Reder S, Herz M, Schwaiger M, Weber W, Tei L, D'Alessandria C. Room Temperature Al¹⁸F Labeling of 2-Aminomethylpiperidine-Based Chelators for PET Imaging. ChemMedChem. 2020 Feb 5;15(3):284-292.

Room Temperature Al¹⁸F Labeling of 2-Aminomethylpiperidine-Based Chelators for PET Imaging

Lisa Russelli⁺,^[a] Jonathan Martinelli⁺,^[b] Francesco De Rose,^[a] Sybille Reder,^[a] Michael Herz,^[a] Markus Schwaiger,^[a] Wolfgang Weber,^[a] Lorenzo Tei,^{*,[b]} and Calogero D'Alessandria^{*,[a]}

Positron emission tomography (PET) is a non-invasive molecular imaging technology that is constantly expanding, with a high demand for specific antibody-derived imaging probes. The use of tracers based on temperature-sensitive molecules (i.e. Fab, svFab, nanobodies) is increasing and has led us to design a class of chelators based on the structure of 2-aminomethylpiperidine (AMP) with acetic and/or hydroxybenzyl pendant arms (2-AMPTA, NHB-2-AMPDA, and 2-AMPDA-HB), which were investigated as such for {Al¹⁸F}²⁺-core chelation efficiency. All the compounds were characterized by HPLC-MS analysis and NMR spectroscopy. The AlF-18 labeling reactions were performed under various conditions (pH/temperature), and the radiolabeled chelates were purified and characterized by radio-

TLC and radio-HPLC. The stability of labeled chelates was investigated up to 240 min in human serum (HS), EDTA 5 mM, PBS and 0.9% NaCl solutions. The *in vivo* stability of [Al¹⁸F(2-AMPDA-HB)]⁻ was assessed in healthy nude mice (*n*=6). Radiochemical yields between 55% and 81% were obtained at pH 5 and room temperature. High stability in HS was measured for [Al¹⁸F(2-AMPDA-HB)]⁻, with 90% of F-18 complexed after 120 min. High stability *in vivo*, rapid hepatobiliary and renal excretion, with low accumulation of free F-18 in bones were measured. Thus, this new Al¹⁸F-chelator may have a great impact on immuno-PET radiopharmacy, by facilitating the development of new fluorine-18-labeled heat-sensitive biomolecules.

Introduction

Positron emission tomography (PET) is a diagnostic imaging technique based on the use of tracers radiolabeled with positron emitters, among which ¹¹C, ⁶⁸Ga, ¹⁸F, ⁶⁴Cu and ⁸⁹Zr are the most used in preclinical studies. The choice of β⁺-emitting radioisotopes for imaging purposes is dictated by several factors such as: the high sensitivity and spatial resolution of PET cameras combined with fast acquisition of data and possibility to acquire dynamic images in tomographic mode,^[1] the availability of biomedical cyclotrons for in-house production of positron emitters and the increasing number of metal-based radiopharmaceuticals, either recently approved by FDA or in late-stage clinical trials.^[2] For PET imaging, the selection of the best radionuclide for a given application is the most crucial decision because the physical half-life of the radionuclide must match the expected biological half-life of the radiotracer *in vivo*.^[3] F-18 with *t*_{1/2} = 109.8 min, ~97% β⁺-emission and a

maximum positron energy of 635 keV can be easily produced in high quantities with an on-site cyclotron. Since the half-life of F-18 is long enough to allow multistep labeling reactions, but also short enough to avoid extended irradiation of patients, in the last decades several radiotracers based on F-18 have been developed.^[4] Fluorine-18 incorporation into large biomolecules can be achieved by either a direct or an indirect labeling approach. Typically, the direct preparation of [¹⁸F]⁻radiotracers involved the attachment of ¹⁸F to a carbon in the organic structure of the radiotracer, often requiring a base and high temperatures. Although there are few examples of direct fluorine-18 labeling of peptides, protein labeling is typically performed using indirect labeling methods.^[5–7] In this approach, a small molecule containing a suitable functional group is radiolabeled by conventional nucleophilic substitution chemistry using [¹⁸F]fluoride and then conjugated to the proteins of interest. The most widely used prosthetic group is N-succinimidyl-4-[¹⁸F]fluorobenzoate ([¹⁸F]SFB) for conjugation to amine functionalities^[8–11] and ¹⁸F-N-[2](4-Fluorobenzamido)ethyl-maleimide ([¹⁸F]FBEM) for conjugation to thiols on cysteine residues.^[12–14] However, while each of these methods has certain advantages, other complications have limited their applications for clinical purposes. Therefore, the requirement of faster labeling methods boosted the search of new strategies based on the fluoride anion complexation/coordination chemistry and thus, the formation of an ¹⁸F-group-13 element bond, i.e. boron, aluminum and gallium.^[15] Among these methods, the complexation of {Al¹⁸F}²⁺ with an appropriate chelator is one of the most studied, and it shows great potential.^{[16][17]} In fact, the aluminum-fluoride bond is stronger than 60 other metal-fluoride bonds (bond energy of 670 kJ/mol),^[18] and it is very stable *in vivo*, making small amounts of

[a] L. Russelli,⁺ F. De Rose, S. Reder, M. Herz, Prof. M. Schwaiger, Prof. W. Weber, Dr. C. D'Alessandria
Department of Nuclear Medicine
Klinikum rechts der Isar TU München
Ismaningerstraße 22
81675 Munich (Germany)
E-mail: calogero.dalessandria@tum.de

[b] Dr. J. Martinelli,⁺ Prof. L. Tei
Department of Science and Technological Innovation
Università del Piemonte Orientale
Viale T. Michel 11
15121 Alessandria (Italy)
E-mail: lorenzo.tei@uniupo.it

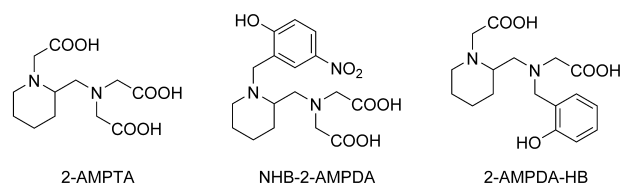
[⁺] These authors contributed equally to this work.

Supporting information for this article is available on the WWW under <https://doi.org/10.1002/cmdc.201900652>

aluminum fluoride chelate compatible with biological systems.^[19] In this method, $^{18}\text{F}^-$ interacts with Al^{3+} to form $\{\text{Al}^{18}\text{F}\}^{2+}$ (fluoranylaluminum(2+)) which can be chelated by a suitable polydentate ligand. If the chelating agent is modified to contain a chemically reactive functional group for conjugation to biomolecules, it is possible to carry out a direct labeling.^[20] Aluminum(III) forms octahedral complexes, therefore a pentadentate chelator is preferable, as it leaves only a binding site available for $^{18}\text{F}^-$. McBride *et al.* were the first to explore the Al^{18}F method in 2009 with the 1,4,7-triazacyclononane-1,4,7-triacetate (NOTA)^[16] chelator. Then, in 2011 both McBride and Shetty identified the pentadentate 1,4,7-triazacyclononane-1,4-diacetate (NODA) chelator as the best among those tested.^[21–23] It has been shown that the most stable Al^{III} complexes are based on multidentate ligands with two neutral N-amines and three negatively charged O-carboxylic or phenolic donor atoms (N_2O_3), providing the ideal coordination sphere for $\{\text{Al}^{18}\text{F}\}^{2+}$. In case of NODA-derivatives conjugated peptides, a kit which contains Al^{III} , a radioprotector (ascorbic acid), a non-volatile buffer (potassium bis-phthalate) and a stabilizing agent (trehalose) has also been developed.^[24] Although these macrocyclic chelators show considerable potential, the high temperature required for the complexation reaction ($\geq 100^\circ\text{C}$)^[25–27] represents a limit to the widespread application of this radiolabeling approach, especially in the presence of thermosensitive biomolecules such as proteins, Fab fragments (55 kDa), scFab (28 kDa) or nanobodies (15 kDa).

Starting from 2016, Cleeren *et al.* developed new classes of chelators^[28,29] that can be used to perform radiofluorination at moderate temperature ($< 40^\circ\text{C}$) using the McBride modified protocol.^[30] They have developed a number of N_2O_3 pentadentate ligands based on ethylenediamine and 1,2-cyclohexanediamine having three acetate pendant arms (in case of ethylenediamine based ligands, also hydroxybenzyl arms were used). The RESCA chelator was conjugated to a series of biomolecules such as HSA, a nanobody targeting the Kupffer cell marker CRIG and an affibody targeting HER2 and labeled with Al^{18}F .^[29]

It is well-known that, to increase the kinetic inertness of a metal complex, it is important to increase the rigidity of the chelator and the pre-organization of the ligand.^[31,32] However, at the same time, it is necessary to maintain a linear and non-macrocyclic structure of the polydentate chelator to allow a fast complexation kinetics and avoid the need to work at high temperatures, not compatible with some biomolecules. Therefore, the ideal structure of the pentadentate chelator should have an intrinsic rigidity provided by a cycloalkane or a heterocycle, and then flexible pendant arms. In the light of this, we designed a new class of chelators (see Scheme 1) based on the structure of 2-aminomethylpiperidine (AMP) with acetic and/or hydroxybenzyl pendant arms (2-AMPTA, NHB-2-AMPDA and 2-AMPDA-HB) and we tested their $\{\text{Al}^{18}\text{F}\}^{2+}$ labeling efficiency and stability in physiological conditions. Moreover, we investigated the *in vivo* stability and biodistribution of the $[\text{Al}^{18}\text{F}(2\text{-AMPDA-HB})]^-$ compound, that has shown the best performance during *in vitro* studies.

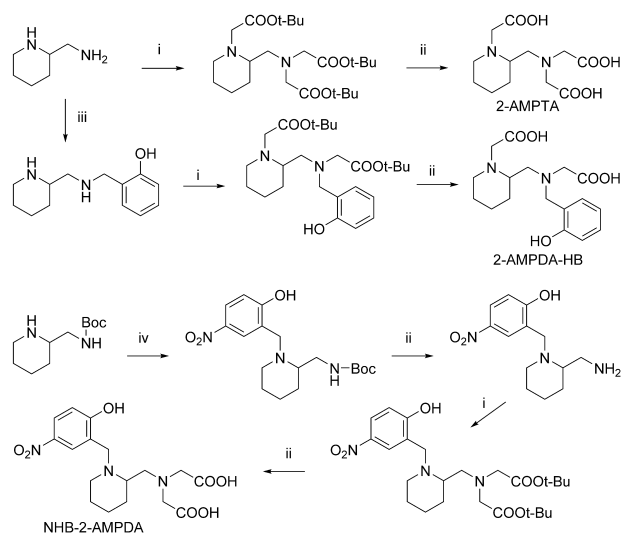


Scheme 1. AMP-based chelators discussed in this work.

Results and Discussion

Synthesis

The chelators 2-AMPTA and 2-AMPDA-HB were synthesized starting from racemic 2-aminomethylpiperidine, whereas NHB-2-AMPDA was obtained starting from racemic Boc-protected 2-AMP, as shown in Scheme 2. The main difference between the three ligands is the relative position of the acetic and hydroxybenzyl arms. Briefly, the triacetic derivative 2-AMPTA was obtained in overall 61% yield by nucleophilic substitution by the amines of 2-AMP on *tert*-butyl bromoacetate followed by deprotection of the carboxylic acids with TFA in DCM. In case of 2-AMPDA-HB, the reductive amination between the primary amine of 2-AMP and salicylaldehyde was followed by the alkylation of the secondary amines with *tert*-butyl bromoacetate and subsequent deprotection of the acid moieties. The synthesis of NHB-2-AMPDA started with the reaction of 2-chloromethyl-4-nitrophenol on the piperidine nitrogen: this step introduced a 4-nitro-2-hydroxybenzyl pendant arm that characterizes this chelator. Then, after removal of the Boc protecting group with TFA/DCM, two *tert*-butyl acetate arms were introduced on the 2-aminomethyl group and, finally, the carboxylates were deprotected. Al^{18}F -complexes were also



Scheme 2. Synthesis of the AMP-based ligands: i) *tert*-butyl 2-bromoacetate, K_2CO_3 , CH_3CN , reflux, on; ii) TFA/DCM 1:1 (v/v), RT, 2 h; iii) salicylaldehyde, dry THF, AcOH cat., 0°C to RT, 1 h; NaBH_4 , 0°C to RT, 2 h; iv) 2-(chloromethyl)-4-nitrophenol, K_2CO_3 , CH_3CN , reflux, on.

prepared following a reported procedure, in order to characterize the cold Al^{19}F -complexes.^[28] AMP-ligands and Al^{19}F -complexes were purified by semi-preparative HPLC-MS (Figures S1–S2) and characterized by ESI MS and ^1H , ^{19}F (Figures S3–S8) and ^{13}C NMR spectroscopy.

In case of $[\text{Al}^{19}\text{F}(\text{2-AMPTA})]^-$ a small amount of $[\text{Al}(\text{H}_2\text{O})(\text{2-AMPTA})]$ was also formed as confirmed by HPLC-MS and ^1H NMR. This hydrated complex was not formed in case of the other two phenol-functionalized complexes probably due to a higher hydrophobicity provided by the aromatic moiety. Moreover, the ^{19}F NMR spectra of the complexes show two peaks (-158 and -171 ppm) in case of $[\text{Al}^{19}\text{F}(\text{2-AMPTA})]^-$, two close peaks around -157 ppm for $[\text{Al}^{19}\text{F}(\text{NHB-2-AMPDA})]^-$, and three peaks for $[\text{Al}^{19}\text{F}(\text{2-AMPDA-HB})]^-$, two around -157 ppm and one at -165 ppm. The presence of more than one ^{19}F NMR resonance in case of the two phenol-functionalized derivatives is probably due to different positions occupied by the fluoride ion in the octahedral coordination geometry of the Al^{III} ion (Figure S9), as already reported previously for other AlF -complexes.^[28,33] Notably, the acquisition of the ^{19}F NMR spectra after two months did not show significant differences proving a good stability of the complexes in water at pH 7 (Figure S10). In addition, ^{19}F NMR spectra of $[\text{Al}^{19}\text{F}(\text{NHB-2-AMPDA})]^-$ acquired at different temperatures (283–353 K, Figure S10) showed an equilibrium between the coordination isomers as the integral ratio between the signals changes with temperature.

Radiolabeling experiments

The preparation of $\{\text{Al}^{18}\text{F}\}^{2+}$ and the subsequent labeling with AMP-based chelators were carried out by slight modification of the procedure reported by Bormans and colleagues.^[28] In particular, labeling reactions were performed at pH 4 and 5 and at three different temperatures for each pH value (room temperature, 37°C and 80°C) for 12 min. RCYs were calculated by radio-TLC analysis. All the radiolabeled complexes were purified using a Sep-Pak Plus Alumina-N-cartridges (Waters), following a previously reported protocol^[30] and characterized via radio-HPLC (Figure S11). At pH 4, only 2-AMPTA chelator is able to efficiently complex $\{\text{Al}^{18}\text{F}\}^{2+}$ with a RCY between 77% and 86% (Figure 1a).

This is consistent with the presence of the acetic pendant arms, which are more acidic compared to the phenol groups that are protonated at pH 4. At this pH, only heating the reaction to 80°C we obtain a good RCY for the other two chelators. On the other hand, at pH 5 all three chelators were successfully labeled, and a RCY between 55% and 81% was obtained at room temperature (55% 2-AMPDA-HB, 69% NHB-2-AMPDA and 81% 2-AMPTA, respectively). Increasing the temperature to 37 and 80°C allowed improving the RCY for 2-AMPDA-HB for which the radiolabeling efficiency reached 75%. Comparing the labeling results for the three chelators, we can conclude that, as already reported previously on for similar pentadentate N_2O_3 ligands,^[28] the most acidic ligand 2-AMPTA, with three carboxylic acids and without a phenol moiety, is more reactive than the ligands containing a phenolate moiety

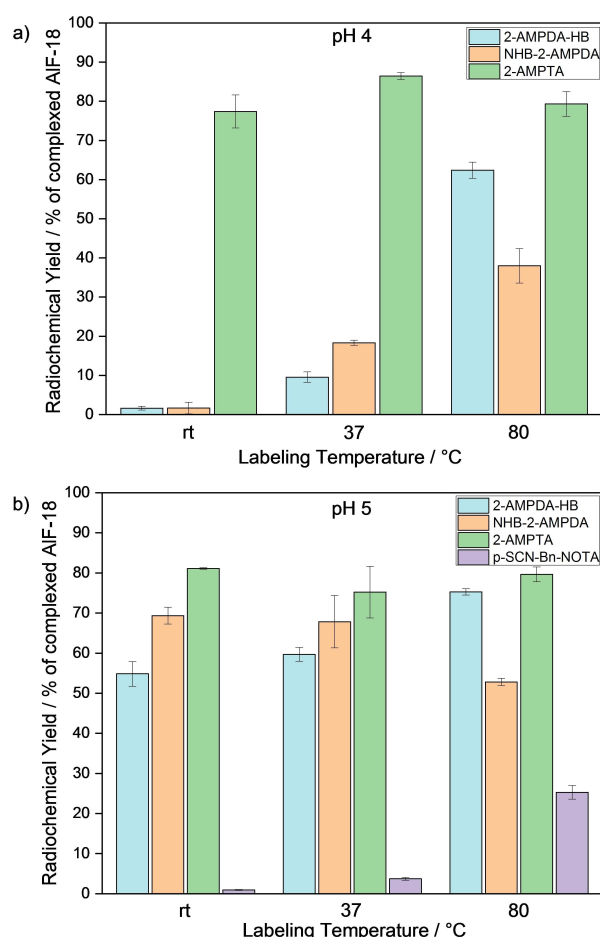


Figure 1. Radiochemical yields (\pm SD) at pH 4 of Al^{18}F -AMP-derivatives (a) and at pH 5 of Al^{18}F -AMP-derivatives and p-SCN-Bn-NOTA (b) at different temperatures analyzed via radio-TLC. On X-axis are reported the reaction temperatures, while on the Y-axis the radiochemical yields as a percentage ($n=3$).

as donor. In fact, phenols in acidic conditions (pH 4) are almost fully protonated, and for this reason less available to chelate $\{\text{Al}^{18}\text{F}\}^{2+}$ ions.

Since a pronounced pH dependence was observed for the labeling reaction of AMP-based chelators with $\{\text{Al}^{18}\text{F}\}^{2+}$, a more detailed study to assess the labeling efficiency at RT versus pH was performed (Figure 2). The pH value and reaction buffer are really important for the radiofluorinations using $\{\text{Al}^{18}\text{F}\}^{2+}$, because at $\text{pH} < 4$ fluorine is present in solution also in the HF form, while at $\text{pH} > 5$ Al^{III} starts to form hydroxide species.^[34] In both cases the species compete with the formation of $\{\text{Al}^{18}\text{F}\}^{2+}$ and, therefore, influence the RCYs. As shown in Figure 2, the three chelators are able to complex $\{\text{Al}^{18}\text{F}\}^{2+}$ with good yield also at higher pH, with a RCY around 50% at pH 6.5. Notably, the ability to form the labeled complex at almost neutral pH is important and can have an impact on the labeling of acid sensitive biomolecules. The different behavior of the three chelators again reflects the different acidity of the donor groups: for 2-AMPTA the higher RCY was measured at pH 4.5, whereas for NHB-2-AMPDA at pH 5 and up to pH 6 in case of 2-

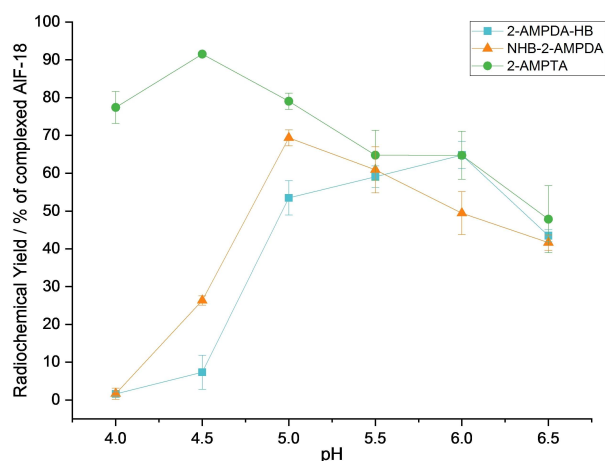


Figure 2. Radiochemical yields profile (\pm SD) evaluated at different pH values ($n=3$). Data reported are representative of the radiolabeling performed at room temperature.

AMPDA-HB, which presents an un-substituted, weaker acid, phenol group.

Head-to-head labeling comparison of 2-AMPDA-HB vs *p*-SCN-Bn-NOTA chelator

As shown in Figure 1b we also performed a parallel labeling experiment on the *p*-SCN-Bn-NOTA chelator at pH 5 using the same labeling conditions reported for the AMP-based chelators. As expected, the NOTA derivative was not able to form a stable complex with $\{Al^{18}F\}^{2+}$ at the tested temperatures (room temperature, 37 °C and 80 °C) and the RCYs were respectively 0.96% (± 0.11), 3.72% (± 0.35), 25.3% (± 1.74). From this comparison, we can then confirm that the new AMP-based chelators have better labeling performance at low temperature compared to *p*-SCN-Bn-NOTA.

In vitro stability studies

Stability studies were performed on purified products after radiofluorination at pH 5 and room temperature (Table 1). The $\{Al^{18}F\}^{2+}$ complexes were incubated at 37 °C for 240 minutes in Human Serum (HS), PBS, EDTA 5 mM (1000-fold excess) and NaCl 0.9% solutions respectively, and the percentage of $^{18}F^-$ coordinated to the Al^{III} -complex measured via radio-TLC analysis. Excellent stability in HS was measured for $[Al^{18}F(2-AMPDA-HB)]^-$ with a $90 \pm 4\%$ of intact complex after 120 min, higher if compared to other reported ligands.^[28]

On the other hand, for $[Al^{18}F(2-AMPTA)]^-$ and $[Al^{18}F(NHB-2-AMPDA)]^-$ complexes, $55 \pm 9\%$ and $46 \pm 4\%$ of coordinated $^{18}F^-$ was measured. Measuring the percentage of coordinated $^{18}F^-$ up to 4 h, a remarkable stability in HS was found for the labeled $[Al^{18}F(2-AMPDA-HB)]^-$ ($87 \pm 5\%$), and great stability also in PBS, EDTA 5 mM and NaCl 0.9%, about 90% after 4 h. The stability study on the labeled complexes shows that $[Al^{18}F(2-AMPDA-HB)]^-$ is substantially more stable than the other chelates. This trend is not the same as that found for RCYs where 2-AMPTA resulted the most reactive among the three chelators. A possible explanation is a higher flexibility of the acetate arms in 2-AMPTA that allows a faster and more efficient complexation, but at the same time a lower stability already after 30 min. Conversely, a higher rigidity provided by the phenol pendant in 2-AMPDA-HB leads to lower RCYs, but at the same time to a higher stability towards dissociation of the complex in physiological conditions. Based on stability results, the theoretical higher specific activity of the most stable compound, $[Al^{18}F(2-AMPDA-HB)]^-$, was calculated to be 32 GBq/ μ mol.

In vivo studies

Due to the high *in vitro* stability measured for $[Al^{18}F(2-AMPDA-HB)]^-$ in HS, we decided to test its stability *in vivo*. Such experiments were performed by injecting healthy female nude mice ($n=6$) with 2.3 ± 0.1 MBq of $[Al^{18}F(2-AMPDA-HB)]^-$ and performing dynamic PET/CT scans for up to 90 minutes. Afterwards, mice were sacrificed 2 h p.i. to perform a biodistribution analysis. In Figure 3, PET-CT images are reported as frames of the dynamic scan extracted at different time points

Table 1. Stability study of $[Al^{18}F(2-AMPDA-HB)]^-$ ($n=3$), $[Al^{18}F(2-AMPTA)]^-$ ($n=3$), $[Al^{18}F(NHB-2-AMPDA)]^-$ ($n=3$). All the complexes were incubated at 37 °C in Human Serum (HS), PBS, EDTA 5 mM and NaCl 0.9%. Data are expressed as % of ^{18}F complexed measured by radio-TLC analysis.

	Incubation solution	10 min	SD (\pm)	30 min	SD (\pm)	60 min	SD (\pm)	120 min	SD (\pm)	240 min	SD (\pm)
$[Al^{18}F(2-AMPDA-HB)]^-$	HS	95%	2%	92%	2%	90%	4%	90%	2%	87%	5%
	PBS	97%	1%	97%	1%	91%	8%	93%	2%	93%	1%
	EDTA 5 [mM]	94%	2%	95%	1%	92%	2%	90%	3%	87%	4%
	NaCl 0.9%	95%	4%	97%	0%	92%	6%	94%	2%	92%	2%
$[Al^{18}F(2-AMPTA)]^-$	HS	91%	1%	83%	6%	72%	7%	55%	9%	32%	6%
	PBS	92%	1%	89%	3%	82%	3%	73%	2%	52%	8%
	EDTA 5 [mM]	93%	2%	91%	3%	90%	1%	81%	3%	68%	7%
	NaCl 0.9%	94%	2%	90%	3%	88%	5%	84%	7%	71%	15%
$[Al^{18}F(NHB-2-AMPDA)]^-$	HS	85%	5%	78%	2%	51%	2%	46%	4%	7%	2%
	PBS	86%	7%	82%	1%	68%	0%	47%	4%	13%	4%
	EDTA 5 [mM]	88%	1%	86%	1%	69%	1%	33%	7%	5%	1%
	NaCl 0.9%	92%	1%	81%	8%	72%	5%	58%	4%	27%	2%

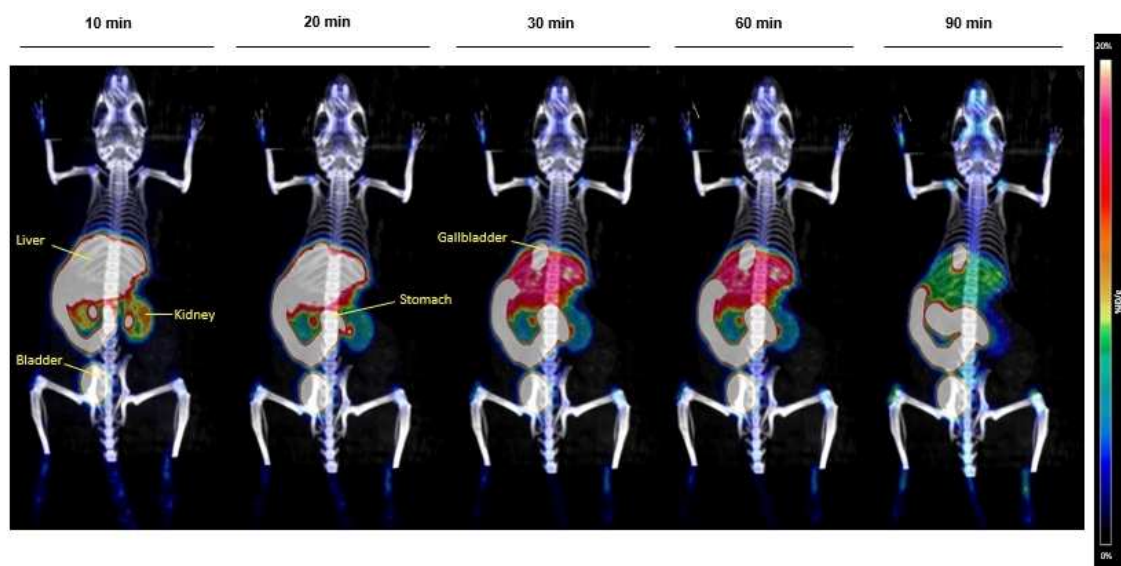


Figure 3. Maximum Image Projections (MIPs) obtained selecting frames at different time points during dynamic PET-CT scans. A hepatobiliary and renal excretion is clearly visible. Scale bar: 0–20%ID/g.

using the Inveon Research Workplace software (Siemens, Knoxville, TN). $[Al^{18}F(2-AMPDA-HB)]^-$ complex presented fast blood clearance, hepatobiliary and renal excretion, as expected due to the $\log P$ value of -2.47 ± 0.4 and the low molecular weight of the compound.^[35]

Performing image-derived uptake calculation on dynamic PET-CT scans by drawing region of interest (ROIs) on selected organs, we were also able to study the biodistribution of the tracer over the time analysis as shown in Figure S12. A fast blood clearance (heart ROI) and kidney elimination was measured over time, and also a fast hepatobiliary clearance was confirmed.

Ex vivo studies

Based on biodistribution results (Figure 4 and Table S1) and according to the dynamic PET-CT ROI calculations, we can confirm that the labeled complex $[Al^{18}F(2-AMPDA-HB)]^-$ shows high stability *in vivo* as shown by the low ^{18}F accumulation measured in femur (%ID/g: $1.63 \pm 0.73\%$) and other organs at 2 h p.i.. Since the aluminum-fluoride bond is very strong (670 kJ/mol),^[18] the activity accumulated in the organs cannot be ascribed to $^{18}F^-$ released from the Al^{III} chelate, but either to the intact complex or $\{Al^{18}F\}^{2+}$ dissociated from the ligand. These results are really promising when compared to other *in vivo* studies reported in literature^[28] showing an accumulation in bones of free $\{Al^{18}F\}^{2+}$ equal to 83% ID \pm 10.65 and $\{Al^{18}F\}^{2+}$ -ligands of 2.5% ID \pm 0.64 60 min p.i.^[28] In fact, radio-TLC analysis of mice's urine performed 2 h p.i. showed that the $68 \pm 0.1\%$ of activity was still present as $[Al^{18}F(2-AMPDA-HB)]^-$ complex (data not shown).

According with PET images, our biodistribution data confirm the fast hepatobiliary/renal excretion of the labeled chelate due

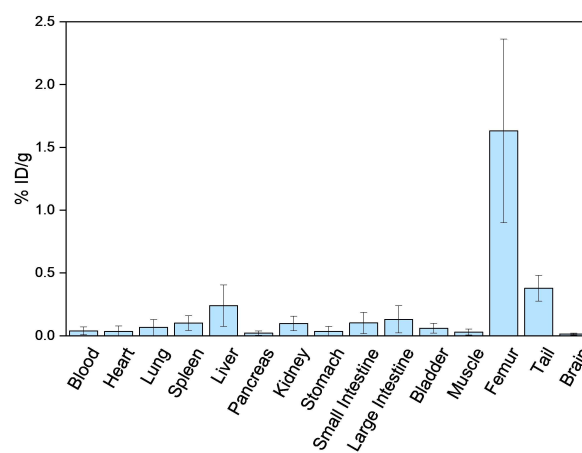


Figure 4. Biodistribution data of $[Al^{18}F(2-AMPDA-HB)]^-$ on female healthy nude mice in selected organs measured 2 h p.i.. The activity accumulated is reported as Percentage of Injected Dose per gram (%ID/g \pm SD) ($n=6$).

to the low molecular weight of 381 Da^[35] and the mild lipophilicity ($\log P = -2.47 \pm 0.4$). A similar behavior was also obtained in previous works based on AlF-18 compounds non conjugated to a biomolecule, which are then in agreement with our results.^{[23][28]} Although, a “naked” and negatively charged $Al^{18}F$ -chelate complex does not persist *in vivo* long enough to encounter challenge to its structural integrity compared to a conjugated version, nevertheless the results obtained speak for a stable $Al^{18}F$ -complex once conjugated with a biomolecule. The accumulation measured at 10 minutes p.i. in the liver (Figure S12) is due to the excretion pathway of the labeled chelator, which only transits through the organ and does not reside in it. As already reported above, the chelator will be conjugated to vector molecules having specific binding

capacity for tumor-associated targets. Therefore, we expect a different biodistribution of the labeled complex dictated by the pharmacokinetic characteristic of the vector molecules.

Conclusions

Three pentadentate ligands based on the structure of 2-aminomethylpiperidine and having acetate and/or hydroxybenzyl pendant arms were synthesized and complexed with Al¹⁸F. The labeling with {Al¹⁸F}²⁺ was carried out at different temperatures and pH, finding the optimal labeling conditions for each chelator. In general, a very good radiochemical yield was obtained for all chelators at pH 5 and 25 °C. The stability tests on the radiolabeled complexes showed that the {Al¹⁸F}²⁺ complex with 2-AMPDA-HB is the most stable in all conditions, presenting 90% of ¹⁸F complexed up to 240 min. With this Al¹⁸F tracer an *in vivo* study was performed on nude mice and a good stability, a low amount of ¹⁸F accumulation in bones and a fast renal excretion were measured. The promising results obtained in this work prompted us towards the synthesis of a bifunctional derivative of 2-AMPDA-HB that will allow the conjugation with temperature-sensitive biomolecules, *e.g.* Fab fragments and/or nanobodies, the labeling at room temperature and then *in vivo* applications. Moreover, we will have the possibility to test and confirm the stability of the [Al¹⁸F(2-AMPDA-HB)]⁻ complex at early time points, *i.e.* 1h, 2hrs and 3 hrs, post tracer injection.

Experimental Section

General

All chemicals were purchased from commercial sources and were used without purification. Water was purified (18 MΩ cm) using a standard Milli-Q system (Millipore, Bedford, MA, USA). Elemental analyses were carried out with a EA3000 CHN Elemental Analyzer (EuroVector, Milano, Italy). NMR spectra (including ¹H-decoupled ¹³C NMR) were recorded on a Bruker Avance III spectrometer operating at 11.74 T, corresponding to a protonic resonance frequency of 499.8 MHz. ¹H and ¹³C NMR chemical shifts are reported relative to TMS and are referenced using the residual proton solvent resonances. ¹⁹F NMR chemical shifts are reported relative to CFC₃. Samples were prepared in 5 mm NMR tubes by dissolving the compounds in appropriate deuterated solvents. Splitting patterns are described as singlet (s), broad singlet (bs), doublet (d), double doublet (dd), triplet (t), multiplet (m) or broad multiplet (bm). ESI mass spectra were recorded on a Waters SQD 3100. Analytical HPLC-MS were carried out on Waters modular system equipped with Waters 1525 binary pump, Waters 2487 UV/Vis and Waters SQD 3100 (ESCI ionization mode) detectors, using an XBridge™ Phenyl 3.5 μm 4.6x150 mm column (Waters). Semi-preparative HPLC purifications were performed with an XBridge™ Prep Phenyl 5 μm OBD™ 19x100 mm column (Waters). The HPLC methods are indicated for each procedure and reported in the Supporting Information (SI). [¹⁸F]fluoride was produced at the PETtrace cyclotron 880 (GE Healthcare, Uppsala, Sweden) *via* the ¹⁸O(p,n)¹⁸F nuclear reaction by irradiating enriched [¹⁸O]water with 16.5 MeV protons in a niobium target (2.5 mL internal volume). The activity during experiments was measured with a Capintec CRC® 15R dose

calibrator. After the labeling reaction, the chelators were purified using a Sep-Pak Alumina N Plus Light Cartridge (Waters) with a saline solution (NaCl 0.9%) and characterized by a Prominence HPLC system (Shimadzu) with a Photo Diode Array detector (Shimadzu) and a GABI Star γ detector (Raytest) with a reverse phase XTerra MS C18 5 μm 4.6x100 mm (Waters) using Method A1 (SI). RCYs were determined by radio-TLC using an elution solution of ACN/H₂O 75%–25% and TLC silica gel 60 plates (Merck Millipore). The stripes were read-out using a radio-TLC-scanner (Bioscan, Eckert & Ziegler) and data were analyzed by the Bio-Chrom Lite software. PET/CT scans of animals were performed using an Inveon Small Animal PET/CT scanner (Siemens, Knoxville, TN). The activity accumulation in specific organs was measured in *ex vivo* experiments using a γ-counter (Perkin Elmer).

Synthesis of 2-AMPTA

tert-Butyl 2-aminomethylpiperidine triacetate (AMPTA(OtBu)₃). 2-Aminomethylpiperidine (1 mL, 8.24 mmol) was dissolved in MeCN (50 mL). K₂CO₃ (5.12 g, 37.04 mmol) was added, followed by *tert*-butyl bromoacetate (4.0 mL, 27.2 mmol), and the mixture was stirred at reflux overnight. The solvent was evaporated under reduced pressure, the residue was suspended in EtOAc (100 mL) and washed with H₂O (50 mL) and brine (2x50 mL). The organic phase was dried over anhydrous Na₂SO₄, filtered and evaporated under vacuum. The crude product was purified by flash chromatography (SiO₂, PetEt/EtOAc 90:10→80:20, R_f^{90:10} = 0.22), leading to the aimed compound as a yellow-colored oil (2.50 g, 66.4%). ¹H NMR (500 MHz, 27 °C, D₂O), δ (ppm): 3.39 (s, 6H, CH₂CO), 2.95 (dd, ¹J_{HH} = 13.2 Hz, ²J_{HH} = 5.1 Hz, 1H, CHCHH'N), 2.80 (m, 1H, NCHH'CH₂), 2.69 (m, 1H, CH), 2.60 (dd, ¹J_{HH} = 13.2 Hz, ²J_{HH} = 5.1 Hz, 1H, CHCHH'N), 2.52 (m, 1H, NCHH'CH₂), 1.81 (m, 1H, NCHCHH'CH₂), 1.66 (m, 1H, NCH₂CHH'), 1.54 (m, 2H, NCHCH₂CH₂), 1.27 (m, 2H, NCH₂CHH' + NCHCHH'CH₂). ¹³C NMR (125 MHz, 27 °C, D₂O), δ (ppm): 170.6 (CO), 80.8 (C¹⁸O), 57.6 (CH), 57.5 (NCHCH₂N), 56.4 (CH₂CO), 53.4 (NCH₂CH₂), 30.5 (NCHCH₂CH₂), 28.1 (CH₃), 25.5 (NCHCH₂CH₂), 23.6 (NCH₂CH₂). ESI⁺ MS: m/z 457.5 [M + H⁺], calc. for [C₂₄H₄₅N₂O₆]⁺ = 457.33 g/mol.

2-AMPTA. AMPTA(OtBu)₃ (0.31 g, 0.69 mmol) was dissolved in DCM (5 mL). TFA (5 mL) was added and the mixture was stirred at room temperature for 6 h. The solvents were evaporated under reduced pressure and the residue was redissolved in TFA (1 mL) and precipitated in Et₂O (10 mL). The suspension was centrifuged (4000 rpm, 15 min, 10 °C) and the precipitate was washed/centrifuged with Et₂O (3x10 mL). The product was purified by preparative HPLC-MS (Method P1, t_R = 5.2 min), and it was obtained as mono-trifluoroacetate salt after lyophilization (184 mg, 66%). HPLC-MS (Method A1): t_R = 8.3 min. Elemental analysis: found C, 41.91; H, 5.29; N, 6.98; calc. for C₁₄H₂₁F₃N₂O₈ C, 41.80; H, 5.26; N, 6.96. ¹H NMR (500 MHz, 27 °C, D₂O), δ (ppm): 3.66 (d, ²J_{HH} = 18.3 Hz, 3H, CHH'COOH), 3.60 (d, ²J_{HH} = 18.3 Hz, 3H, CHH'COOH), 3.6–3.4 (m, 3H, CH + NCHH'CH₂ + NCHCHH'), 3.18 (m, 2H, NCHH'CH₂ + NCHCHH'), 3.06 (d, ²J_{HH} = 11.2 Hz, 2H, NCHCH₂N), 1.77 (m, 2H, NCHCH₂CH₂), 1.53 (m, 2H, NCH₂CH₂). ¹³C NMR (125 MHz, 27 °C, D₂O), δ (ppm): 175.1 (COOH), 59.1 (NCH), 56.4 (NCH₂CO), 56.0 (NCHCH₂N), 54.3 (NCH₂CH₂), 49.8 (NCHCH₂), 22.0 (NCH₂CH₂), 18.7 (NCHCH₂CH₂). ESI⁺ MS: m/z 289.4 [M + H⁺], calc. for [C₁₂H₂₁N₂O₆]⁺ = 289.14 g/mol.

Synthesis of NHB-2-AMPDA

2-(Boc-aminomethyl)-N-(2-hydroxy-4-nitrophenylmethyl)piperidine. 2-(Boc-aminomethyl)piperidine (322 mg, 1.50 mmol) was dissolved in DMF (10 mL). K₂CO₃ (415 mg, 3.00 mmol) was added, followed by 2-chloromethyl-4-nitrophenol (563 mg, 3.00 mmol), and the mixture was stirred at reflux overnight. The solvent was evaporated under reduced pressure, the residue was suspended in

EtOAc (40 mL) and washed with H₂O (2×50 mL) and brine (50 mL). The organic phase was dried over anhydrous Na₂SO₄, filtered and evaporated under vacuum. The crude product was purified by flash chromatography (SiO₂, cyclohexane/acetone 95:5→80:20, R_f^{90:10} = 0.34), leading to the aimed compound as a yellow solid (262 mg, 48%). ¹H NMR (500 MHz, 27 °C, CDCl₃), δ (ppm): 7.94 (d, ²J_{HH} = 8.9 Hz, 1H, CHCHCNO₂), 7.82 (s, 1H, CCHCNO₂), 6.70 (d, ²J_{HH} = 8.9 Hz, 1H, CHCOH), 4.37 (d, ²J_{HH} = 12.1 Hz, 1H, NCH₂Ar), 3.61 (d, ²J_{HH} = 12.1 Hz, 1H, NCH₂Ar), 3.40 (m, 1H, CH₂NH), 3.33 (m, 1H, CH₂NH), 2.85 (m, 1H, NCH), 2.60 (m, 1H, NCH₂CH₂), 2.27 (m, 1H, NCH₂CH₂), 1.69 (m, 1H, NCHCH₂CH₂), 1.68 (m, 1H, NCHCH₂CH₂), 1.55 (m, 1H, NCHCH₂CH₂), 1.49 (m, 2H, NCHCH₂CH₂ + NCH₂CH₂), 1.39 (m, 1H, NCH₂CH₂), 1.32 (s, 9H, CH₃). ¹³C NMR (125 MHz, 27 °C, CDCl₃), δ (ppm): 165.2 (COH), 156.0 (COO), 139.5 (CNO₂), 125.0 (CCHCNO₂), 124.6 (NCH₂C), 121.5 (CHCHCNO₂), 116.3 (CHCOH), 79.5 (C¹⁸), 60.5 (NCH), 60.3 (NCH₂CH₂), 56.3 (NCH₂Ar), 50.8 (CH₂NH), 40.9 (NCHCH₂CH₂), 28.2 (CH₃¹⁸), 24.1 (NCH₂CH₂), 20.9 (NCHCH₂CH₂). ESI⁺ MS: m/z 366.6 [M + H⁺], calc. for [C₁₈H₂₈N₃O₅]⁺ = 366.20 g/mol.

2-Aminomethyl-*N*-(2-hydroxy-4-nitrophenylmethyl)piperidine. 2-(Boc-aminomethyl)-*N*-(2-hydroxy-4-nitrophenylmethyl)piperidine (235 mg, 0.64 mmol) was dissolved in DCM (5 mL). TFA (5 mL) was added and the mixture was stirred at room temperature for 3 h. The solvents were evaporated under reduced pressure and the residue was redissolved in TFA (1 mL) and precipitated in Et₂O (10 mL). The suspension was centrifuged (4000 rpm, 15 min, 10 °C) and the precipitate was washed/centrifuged with Et₂O (3×10 mL). The product was obtained in the trifluoroacetate form as a yellow solid (216 mg, 89%). ¹H NMR (500 MHz, 27 °C, CD₃OD), δ (ppm): 8.31 (s, 1H, CCHCNO₂), 8.17 (d, ²J_{HH} = 9.0 Hz, 1H, CHCHCNO₂), 7.02 (d, ²J_{HH} = 8.9 Hz, 1H, CHCOH), 4.54 (d, ²J_{HH} = 13.2 Hz, 1H, NCH₂Ar), 4.30 (d, ²J_{HH} = 13.2 Hz, 1H, NCH₂Ar), 3.72 (m, 1H, CH₂NH), 3.68 (m, 1H, NCH), 3.46 (m, 1H, CH₂NH), 3.37 (m, 1H, NCH₂CH₂), 3.07 (m, 1H, NCH₂CH₂), 2.12 (m, 1H, NCH₂CH₂), 1.86–1.83 (m, 4H, NCHCH₂CH₂ + NCH₂CH₂), 1.62 (m, 1H, NCHCH₂CH₂). ¹³C NMR (125 MHz, 27 °C, CD₃OD), δ (ppm): 162.6 (COH), 140.4 (CNO₂), 128.8 (CCHCNO₂ + CCHCNO₂), 127.8 (CHCHCNO₂), 116.1 (CHCOH), 60.5 (NCH), 51.2 (NCH₂CH₂), 48.7 (NCH₂Ar), 38.9 (CH₂NH₂), 24.8 (NCH₂CH₂), 20.3 (NCHCH₂CH₂ + NCHCH₂CH₂). ESI⁺ MS: m/z 266.2 [M + H⁺], calc. for [C₁₃H₂₀N₃O₅]⁺ = 266.15 g/mol.

***tert*-Butyl 2-aminomethyl-*N*-(2-hydroxy-4-nitrophenylmethyl)piperidine diacetate (NHB-2-AMPDA(OtBu)₂).** 2-Aminomethyl-*N*-(2-hydroxy-4-nitrophenylmethyl)piperidine (216 mg, 0.57 mmol) was dissolved in DMF (2 mL). K₂CO₃ (157 mg, 1.14 mmol) was added, followed by *tert*-butyl bromoacetate (0.167 mL, 1.14 mmol), and the mixture was stirred at room temperature overnight. The solvent was evaporated under reduced pressure, the residue was suspended in EtOAc (10 mL) and washed with H₂O (2×5 mL) and brine (5 mL). The organic phase was dried over anhydrous Na₂SO₄, filtered and evaporated under vacuum. The crude product was purified by flash chromatography (SiO₂, PetEt/EtOAc 60:40→20:80, R_f^{30:70} = 0.24), leading to the aimed compound as a yellow solid (194 mg, 69%). ¹H NMR (500 MHz, 27 °C, CDCl₃), δ (ppm): 8.31 (d, ²J_{HH} = 8.9 Hz, 1H, CHCHCNO₂), 7.85 (s, 1H, CCHCNO₂), 6.75 (d, ²J_{HH} = 8.9 Hz, 1H, CHCOH), 3.93 (d, ²J_{HH} = 12.1 Hz, 1H, NCH₂Ar), 3.79 (d, ²J_{HH} = 12.1 Hz, 1H, NCH₂Ar), 3.5–3.3 (m, 5H, NCH + NCH₂CO), 3.30 (m, 1H, CHCH₂N), 3.08 (m, 1H, NCH₂CH₂), 2.88 (m, 1H, CHCH₂N), 2.75 (m, 1H, NCH₂CH₂), 2.04 (m, 1H, NCH₂CH₂), 1.8–1.7 (m, 4H, NCHCH₂CH₂ + NCH₂CH₂), 1.63 (m, 1H, NCHCH₂CH₂), 1.42 (s, 18H, CH₃). ¹³C NMR (125 MHz, 27 °C, CDCl₃), δ (ppm): 169.8 (COO), 163.8 (COH), 140.6 (CNO₂), 129.4 (CCHCNO₂), 127.3 (NCH₂C), 125.3 (CHCHCNO₂), 118.0 (CHCOH), 83.0 (C¹⁸), 60.6 (NCH), 57.9 (NCH₂CO), 56.1 (NCHCH₂N), 50.6 (NCH₂CH₂), 39.9 (NCH₂Ar), 28.8 (CH₃¹⁸), 26.2 (NCH₂CH₂), 22.4 (NCHCH₂CH₂), 21.4 (NCHCH₂CH₂). ESI⁺ MS: m/z 494.4 [M + H⁺], calc. for [C₂₅H₄₀N₃O₇]⁺ = 494.29 g/mol.

NHB-2-AMPDA. NHB-2-AMPDA(OtBu)₂ (27 mg, 0.055 mmol) was dissolved in DCM (1 mL). Triisopropylsilane (1 drop) was added, followed by TFA (1 mL), and the mixture was stirred at room temperature for 15 h. The solvents were evaporated under reduced pressure, the residue was dissolved in TFA (1 mL) and precipitated in Et₂O (10 mL). The suspension was centrifuged (4000 rpm, 15 min, 10 °C) and the precipitate was washed/centrifuged with Et₂O (3×10 mL) and dried under vacuum. The residue was redissolved in concentrated HCl (5 mL) and stirred at ambient temperature for 30 min. After lyophilization, the product was obtained as monohydrochloride salt (14 mg, 61%) and it was used for complexation experiments without further purification. Elemental analysis: found C, 48.92; H, 5.81; N, 10.10; calc. for C₁₇H₂₄CIN₃O₇·C, 48.87; H, 5.79; N, 10.06. ¹H NMR (500 MHz, 27 °C, D₂O), δ (ppm): 7.93 (m, 2H, CHCHCNO₂ + CCHCNO₂), 6.88 (d, ²J_{HH} = 8.8 Hz, 1H, CHCOH), 3.90 (s, 2H, NCH₂Ar), 3.71 (m, 2H, NCH + NCHCH₂N), 3.51 (m, 5H, NCHCH₂N + NCH₂CO), 3.32 (m, 1H, NCH₂CH₂), 3.09 (m, 1H, NCH₂CH₂), 2.08 (m, 1H, NCH₂CH₂), 1.9–1.7 (m, 4H, NCHCH₂CH₂ + NCH₂CH₂), 1.58 (m, 1H, NCHCH₂CH₂). ¹³C NMR (125 MHz, 27 °C, D₂O), δ (ppm): 173.2 (COOH), 161.8 (COH), 141.0 (CNO₂), 128.8 (CCHCNO₂), 127.0 (NCH₂C), 125.8 (CHCHCNO₂), 116.4 (CHCOH), 66.7 (NCH₂CO), 60.6 (NCH), 51.8 (NCH₂CH₂), 39.5 (NCHCH₂N), 30.8 (NCH₂Ar), 25.1 (NCH₂CH₂), 20.3 (NCHCH₂CH₂ + NCHCH₂CH₂). ESI⁺ MS: m/z 382.2 [M + H⁺], calc. for [C₁₇H₂₄N₃O₇]⁺ = 382.16 g/mol.

Synthesis of 2-AMPDA-HB

2-(*N*-(2-Hydroxybenzyl)aminomethyl)piperidine. (DL)-2-aminomethylpiperidine (0.50 mL, 4.12 mmol) was dissolved in dry MeOH (10 mL). At 0 °C, AcOH (1 drop) was added, followed by salicylaldehyde (0.48 mL, 4.53 mmol), and the resulting yellow mixture was stirred at room temperature for 2 h. NaBH₄ (850 mg, 22.47 mmol) was then added portionwise at 0 °C, and the suspension was stirred at room temperature for further 15 h. H₂O (3 mL) was added and stirring was continued at room temperature for 30 min. The volatiles were evaporated under reduced pressure, and the residue was suspended in EtOH (10 mL) and filtered through a PTFE membrane. The solvent was evaporated and the crude product (1.00 g) was used as such without further purification. ESI⁺ MS: m/z 221.1 [M + H⁺], calc. for [C₁₃H₂₁N₂O]⁺ = 221.32 g/mol.

***tert*-Butyl 2-(*N*-(2-hydroxybenzyl)aminomethyl)piperidine diacetate (2-AMPDA-HB(OtBu)₂).** 2-(*N*-(2-Hydroxybenzyl)aminomethyl)piperidine (1.00 g, 4.54 mmol, theoretical) was dissolved in MeCN (50 mL). K₂CO₃ (2.51 g, 18.16 mmol) was added, followed by *tert*-butyl bromoacetate (2.00 mL, 13.64 mmol), and the mixture was heated to reflux and stirred overnight. The solvent was evaporated under reduced pressure, the residue was suspended in EtOAc (50 mL) and washed with H₂O (2×25 mL) and brine (25 mL). The organic phase was dried over anhydrous Na₂SO₄, filtered and evaporated under vacuum. The crude product was purified by flash chromatography (SiO₂, PetEt/EtOAc 80:20→70:30, R_f^{80:20} = 0.24), leading to the aimed compound as a colorless oil (855 mg, 42%). ¹H NMR (500 MHz, 27 °C, CD₃OD), δ (ppm): 7.17 (t, ³J_{HH} = 7.2 Hz, 1H, CHCHCOH), 6.95 (d, ³J_{HH} = 7.1 Hz, 1H, CHCCH₂), 6.83 (d, ³J_{HH} = 8.0 Hz, 1H, CHCOH), 6.76 (t, ³J_{HH} = 7.4 Hz, 1H, CHCHCCH₂), 3.90 (s, 2H, NCH₂Ar), 3.71 (m, 3H, NCH + NCHCH₂N), 3.51 (m, 5H, NCHCH₂N + NCH₂CO), 3.32 (m, 1H, NCH₂CH₂), 3.09 (m, 1H, NCH₂CH₂), 2.08 (m, 1H, NCH₂CH₂), 1.9–1.7 (m, 4H, NCHCH₂CH₂ + NCH₂CH₂), 1.58 (m, 1H, NCHCH₂CH₂), 1.48 (s, 9H, 3×CH₃), 1.46 (s, 9H, 3×CH₃). ¹³C NMR (125 MHz, 27 °C, CD₃OD), δ (ppm): 170.3 (CO), 157.5 (COH), 129.5 (CHCCH₂), 129.2 (CHCHCOH), 122.0 (CCH₂), 119.2 (CHCHCCH₂), 116.4 (CHCOH), 82.3 (C¹⁸), 59.4 (NCH₂CO), 58.8 (NCH₂Ar), 60.6 (NCH), 51.8 (NCH₂CH₂), 39.5 (NCHCH₂N), 28.2 (CH₃), 25.1 (NCH₂CH₂), 20.3

(NCHCH₂CH₂ + NCHCH₂CH₂). ESI⁺ MS: m/z 449.5 [M + H⁺], calc. for [C₂₅H₄₁N₂O₅]⁺ = 449.30 g/mol.

2-AMPDA-HB. 2-AMPDA-HB(OtBu)₂ (200 mg, 0.44 mmol) was dissolved in DCM (3 mL). Triisopropylsilane (1 drop) was added, followed by TFA (3 mL), and the mixture was stirred at room temperature for 15 h. The solvents were evaporated under reduced pressure and the residue was redissolved in TFA (1 mL) and precipitated in Et₂O (10 mL). The suspension was centrifuged (4000 rpm, 15 min, 10 °C) and the precipitate was washed/centrifuged with Et₂O (3 × 10 mL) and dried under vacuum. The product was purified by preparative HPLC-MS (Method P2, t_R = 5.6 min), and the product was obtained after lyophilization as mono-trifluoroacetate salt (38 mg, 19%). HPLC-MS (Method A2): t_R = 9.6 min. Elemental analysis: found C, 50.59; H, 5.59; N, 6.19; calc. for C₁₉H₂₅F₃N₂O₇: C, 50.67; H, 5.59; N, 6.22. ¹H NMR (500 MHz, 27 °C, CD₃OD), δ (ppm): 7.19 (m, 2H, 2 × CH^A), 6.85 (m, 2H, 2 × CH^A), 4.32 (d, ²J_{HH} = 17.2 Hz, 1H, NCHH'Ar), 4.04 (d, ²J_{HH} = 17.2 Hz, 1H, NCHH'Ar), 4.00 (d, ²J_{HH} = 13.1 Hz, 1H, NCHH'COOH), 3.72 (m, 1H, NCH), 3.70 (d, ²J_{HH} = 13.1 Hz, 1H, NCHH'COOH), 3.47 (d, ²J_{HH} = 18.0 Hz, 1H, NCHH'COOH), 3.41 (d, ²J_{HH} = 18.0 Hz, 1H, NCHH'COOH), 3.33 (m, 1H, NCHCH₂N), 3.17 (m, 2H, NCHCH₂N + NCHH'CH₂), 2.88 (m, 1H, NCHH'CH₂), 1.9–1.5 (m, 6H, NCH₂CH₂CH₂CH₂). ¹³C NMR (125 MHz, 27 °C, CD₃OD), δ (ppm): 174.5 (COOH), 168.4 (COOH), 156.5 (COH), 132.0 (CH^A), 129.9 (CH^A), 123.5 (CH₂C^A), 120.1 (CH^A), 115.9 (CH^A), 60.7 (NCH), 54.6, 54.3 (NCH₂Ar + 2 × NCH₂COOH + NCH₂CH₂), 51.4 (NCHCH₂N), 23.5 (NCH₂CH₂), 20.1 (NCH₂CH₂CH₂CH₂), 19.8 (NCH₂CH₂CH₂). ESI⁺ MS: m/z 337.5 [M + H⁺], calc. for [C₁₇H₂₅N₂O₅]⁺ = 337.18 g/mol.

Preparation of Al¹⁸F-complexes

General procedure. AlCl₃ (1 equiv) and NaF (1 equiv) were dissolved in H₂O (5 mL/mmol), and the pH was adjusted to 4 with dropwise addition of 0.1 M NaOH. After stirring for 10 min, a solution of ligand (1 equiv) in H₂O (5 mL/mmol) was added dropwise, the pH was again adjusted to 4 and the mixture was heated to 40 °C and stirred for 2 h. Upon freeze-drying, the crude product was purified by preparative HPLC-MS (Method P3) and lyophilized.

Al¹⁸F-2-AMPTA. HPLC-MS (Method A3): t_R = 5.5 min. ¹⁹F NMR (470 MHz, 27 °C, D₂O), δ (ppm): −171.5. ESI[−] MS: m/z 331.3 [L−3H + AlF][−], calc. for [C₁₂H₁₇AlFN₂O₆][−] = 331.26 g/mol.

Al¹⁸F-NHB-2-AMPDA. HPLC-MS (Method A3): t_R = 8.4 and 8.9 min. ¹H NMR (500 MHz, 27 °C, D₂O), δ (ppm): 8.34 (m, 1H, CH^A), 8.22 (m, 1H, CH^A), 7.04 (m, 2H, CH^A), 4.45 (m, 2H, NCH₂Ar), 3.50 (bm, 5H, NCH₂CO + NCHCHH'N), 3.33 (m, 2H, NCHCHH'N + NCHCH₂N), 3.13 (m, 2H, NCH₂CH₂), 1.9–1.6 (m, 6H, NCH₂CH₂CH₂CH₂). ¹⁹F NMR (470 MHz, 27 °C, D₂O), δ (ppm): −157.2, −157.9. ESI[−] MS: m/z 424.3 [L−3H + AlF][−], calc. for [C₁₇H₂₀AlFN₃O₇][−] = 424.34 g/mol.

Al¹⁸F-2-AMPDA-HB. HPLC-MS (Method A3): t_R = 10.5 and 11.1 min. ¹H NMR (500 MHz, 27 °C, D₂O), δ (ppm): 7.15 (m, 1H, CH^A), 6.97 (m, 1H, CH^A), 6.69 (m, 2H, CH^A), 4.07 (d, ²J_{HH} = 13.8 Hz, 1H, NCHH'Ar), 3.8–3.6 (m, 3H, NCHH'Ar + N¹⁸FCHH'CO + NCHH'CO), 3.36 (d, ²J_{HH} = 18.5 Hz, 1H, N¹⁸FCHH'CO), 3.15 (d, ²J_{HH} = 18.2 Hz, 1H, NCHH'CO), 3.07 (m, 1H, NCH), 2.82 (m, 2H, NCHCH₂N), 2.7–2.6 (m, 2H, NCH₂CH₂), 1.8–1.4 (m, 6H, NCH₂CH₂CH₂CH₂). ¹⁹F NMR (470 MHz, 27 °C, D₂O), δ (ppm): −157.2, −157.9, −165.5. ESI[−] MS: m/z 379.4 [L−3H + AlF][−], calc. for [C₁₇H₂₁AlFN₂O₅][−] = 379.34 g/mol.

Radiolabeling experiments. All the 3 chelators, and the p-SCN-Bn-NOTA as comparison, were labeled with AlF-18 using the protocol already described elsewhere,^[30] slightly modified. [¹⁸F]fluoride was produced at the PETtrace cyclotron 880 (GE Healthcare, Uppsala, Sweden) via the ¹⁸O(p,n)¹⁸F nuclear reaction by irradiating enriched

[¹⁸O]water with 16.5 MeV protons in a niobium target (2.5 mL internal volume). The [¹⁸F]fluoride was then transferred through Tefzel tubing to a QMA Sep-Pak light cartridge for trapping. For experiments with less activities the niobium target was rinsed with the same amount of ultrapure [¹⁶O]water after a production of 130–190 GBq [¹⁸F]fluoride gaining approx. 3–5 GBq.

[¹⁸F]F[−] was eluted from a Sep-Pak Accell Plus QMA Plus Light anion exchange cartridge (Cl[−] form; Waters) with 500 μL of NaCl 0.9% solution (2.5–6 GBq of collected activity). 50 μL of these solution (250–600 MBq) were added at room temperature to 22.5 μL (45 nmol) of AlCl₃ in NaOAc 0.1 M at both pH 4 and 5. After 5 min the chelators were labeled by adding 72.5 μL of [Al¹⁸F]²⁺ to 500 μL total volume of a solution prepared by adding 15 μL (75 nmol) of chelator, 100 μL of EtOH and 385 μL of NaOAc 0.1 M (pH 4 or 5). The final solution (572.5 μL) was incubated for 12 min at different temperature (rt, 37 and 80 °C). The products were purified using a Sep-Pak Alumina N Plus Light cartridges preconditioned with 5 mL of 0.9% NaCl solution and then eluted with 1.5 mL of 0.9% NaCl solution. RCYs were calculated by radio-TLC as well as radio-HPLC analysis using the Method A1 reported in the Supporting Information (MeOH/H₂O 0–2 min 1% A, 2–16 min 1% → 100% A, 16–19 min 100% A). Using the same protocol, labeling tests on AMP-based chelators at pH 4.5, 5.5, 6.0 and 6.5 were performed and RCYs determined.

Partition coefficient test. The partition coefficient of [Al¹⁸F(2-AMPDA-HB)][−] was determined as reported elsewhere^[36] by measuring the distribution of the radioactivity associated to the complex in equal volumes of 1-octanol and PBS (pH 7.4, 0.1 M sodium phosphate, 0.15 M sodium chloride). Briefly, 7 ± 0.2 MBq of the radiolabeled compound was loaded into an Eppendorf tube containing 500 μL of PBS and 500 μL of 1-octanol (Merck, Darmstadt, Germany). After vigorous mixing for 3 min at room temperature, samples were centrifuged at 15000 rpm for 1 min to ensure complete separation of the solvents. Then the 2 solutions were separated and the respectively activity was counted in a dose calibrator. The partition coefficient was then calculated as “log P” dividing the activity in octanol to the activity in PBS solution. The experiment were performed two times in triplicates.

In vitro stability studies. After the purification step and characterization of the radioactive complex via HPLC, the stability evaluation of the complex at different time points and in different solutions was carried out. [Al¹⁸F(2-AMPDA-HB)][−], [Al¹⁸F(2-AMPTA)][−], [Al¹⁸F(NHB-2-AMPDA)][−] were dissolved in NaCl 0.9% solution, EDTA 5 mM (pH 5), PBS buffer and Human Serum (1:5) and were incubated at 37 °C up to 240 min. Each time point the stability was evaluated by radio-TLC using a thin-layer chromatographic strip (TLC, Agilent) and a mixture of ACN/H₂O 75%–25% as eluent.

In vivo studies. All animal experiments were approved by local authorities (animal license: 55.2-1-54-2532-216-15) and handled according to guidelines for the welfare and use of animals in experimental procedures. In order to study the biodistribution and the *in vivo* stability of the [Al¹⁸F(2-AMPDA-HB)][−], 8 weeks old pathogen-free female athymic Nude-Foxn^{1^{nu/nu}} mice (Charles River Laboratories, Sulzfeld, Germany) (n = 6) were injected via catheter in the tail vein with 2.3 ± 0.1 MBq of [Al¹⁸F(2-AMPDA-HB)][−] in 250 μL NaCl 0.9% solution and imaged for 90 minutes with a PET/CT dynamic acquisition using an Inveon Small Animal PET/CT scanner (Siemens, Knoxville, TN). Image-derived uptake calculation on dynamic PET-CT scans were performed by drawing region of interest (ROIs) on selected organs, to study the biodistribution of the [Al¹⁸F(2-AMPDA-HB)][−] over the time and calculate the activity accumulation.

Ex vivo studies. *Ex vivo* biodistribution study was also performed to further probe the biological behavior of the $[Al^{18}F(2\text{-AMPDA-HB})]^-$ complex. After sacrifice the mice by neck dislocation, blood and several organs were collected, weighed and the activity was calculated by a γ -counter. The tracer accumulation in selected organs was expressed as percentage of injected dose per gram of tissue (%ID/g). *In vivo* and *ex vivo* accumulation data were compared for correlation analysis.

Acknowledgements

The authors thank Markus Mittelhäuser for technical support during animal injections and PET-CT scans, and Dr. Alberto Fraccarollo (Università del Piemonte Orientale) for help with the molecular design. This work was supported by the Deutsche Forschungsgemeinschaft (SFB824 Project C10) granted to C.D. and by the Alexander von Humboldt Foundation granted to L.T.

Keywords: PET imaging · AIF-18 · radiofluorination · polydentate chelators

- [1] A. Rahmim, H. Zaidi, *Nucl. Med. Commun.* **2008**, *29*, 193–207.
- [2] E. Boros, A. B. Packard, *Chem. Rev.* **2019**, *119*, 870–901.
- [3] E. Boros, J. P. Holland, *J. Labelled Compd. Radiopharm.* **2018**, *61*, 652–671.
- [4] M. G. Campbell, J. Mercier, C. Genicot, V. Gouverneur, J. M. Hooker, T. Ritter, *Nat. Chem.* **2017**, *9*, 1–3.
- [5] L. Mu, A. Höhne, P. A. Schubiger, S. M. Ametamey, K. Graham, J. E. Cyr, L. Dinkelborg, T. Stellfeld, A. Srinivasan, U. Voigtman, *Anal. Biochem.* **2008**, *47*, 4922–4925.
- [6] J. Becaud, L. Mu, P. A. Schubiger, S. M. Ametamey, K. Graham, T. Stellfeld, L. Lehmann, S. Borkowski, D. Berndorff, L. Dinkelborg, *Bioconjugate Chem.* **2009**, *20*, 2254–2261.
- [7] A. Höhne, L. Mu, M. Honer, P. A. Schubiger, S. M. Ametamey, K. Graham, T. Stellfeld, S. Borkowski, D. Berndorff, U. Klar, *Bioconjugate Chem.* **2008**, *19*, 1871–1879.
- [8] F. Wüst, C. Hultsch, R. Bergmann, B. Johannsen, T. Henle, *Appl. Radiat. Isot.* **2003**, *59*, 43–48.
- [9] G. Vaidyanathan, M. R. Zalutsky, *Nat. Protoc.* **2006**, *1*, 1655–1661.
- [10] G. Vaidyanathan, D. McDougald, J. Choi, M. Pruszyński, E. Koumariou, Z. Zhou, M. R. Zalutsky, *Org. Biomol. Chem.* **2016**, *14*, 1261–1271.
- [11] Z. Li, Z. Wu, Q. Cao, D. W. Dick, J. R. Tseng, S. S. Gambhir, X. Chen, *Mol. Imaging Biol.* **2008**, *10*, 92–98.
- [12] H. Gao, G. Niu, M. Yang, Q. Quan, Y. Ma, E. N. Murage, J. Ahn, D. O. Kiesewetter, X. Chen, *Mol. Pharm.* **2011**, *8*, 1775–1782.
- [13] D. O. Kiesewetter, O. Jacobson, L. Lang, X. Chen, *Appl. Radiat. Isot.* **2011**, *69*, 410–414.
- [14] H. Wang, H. Ding, J. Chen, C. Chao, Y. Lu, W. Lin, C. Kao, T. Veterans, G. Hospital, R. Sciences, *Cancer Imaging* **2012**, *12*, 464–474.
- [15] K. Chansaenpak, B. Vabre, F. P. Gabbai, *Chem. Soc. Rev.* **2016**, *45*, 954–971.
- [16] W. J. McBride, R. M. Sharkey, H. Karacay, C. A. D'Souza, E. A. Rossi, P. Laverman, C.-H. Chang, O. C. Boerman, D. M. Goldenberg, *J. Nucl. Med.* **2009**, *50*, 991–998.
- [17] W. J. McBride, R. M. Sharkey, D. M. Goldenberg, *EJNMMI Res.* **2013**, *3*, 1–11.
- [18] R. B. Coord, *Chem. Rev.* **1996**, *141*, 23–32.
- [19] L. Li, *Crit. Rev. Oral Biol. Med.* **2003**, *14*, 100–114.
- [20] C. Fersing, A. Bouhlef, P. Garrigue, V. Lisowski, B. Guillet, *Molecules* **2019**, *24*, 2866.
- [21] C. A. D'Souza, W. J. McBride, R. M. Sharkey, L. J. Todaro, D. M. Goldenberg, *Bioconjugate Chem.* **2011**, *22*, 1793–1803.
- [22] S. Lütje, G. M. Franssen, R. M. Sharkey, P. Laverman, E. A. Rossi, D. M. Goldenberg, W. J. G. Oyen, O. C. Boerman, W. J. McBride, *Bioconjugate Chem.* **2014**, *25*, 335–341.
- [23] D. Shetty, Y. Choi, M. Jeong, Y. Lee, L. Hoigebazar, Y. Lee, S. Lee, J. Chung, C. Lee, *Chem. Commun.* **2011**, *47*, 9732–9734.
- [24] W. J. McBride, C. A. D. Souza, H. Karacay, R. M. Sharkey, D. M. Goldenberg, *Bioconjugate Chem.* **2012**, *23*, 538–547.
- [25] K. L. S. Chatalic, G. M. Franssen, W. M. van Weerden, W. J. McBride, P. Laverman, E. de Blois, B. Hajjaj, L. Brunel, D. M. Goldenberg, J.-A. Fehrentz, *J. Nucl. Med.* **2014**, *55*, 2050–2056.
- [26] J. M. U. Silvola, X. Li, J. Virta, P. Marjamäki, H. Liljenbäck, J. P. Hytönen, M. Tarkia, V. Saunavaara, S. Hurme, S. Palani, *Nat. Sci. Reports* **2018**, *8*, 1–15.
- [27] S. Boschi, J. T. Lee, S. Beykan, R. Slavik, L. Wei, C. Spick, U. Eberlein, A. K. Buck, F. Lodi, G. Cicoria, *Eur. J. Nucl. Med. Mol. Imaging* **2016**, *43*, 2122–2130.
- [28] F. Cleeren, J. Lecina, E. M. F. Billaud, M. Ahamed, A. Verbruggen, G. M. Bormans, *Bioconjugate Chem.* **2016**, *27*, 790–798.
- [29] F. Cleeren, J. Lecina, M. Ahamed, G. Raes, N. Devoogdt, V. Caveliers, P. McQuade, D. J. Rubins, W. Li, A. Verbruggen, *Theranostics* **2017**, *7*, 2924–2939.
- [30] F. Cleeren, J. Lecina, J. Bridoux, N. Devoogdt, T. Tshibangu, C. Xavier, G. Bormans, *Nat. Protoc.* **2018**, *13*, 2330–2347.
- [31] F. K. Kálmán, G. Tircsó, *Inorg. Chem.* **2012**, *51*, 10065–10067.
- [32] A. Vágner, E. Gianolio, S. Aime, A. Maiocchi, I. Tóth, Z. Baranyai, L. Tei, *Chem. Commun.* **2016**, *52*, 11235–11238.
- [33] R. Bhalla, C. Darby, W. Levason, S. K. Luthra, G. McRobbie, G. Reid, G. Sanderson, W. Zhang, *Chem. Sci.* **2014**, *5*, 381–391.
- [34] J. D. Hem, *Adv. Chem. Ser.* **1968**, *73*, 98–114.
- [35] X. Yang, Y. A. Gandhi, D. B. Duignan, M. E. Morris, *AAPS J.* **2009**, *11*, DOI 10.1208/s12248-009-9124-1.
- [36] S. Stangl, L. Tei, F. De Rose, S. Reder, J. Martinelli, W. Sievert, M. Shevtsov, R. Öllinger, R. Rad, M. Schwaiger, *Cancer Res.* **2018**, *78*, 6268–6281.

Manuscript received: November 20, 2019
 Revised manuscript received: December 2, 2019
 Accepted manuscript online: December 12, 2019
 Version of record online: January 7, 2020